SOL-GEL PROCESSING OF RUTHENIUM AND IRIDIUM DIOXIDES

Julian Robert Osman

A Thesis Submitted for the Degree of PhD
at the
University of St Andrews

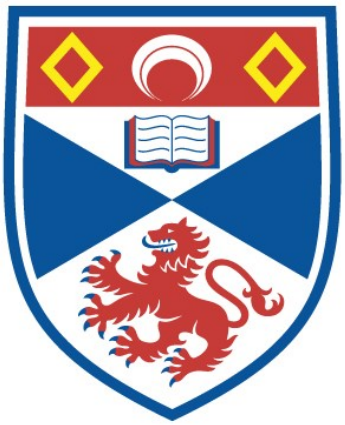

1998

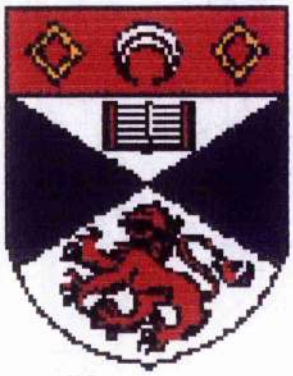

Sol-Gel Processing of Ruthenium and Iridium Dioxides

A thesis presented by Julian Robert Osman BSc.,

to the University of St. Andrews in application

for the degree of Doctor of Philosophy

1998

ProQuest LLC.
789 East Eisenhower Parkway
P.O. Box 1346
Ann Arbor, MI 48106 – 1346

Declaration

I, Julian Robert Osman, hereby certify that this thesis, which is approximately 41,000 words in length, has been written by me, that it is a record of work carried out by me and that it has not been submitted in any previous application for a higher degree.

Signed _____ Date 18/5/98

I was admitted as a research student in October 1994 as a candidate for the degree of Doctor of Philosophy; the higher study for which this is a record was carried out in the University of St. Andrews between October 1994 and February 1998.

Signed _____ Date 18/5/98

I hereby certify that the candidate has fulfilled the conditions of the Resolution and Regulations appropriate for the degree of Doctor of Philosophy in the University of St. Andrews and that the candidate is qualified to submit this thesis in application for that degree.

Signed Date 18/5/98

Signed _____ Date 18/5/98

Declaration

In submitting this thesis to the University of St. Andrews I understand that I am giving permission for it to be made available for use in accordance with the regulations of the University library for the time being in force, subject to any copyright vested in the work not being affected thereby. I also understand that the title and abstract will be published and that a copy of the work may be made and supplied to any bona fide library or research worker.

Signed _____ Date 18/5/93

CONTENTS

Chapter 4

Non Aqueous Sol-Gel Processing of RuO_2 and RuO_2-TiO_2 Mixed Oxides

Chapter 5

Aqueous and Non-Aqueous Sol-Gel processing of IrO_2 and IrO_2-TiO_2 Mixed Metal Oxides

Chapter 6

Oxygen Evolution and Electrochemical Studies on Sol-Gel derived Iridium Dioxide

Acknowledgements

I would like to express my sincerest thanks to my supervisors, Dr. Joe Crayston and Dr. Dave Richens for their invaluable assistance, guidance and enthusiasm over the course of my research in St. Andrews. I would also like to thank my industrial supervisors Dr. Allin Pratt, Dr. David Boyd and Dr. Barry Murrer for their help and insights. Thanks too must go to Dr. Ann Keep at JM for getting me the iridium acetate.

Thanks are also due to a number of people without whom the project would have been a great deal more difficult. I would like to thank the staff at the Johnson Matthey Technology Centre for their extensive analytical work on the samples I sent them. The EXAFS work would have been impossible without the expertise of Dr. Gert Van Dorssen and Dr. Bob Billborrow at Daresbury. Thanks must go to Dr. Iain Shannon without whom analysis of our data would have proved far more difficult. I would also like to thank the technical staff of the School of Chemistry in St. Andrews for their help.

This work would not have been possible without assistance the following souls who have spent the last three and a half years in the lab with me. I would, therefore, like to say a big thank you to Andy Taylor, John Morrison, Graeme Hunt, Patricia Marr, Alex Thomas and Chanaka De Alwis for their help and for putting up with my moods and my hangovers. Special thanks too must go to Dave Butler, Richard Gover and Brian Mitchell. I would also like to thank Malcolm at the Cellar Bar and Steven at the Whey Pat for providing the fine ales that have nourished me during my studies.

Finally I am indebted to the EPSRC and Johnson Matthey Plc for the funding of this project and the loan of metals from the latter.

List of Abbreviations

δ	Relative to TMS
δ_i	Partial Positive or Negative Charge
η	Hardness
μ	Absorption Coefficient
χ	Electronegativity
A	Debye Waller Factor
Acac	2,4-Pentanedione
AFAC	Amplitude Reduction Factor
Bipy	Bipyridine
DMSO	Dimethylsulphoxide
DTA	Differential Thermal Analysis
EDX	Energy Dispersive Analysis of X-Rays
EXAFS	Extended X-Ray Absorption Fine Structure
FAB	Fast Atom Bombardment
FI	Fit Index
h	Hydrolysis Ratio
I_o	Incident X-Ray Energy
I_t	Transmitted X-ray intensity
L_{OEt}	Cyclopentadienyltris(diethylphosphito)cobalt
MeCN	Acetonitrile
MiBK	Methyl Isobutyl Ketone
MIDA	Methyliminodiacetic acid
MS	Mass Spectrum
NMR	Nuclear Magnetic Resonance
OEt	Ethoxide group
O^iPr	Isopropoxide group
OR	Alkoxide group
Pts	p-toluene Sulphonate
Py	Pyridine

R	Discrepancy Index
SEM	Scanning Electron Microscopy
SIMS	Secondary Ion Mass Spectrometry
Tacn	1,4,7-Triazacyclononane
TEM	Transmission Electron Microscopy
TGA	Thermogravimetric Analysis
TMS	Trimethylsilane
UV-Vis	Ultraviolet and Visible
XAS	X-ray Absorption Spectroscopy
XANES	X-Ray Absorption Near Edge Structure
XRD	X-Ray Diffraction
XRF	X-Ray Fluorescence
XPS	X-Ray Photoelectron Spectroscopy
YBCO	Yttrium Barium Copper Oxide

Abstract

The synthesis of the $Ru_4O_6^{4+}(aq)$ ion and attempts to produce derivative complexes of it are explored. Although crystals suitable for examination by single crystal X-Ray crystallography were not obtained, the core structure of the $Ru_4O_6^{4+}$ ion in solution has been successfully determined using Ru K edge EXAFS spectroscopy. The refined results for solutions of the ion in aqueous acid, provide strong indications that the ion has an adamantanoid core arrangement in solution and that core structures based on μ-hydroxo groups i.e $Ru_4(OH)_{12}^{4+}$ can be ruled out.

Preparation and controlled hydrolysis of a variety of ruthenium precursors aimed at preparing gels of $RuO_2.nH_2O$ gave at best powders. For example, only RuO_2 powders were obtained by raising the pH of solutions of the $Ru_4O_6^{4+}$ ion. However, gels of a RuO_2-TiO_2 mixed oxide were readily prepared from the alkoxides. From TGA/DTA, X-Ray, and electron microscopy data these proved to be a mixture of two different oxide phases rather than a solid solution. In some samples the RuO_2 phase contains some of the smallest RuO_2 nanoparticles so far reported. The mixed oxide gels and powders obtained were found to contain a number of impurities.

Work performed on the iridium aqua ion $[Ir(H_2O)_6]^{3+}$ is reported along with experiments to produce mixed IrO_2-TiO_2 oxides using iridium ethoxide and iridium acetate complexes as starting materials. The aqua ion was found to give a powder product but gels were obtained from the other two precursors. The gels have been characterized and it was found that IrO_2 is highly dispersed within a TiO_2 matrix. The electrocatalytic properties of the IrO_2 containing gels have been determined by studying the rates of oxygen evolution and the rate of consumption of cerium(IV) ions. The

results show that the sol-gel derived IrO_2 systems show good activity towards catalysing oxygen evolution by these ions.

CHAPTER 1

Introduction

1.1 Ruthenium and Iridium Dioxides

The element ruthenium was first reported in 1826 by Osann but it was not until 1844 that K. K. Klaus isolated the pure metal by treating chloride salts of the metal with hydrogen sulphide. Klaus named the metal ruthenium in honour of his motherland, Russia[2]. Iridium had been isolated much earlier than ruthenium by Smithson Tennant and was named after iris, the Greek word for rainbow due to the colourful nature of its salts. Ruthenium was then the last of the platinum group metals to be isolated[2].

Ruthenium dioxide, RuO_2, is the only stable solid species formed by heating ruthenium metal in oxygen. RuO_2 can be made by a number of different thermal and chemical methods. The simplest of these are: i) the action of base on aqueous solutions of ruthenium trichloride, $RuCl_3.nH_2O$;. ii) By the reduction of the tetroxide RuO_4 into aqueous solution or acid or; iii), by the Adams method of thermal treatment of the trichloride and sodium nitrate. RuO_2 has also been prepared from RuO_4, ruthenocene and $Ru(acac)_3$ using chemical vapour deposition techniques although this method has proved problematic[3]. The compound exists in two forms: anhydrous and hydrated. The former has a well defined rutile structure. The hydrated form contains a number of molecules of coordinated water and can be amorphous.

Ruthenium dioxide has a number of uses within the electronics industry.

Because of its high electrical conductivity, chemical stability and its ability to act as a good barrier to ionic diffusion, it has applications as both thick film or thin film resistors with resistivities in the range 0.3 – 1 $\mu\Omega m$[4] (Fig.1.1). Ruthenium oxide shows some promise as the active layer in electrochemical capacitors[5-9] in which the specific capacitance of a RuO_2 based system is found to be strongly dependent upon its crystallinity: high values only being obtainable if the sample is amorphous[8]. Capacitance is dependent upon the ease of intercalation of protons into the RuO_2 layer[5,8] with extrapolation of existing data suggesting that energy densities of 10-100

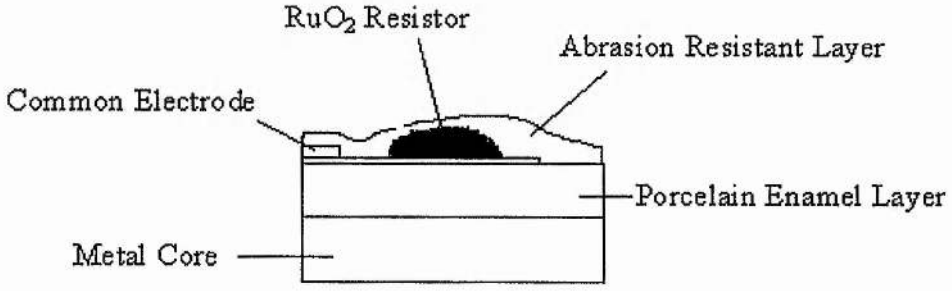

kJ kg^{-1} are possible.

Fig. 1.1: Diagram for the construction of a thermal printing head containing a RuO_2 resistor reproduced from Yosida et al, J. Electrochem. Soc. 1995, **142**, 3165.

IrO_2 can again be prepared via the Adams method of heating the trichloride with $NaNO_3$, or by reaction of the trichloride with aqueous base. Higher oxidation states of iridium are not as stable as those of ruthenium and thus routes to the dioxide by

reduction are rare. Films of IrO_2 have been shown to exhibit electrochromism properties. Electrochromism is defined as a persistent but reversible change produced electrochemically. That is to say a material that can be reversibly coloured by the application of an electric field or the passage of ions and current through it. IrO_2 films change colour from transparent at a negative potential to blue/black at a positive potential[10] leading to possible applications of IrO_2 as a material in display devices such as Fig. 1.2.

The principal use of ruthenium and iridium dioxides is in modified electrodes for the oxidation of chloride to chlorine or the oxidation of water to oxygen. The processes and problems involved in producing these electrodes and evolving the gasses are discussed below.

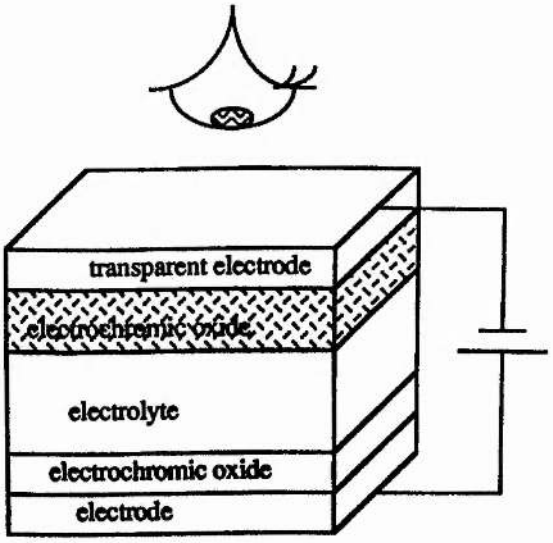

Fig 1.2: An electrochromic cell. Reproduced from G. R. Lee, Ph.D Thesis, University of St. Andrews, 1992.

1.2 Gas Evolution Catalysed by RuO_2 and IrO_2

1.2.1 Water and Chloride oxidation

In these days of increased interest in alternative sources of energy from renewable sources the conversion of solar energy to fuel is of some importance. One system being investigated is the photochemical conversion of water to hydrogen and oxygen or conversion of hydrochloric acid to hydrogen and chlorine. The incident photons should generate a strong oxidant to oxidize water to O_2 and a strong reductant to reduce hydrogen to H_2. It is necessary to include a redox catalyst as the present oxidants are unable to produce O_2 at a measurable rate under ambient conditions. This redox catalyst is a substance, heterogeneous or homogenous, which is able to lower the activation energy of the system where there are two or more redox couples present not in equilibrium thus raising the rate of electron transfer to a measurable value. It has been shown that in many cases an important role of this catalyst is as a conductor of electrons[12,13] (Fig. 1.3).

The mechanism of water and chloride oxidation on a particle of oxidation catalyst or an evolution electrode is given below:-

Oxygen

$$S\text{-}OH \rightarrow S\text{-}O + H^+ + e \qquad (1.1)$$

$$S\text{-}O + OH^- \rightarrow HO\text{-}S\text{-}O + e \qquad (1.2)$$

$$2(HO\text{-}S\text{-}O) \rightarrow 2(S\text{-}OH) + O_2 \qquad (1.3)$$

Chlorine

$$S\text{-}OH \rightarrow S\text{-}O + H^+ + e \qquad (1.4)$$

$$S\text{-}O + Cl^- \rightarrow Cl\text{-}S\text{-}O + e \qquad (1.5)$$

$$2(Cl\text{-}S\text{-}O) + H^+ \rightarrow 2(S\text{-}OH) + Cl_2 \qquad (1.6)$$

Where S represents an atom at the surface of the particle or electrode.

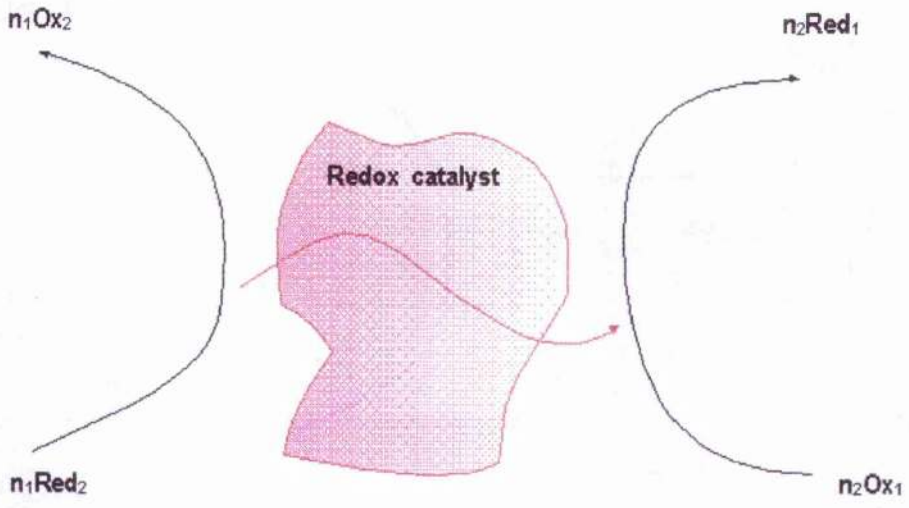

Fig. 1.3 Schematic representation of the electron conducting role of a heterogeneous redox catalyst in reactions 1.7 and 1.8 below.

The general redox reaction

$$Ox_1 + n_1e^- \leftrightarrow Red_1 \qquad E_1 \qquad (1.7)$$

$$Red_2 \leftrightarrow Ox_2 + n_2e^- \qquad E_2 \qquad (1.8)$$

is thermodynamically favourable if $\Delta E = E_1 - E_2 > 0V$, where E_1 and E_2 are the equilibrium reduction potentials of redox couples 1 and 2 respectively.

Solutions of cerium(IV) and permanganate are examples of species which are thermodynamically unstable as both have redox potentials greater than that of the O_2/H_2O and Cl_2/Cl^- couples[11]. These species are, however, stable kinetically due to a large activation barrier arising from the multi-electron transfer processes involved. Hence the need for a redox catalyst to allow production of oxygen hydrogen and chlorine at reasonable rates.

One of the major problems in finding suitable oxidation catalyst materials is finding suitable compounds that are not dissolved or passivated by the strongly oxidizing conditions used[14]. Hydrated RuO_2 is one of the most popular water oxidation catalysts although the type of hydrated RuO_2 used is of great significance. A number of studies[14-19] have shown that $RuO_2.xH_2O$ generated by alkaline hydrolysis in aqueous solution is not a good catalyst with problems arising from oxidation of the RuO_2 to RuO_4. It is found that thermal treatment at temperatures in excess of 144 °C for 5 hours prevents this corrosion. It is thought that this thermal treatment induces condensation reactions between hydroxyl groups at surface defect sites where oxidative loss occurs. The loss of defect sites is responsible for the observed reduction in corrosion. One of the most important advantages of using RuO_2 as an oxidation catalyst is that it has the same rutile structure as many of the metal oxides commonly used as catalyst supports for the such as TiO_2 and SnO_2. There is good agreement amongst published results that the TiO_2-RuO_2 mixed oxide system produces a solid solution over the entire range of metal ratios at firing temperatures between 400 and 700 °C although some authors[21] find segregation into anatase TiO_2 and rutile RuO_2 under certain conditions. Hydrated

IrO_2 has also been studied as a water oxidation catalyst[15,22] and again it has been shown that thermal activation of the hydrate is necessary. Both RuO_2 and IrO_2 have also been shown[13] to be effective catalysts for hydrogen evolution although stabilizers are required to prevent reduction of the catalyst by liberated H_2.

1.2.2 Ruthenium and iridium dioxide based coatings

Several classes of transition metal oxide have been found to be superior to all others for water and chlorine oxidation electrodes: rutiles (dioxides), spinels and perovskites. The past 25 years have witnessed the large scale adoption of platinum group metal coatings for a number of electrolytic processes. In particular the chlorine industry is heavily reliant on RuO_2 based coatings. It is estimated that by 1980 60% of the worlds' chlorine was being manufactured on ruthenised titania[1], a material that consists of layers of RuO_2 and TiO_2 prepared by painting precursors onto a titanium or TiO_2 support and firing at high temperature.

These electrodes typically consist of a few microlayers of electrocatalyst painted onto a base metal substrate. The mechanism of oxidation of water and chlorine oxidation and hydrogen reduction depends on the ease of changing the oxidation state of the oxide species[13]. Oxide layers on electrodes can be "cracked" or "compact", amorphous or crystalline depending on the techniques employed in producing the electrode and the conditions used. The oxide layer is usually prepared by pyrolysis of the chloride salts of the metals involved after painting or spraying isopropanol solutions of these precursors onto a metal backplate, usually titanium. In many cases simple alkoxide compounds of the less valuable base metal such as $Ti(OEt)_4$ are used

rather than chlorides. Non stoichiometric, structurally defective oxides are obtained, the properties of which depend upon the means by which the oxide was produced. If pyrolysis is performed at temperatures below 800°C the oxide layer contains chloride impurities although the contamination is lower as the pyrolysis temperature or the calcination time is increased . It is found for both iridium and ruthenium that the chloride contamination is more extensive in the bulk than at the surface. It is also found that iridium oxide prepared by pyrolysis of hydrated $IrCl_3$ contains chloride at higher temperatures (850-950°), a problem thought to arise from passivation of the trichloride by oxide formed at the surface during the pyrolysis[23]. One possibility for the higher bulk contamination was suggested by Daolio et al,[24] who studied the surface and bulk of RuO_2-TiO_2 coatings using SIMS. They proposed that residual chloride reacts with water of crystallization at the surface leading to oxygen enrichment and loss of HCl. Carbon impurities are also often found in coatings due to incomplete pyrolysis of metal organic precursors and when these impurities are removed porosity arises in the coating which can affect its electrocatalytic behaviour. Another important discovery was made during the SIMS studies on RuO_2-TiO_2 films concerning the surface and bulk compositions in relation to the two metals: it was found that in a sample treated at 400 °C the ruthenium penetrates into the bulk and accumulates in the near surface region. In pyrolysed samples RuO_2 is found to be oxygen deficient whereas IrO_2 has excess oxygen. RuO_2 and TiO_2 form a solid solution over the entire composition range, but a minimum of 20% RuO_2 is required in a RuO_2-TiO_2 mixed oxide electrode. TiO_2 is non-conducting so for any conduction to occur the electrode coating requires chains of touching RuO_2 grains. If tin oxide, doped with a small percentage of antimony to make it conducting, is used as the base metal oxide as little

as 2-3% ruthenium is required. For IrO_2-TiO_2 electrodes the solid solution is less stable and problems can arise from oxidation of the metal backplate at higher calcination temperatures leading to an insulating layer between the coating and the substrate.

Ruthenium and iridium oxide coatings are usually prepared from a mixture of a precious metal precursors and a base metal, usually titanium, precursor . The rationale behind this mixing of metal oxides is that the precious metal oxide provides the electrocatalytic activity whereas the base metal oxide provides inertness, improves mechanical integrity and adhesion properties of the coating along with changing the electrochemical behaviour of the coating. A titanium metal backplate is considered to be self-healing as, in areas where the coating has corroded, the metal is protected by an oxide coating. It is found that IrO_2, although less active than RuO_2 can stabilize a RuO_2-TiO_2 electrode. In principle the best oxygen evolving compound of ruthenium is RuO_4 produced by oxidation of the RuO_2 electrode. This compound is a gas however, and thus rapid corrosion of the electrode occurs as this species is lost from the electrode before reduction back to RuO_2. For an IrO_2-only based system the oxidized iridium species involved in oxygen evolution is in the +6 oxidation state and has 3-5 electrons in its t_{2g} band whereas for a RuO_2-only system the oxygen involving species is in the +8 oxidation state and has only two electrons in the t_{2g} band. Orbital overlap arising from mixing of the t_{2g} bands of RuO_2 and IrO_2, as shown by XPS spectroscopy[25], in a solid solution of RuO_2-IrO_2-TiO_2 leads to a shared d band with the electrons available on IrO_2 sites being shared with RuO_2 sites. This shifts the oxidation potentials for the reactions involved and prevents the production of RuO_4, slowing corrosion considerably at the cost of slightly reducing the activity. As little as 20% IrO_2 has been shown to be sufficient to dramatically reduce corrosion.

Oxide electrodes possess reactive surfaces with a strong hydrophilic character. Water molecules can become bonded to surface atoms and transfer protons to neighbouring oxygen atoms leading to a "carpet" of OH which can mediate the interactions of the oxide with the solution species. It is found that in RuO_2 and IrO_2 protons can penetrate through cracks, pores and grain boundaries into the inner surface of a layer through transfer between surface OH and O groups. The presence of these OH groups at the surface means that the surface charging is pH dependent.

The mechanism of gas evolution at these electrodes is given earlier. This mechanism is only possible because of the many available valence states for transition metal ions[13] such as ruthenium and iridium. For oxides with only one oxidation state the oxidation and reduction of surface sites becomes harder and their resistance to anodic dissolution higher hence their use to protect the more active species.

1.3 The Aqueous Chemistry of Ruthenium and Iridium

1.3.1 Ruthenium

Ruthenium has the richest redox chemistry of any element. Compounds exist in all valence states between -2 and +8. Next to vanadium and molybdenum it has the richest aqueous chemistry of cationic aqua species with oxidation states +2, +3 and +4 all represented[26]. In terms of finding precursors for aqueous (colloidal) sol-gel processing of RuO_2 the $[Ru_4O_6^{4+}]$ tetrameric aqua ion has potential along with a number of oxo, aqua, acetate and halide compounds.

1.3.1.1 The tetrameric $[Ru_4O_6^{4+}]$ aqua ion

One possible precursor for the colloidal sol-gel processing of RuO_2 is the tetrameric aqua cluster $Ru_4O_6^{4+}(aq)$. The existence of a red brown Ru(IV) ion has been documented since the 1950s in papers by Werner and Hindmann[27], Niedrach and Terebaugh[28] and Atwood and De Vries[29]. Initially, it was thought that the species was monomeric $[RuO]^{2+}$ or $[Ru(OH)_2]^{2+}$ or a dimeric species. Further work, however, pointing to the presence of oxo or hydroxo bridges[29] suggested otherwise. The detection of fractional oxidation states and subsequent electrochemical studies[30,31], in conjunction with charge to metal and charge/species determination, provided compelling evidence for a tetranuclear structure. The cluster can be prepared in three ways: electrochemically by oxidation of $[Ru(OH_2)_6]^{2+}$ or $[Ru(OH_2)_6]^{3+}$; by reduction of RuO_4 produced from $RuCl_3$ or RuO_2; or by treatment of K_2RuBr_6 with BrO_3^- (scheme 1)[26]. Care must be taken in the chemical preparations as the tetrameric structure is destroyed by halide ions. Reduction of RuO_4 is the most facile route to the tetramer and is achieved by extraction of RuO_4 into CCl_4 and reduction by H_2O_2 into 2M $HClO_4$. The reduction allows Ru(IV) to pass into the aqueous phase. Stronger reducing agents than H_2O_2 are found to reduce RuO_4 to Ru(II) and it is found that the use of less concentrated acid leads to extensive precipitation of $RuO_2.nH_2O$. After standing overnight to allow excess peroxide to decompose, the red/brown solution of the tetramer is subjected to purification by cation exchange chromatography. Problems arise with this method as it is found that the Dowex resin used for the purification retains much of the aqua ion, a problem thought to be due to protonation of the aqua

ion on the column, and that displacement of the aqua ion by elution with lanthanum (previously thorium) salts is necessary. This leads to lanthanum contamination of the final solution.

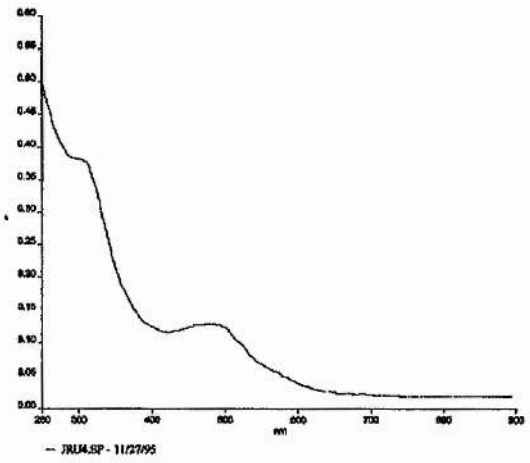

Fig. 1.4: UV-Visible spectrum of the $[Ru_4O_6]^{4+}$ aqua ion in 2M perchloric acid.

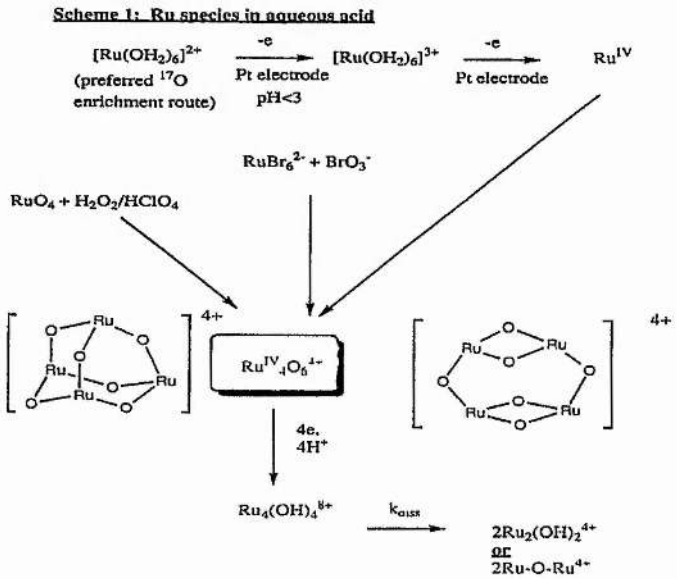

The aqua ion is most easily characterized in solution by UV-Vis spectrophotometry. The spectrum of the ion in perchloric acid of the ion is given in Fig. 1.4. The spectrum contains a characteristic broad shoulder at 487 nm ($\varepsilon = 709$ M^{-1} cm^{-1} per Ru) and a shoulder at around 302 nm ($\varepsilon \approx 2200$ M^{-1} cm^{-1} per Ru). It is found that the peak at 487nm shifts to lower wavelengths at higher pH and that above pH 4 a precipitate, postulated to by ruthenium hydroxide, is formed[32].

The exact structure of the core of the aqua ion cluster is not known and two possibilities have been suggested (Scheme 1). The main evidence for the first, "stacked dimer", structure is the observation that reduction leads to dimeric products via cleavage of the two $Ru(\mu\text{-}O)_2Ru$ units. However, the ^{17}O-NMR spectrum of the aqua ion (Fig. 1.5) contains only three peaks, one of which corresponds to bound water

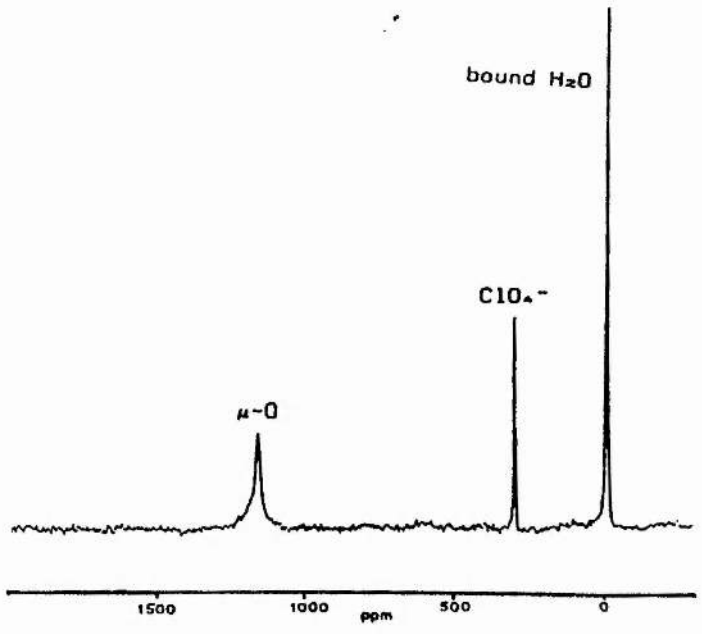

Fig. 1.5: O^{17} NMR spectrum of the tetrameric $[Ru_4O_6]^{4+}$ aqua ion in perchloric acid reproduced from A. Patel, Ph.D Thesis, University of Stirling, 1988.

molecules, one to the perchlorate counterion and only one for bridging oxygen. This spectrum could be explained by a more symmetric structure e.g adamantanoid structure. Mass spectrometric studies[32,33] on a tris-pyrazolyl borate derivative have confirmed the presence of the Ru_4O_6 core.

Patel[32], in addition to the mass spectrometric studies, made several attempts to grow a suitable crystal of derivatives of the aqua ion for X-ray diffraction but was only partially successful. Although these attempts did not produce crystals, success has been had with similar species. Crystals of a molybdenum aqua oligomer, an oxo bridged trimer similar in nature to the $[Ru_4O_6]^{4+}$ aqua ion, have been obtained from solutions in p-toluenesulphonic acid at low temperature[34]. Ruthenium oxo dimers have been characterized using the anionic tripod ligand $[(^5\eta C_5H_5)Co[(CH_3CH_2O)_2P{=}O]_3]$[35] and a manganese cluster with an adamantane skeleton has been characterized using triazacyclononane[36]. None of these ligands have been used previously in attempts to obtain crystals of the $[Ru_4O_6]^{4+}$ aqua ion.

It is hoped that derivatives of the $[Ru_4O_6]^{4+}$ aqua ion with organic counterions, prepared to yield crystals, would prove to be soluble in non-aqueous solvents leading to new possibilities for the sol-gel processing of RuO_2. The hydrolytic instability of the species in aqueous solution make it an ideal candidate for colloidal sol-gel processing. That is to say that the inherent instability of the aqua ion with respect to formation of RuO_2 above a certain pH can be exploited as a means of producing the dioxide in a controlled fashion as either gels or powders.

1.3.1.2 Chloride based sol-gel precursors

Commercial ruthenium trichloride is the starting material for the synthesis of many ruthenium compounds and is prepared by reduction of RuO_4 in the presence of HCl. The compound is highly soluble in both ethanol and water. This compound is of little use on its own as a sol-gel precursor due to its mixed nature: the compound is in fact a mixture of Ru(III) and Ru(IV) chloro and oxo species the main constituent of which is the compound referred to in the early literature as $Ru(OH)Cl_3$[37] or more recently as $Cl_xRuORuCl_y$. Its use as a starting material for preparing other sol-gel precursors such as the ruthenium alkoxides postulated by Kameyama et al[21] or the $Ru(acac)_3$[38] used by Guglielmi et al in their sol-gel studies on ruthenium make it an important compound. $RuCl_3$ can be prepared in the pure form by direct combination of the metal with Cl_2. The compound exists in two allotropic states: α-$RuCl_3$ (soluble in both water and ethanol) and β-$RuCl_3$ (water and ethanol insoluble), the former having recently been used to prepare mixed RuO_2-TiO_2 aerogels[39].

1.3.1.3 Oxo centered triaqua ruthenium complexes.

The ruthenium analogue of the $Fe(III)_3$ complex $[Fe_3(\mu_3\text{-}O)(\mu\text{-}O_2CCH_3)_6(OH_2)_3]^+$ was first reported by Wilkinson and co-workers in 1970[40] as the acetate salt obtained by treatment of $RuCl_3.nH_2O$ with a mixture of acetic acid and acetic anhydride. Since then it has been characterized as its BF_4^- and ClO_4^- salts (Fig. 1.6). The complex is interesting as it exists in two valence forms: $[Ru(III)_3(\mu_3\text{-}O)(\mu\text{-}O_2CCH_3)_6(OH_2)_3]^+$ and

$[Ru(III,III,IV)_3(\mu_3\text{-}O)(\mu\text{-}O_2CCH_3)_6(OH_2)_3]^{2+}$. Perchlorate salts of both cations are isolatable depending upon the conditions used: slow evaporation allows oxidation by perchlorate, a phenomenon not seen if high ionic strength solutions are used. Up to five valence forms of the compound can be obtained in total.

The water exchange rate constant at 25°C for this compound is (1.008 ± .007) x 10^{-3} s^{-1}, three orders of magnitude faster than for $[Ru(OH_2)_6^{3+}]$ and this is thought to arise from a *trans* influence from the planar μ_3-O group. This *trans* effect is also thought to be responsible for the slightly longer than expected Ru-OH_2 bond lengths found (212 pm compared to 203 pm in $[Ru(OH_2)_6^{3+}]$.

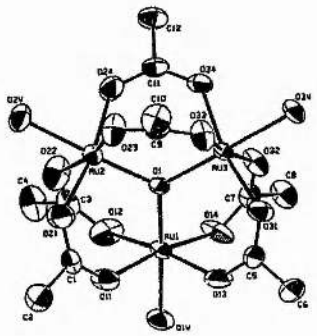

Fig. 1.6: The crystal structure of $[Ru_3(\mu_3\text{-}O)(\mu\text{-}O_2CCH_3)_6(OH_2)_3]^+$ first reported by Wilkinson et al[40], reproduced from D. T. Richens, *The Chemistry of Aqua ions*, Wiley, Chichester, 1997.

1.3.1.4 Hexaaqua ruthenium compounds, $[Ru(H_2O)_6]^{n+}$ (n = 2,3)

The aqua ion in the +2 state can be isolated as its p-toluenesulphonate

($CH_3C_6H_4SO_3^-$) or $CH_3SO_3^-$ salt by reduction of RuO_4 with metallic lead followed by decantation into 2M H_2SO_4 and removal of contaminating lead sulphate by filtration. The red purple aqua ion is then purified by ion exchange chromatography, followed by elution with the corresponding acid and crystallization by evaporation.

Like the tetrameric Ru(IV) aqua ion the compound's core contains only ruthenium, oxygen and hydrogen and thus is of interest as a sol-gel precursor. Air oxidation of pure solutions of the Ru(II) aqua ion gives the Ru(III) aqua ion. Hydrolysis of this species has been investigated by a number of authors. Below pH 3 it is found that E^θ is independent of pH but above this threshold it is found that E^θ varies linearly with increasing pH[26] although little data actually exists on the products of hydrolytic polymerization.

1.3.2 Iridium

Less is known about the solution chemistry of iridium in higher oxidation states, with only a few examples in the IV or V state[41-43] due to the increasing effective nuclear charge on the metal. Ir(V) is generated in conditions of high dilution by exhaustive anodic electrolysis of $[Ir(OH_2)_6]^{3+}$ [44]. ^{17}O-NMR has been used along with UV-Vis spectrophotometry to examine the electrochemical and chemical reduction of Ir(V). Initial reduction produces a blue Ir(IV) solution which slowly transforms to a purple Ir(IV) species. This purple species then undergoes a two stage spontaneous decay into Ir(III) (Scheme 2).

It is possible that the techniques used to examine the polymerization processes of Cr(III) solutions[45,46] could also be applied to investigate such processes for Ir.

Deprotonation of the Cr(III) aqua ion leads to oligomerization (up to the hexamer have been characterized). Deprotonation facilitates the formation of oligomers in several ways: (i) by generating a hydroxide which is a better nucleophile than coordinated water, (ii) by increasing the lability of the primary coordination shell on the Cr(III) through a *trans* effect, (iii) reducing the charge on the reactants thus increasing ion-pair association constants and (iv) bringing the reactants closer together through hydrogen bond formation. Studies have shown that labilization of the coordination sphere is more important than the nucleophilicity of the incoming nucleophile. ^{17}O-NMR can be used to further characterize hydroxo bridged species and their structures can be confirmed using new assignments for the bridging groups[47,48].

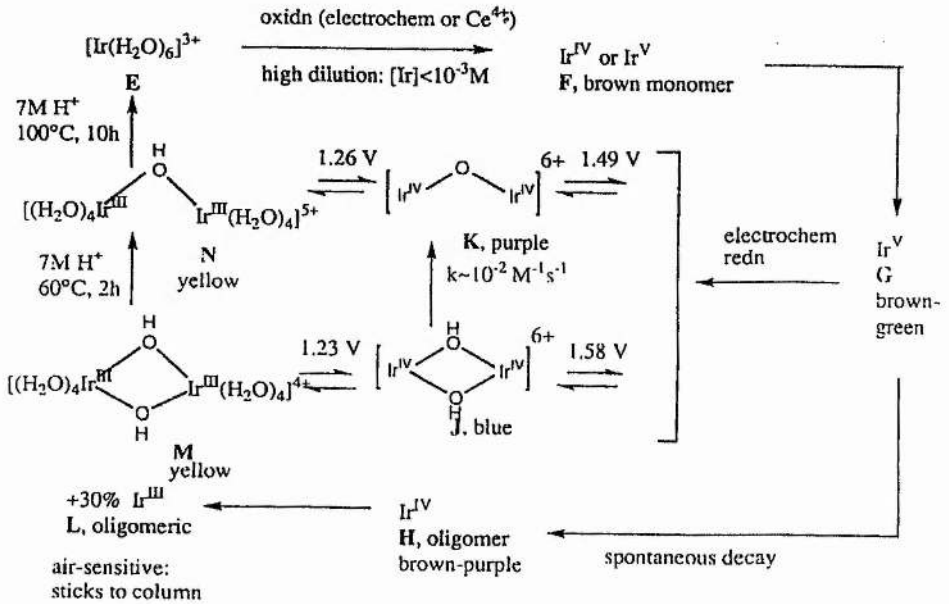

Scheme 2 Ir species in aqueous solution

The procedures used to examine the polymeric ageing process after deprotonation for Rh(III) (like Ir(III) a kinetically inert species) involve acid quenching and then the use of UV-Vis spectrophotometry or ^{17}O-NMR spectroscopy. The detection of oligomers and polymers can be used to examine the possibility of producing gels or colloids for Ir. These species will then be compared to the IrO_2 produced from other sources. Hydrated Ir_2O_3 oxides are important in understanding the electrochemistry of oxide electrodes such as $Ir(OH)_3$ which has shown electrochromic properties. The hydrolysis of $[Ir(OH_2)_6]^{3+}$ to give $[Ir(OH)_3(OH_2)_3]$ has been studied[49]. It has been postulated that the hydroxide hydrate is isomorphous with active $Cr(OH)_3(OH_2)_3$ in that the hydrolysis is reversible and the hydroxide redissolvable. The solubility of precipitated $[Ir(OH)_3(OH_2)_3]$ is low but it is possible that this compound could polymerize in the solid state[50]. Another active hydroxide of Cr is the $Cr_2(OH)_6(OH_2)_6$ dimer which has been used to form mesitylene sulphonic acid salts which have allowed crystals to be produced. An analogous Ir compound could be obtained by adding OH^- to the hydroxy bridged Ir(III) dimer.

There is evidence to suggest that aqua Ir(V) can decay spontaneously into oligomeric Ir(IV) and Ir(III) aqua hydroxo species which may be useful in triggering homogenous nucleation leading to monodisperse powders.

Non aqueous routes to IrO_2 would involve the use of phase transfer reagents to extract the above Ir salts into non aqueous media. The alkoxide route used to produce ultrafine powders of RuO_2 has also been applied to IrO_2[51] but little manipulation of the sol-gel parameters been carried out.

The trinuclear compound, iridium acetate $[Ir(III)_3(\mu_3\text{-}O)(\mu\text{-}O_2CCH_3)_6(OH_2)_3]^+$, also has potential as a sol-gel precursor. First prepared as a pyridine adduct by Uemura

et al[52], this compound was found[53] to be analogous to the iron and ruthenium acetates and has the same triply oxygen bridged core structure.

1.4 Sol-gel Processing: Hydrolysis, Condensation and the Partial Charge Model

Traditionally ceramic materials are prepared by mixing fine grained solid powders of oxides and firing at high temperature. For ruthenium and iridium oxides and this is done by the Adams method mentioned above. The problems associated with this method are well known: firstly, high temperatures are required to sinter large particles in order to facilitate diffusion across the large distances between particles; large particles lead to defects and voids which can have a deleterious affect on the properties of the final product; the correct atomic scale stoichiometry and chemical homogeneity is hard to achieve due to the relatively large particle size and, finally, it is hard to produce some metastable phases due to the high temperatures involved.

Sols, submicroscopically homogenous suspensions of solid particles in a liquid, were investigated for the first time at the beginning of the twentieth century. Lord Rayleigh[54] studied precipitation of these sols whilst Weiser and Milligan[55] worked on gelation phenomena. The first work on the relatively recent non-hydrolytic sol-gel route to metal oxide was reported by Gerrard and Kilburn in 1956[56]. It was not until after the second world war that sol-gel processing as a route to metal oxides really took off.

Sol-gel processing is the controlled hydrolysis and condensation of a soluble metal precursor to form a sol[57]. In turn the sol particles can grow and condense to form

a continuous network polymer or gel containing trapped solvent particles. The method of drying then determines the nature of the final product: the gel can either be heated to drive off the trapped solvent molecules leading to capillary pressure and a collapse of the gel network or alternatively the gel may be dried supercritically which allows solvent removal without network collapse. The final product obtained from supercritical drying is called an aerogel, that from heating is called a xerogel. Gels are not the only form for the final product obtainable, Fig. 1.7 shows the various routes to different product types available.

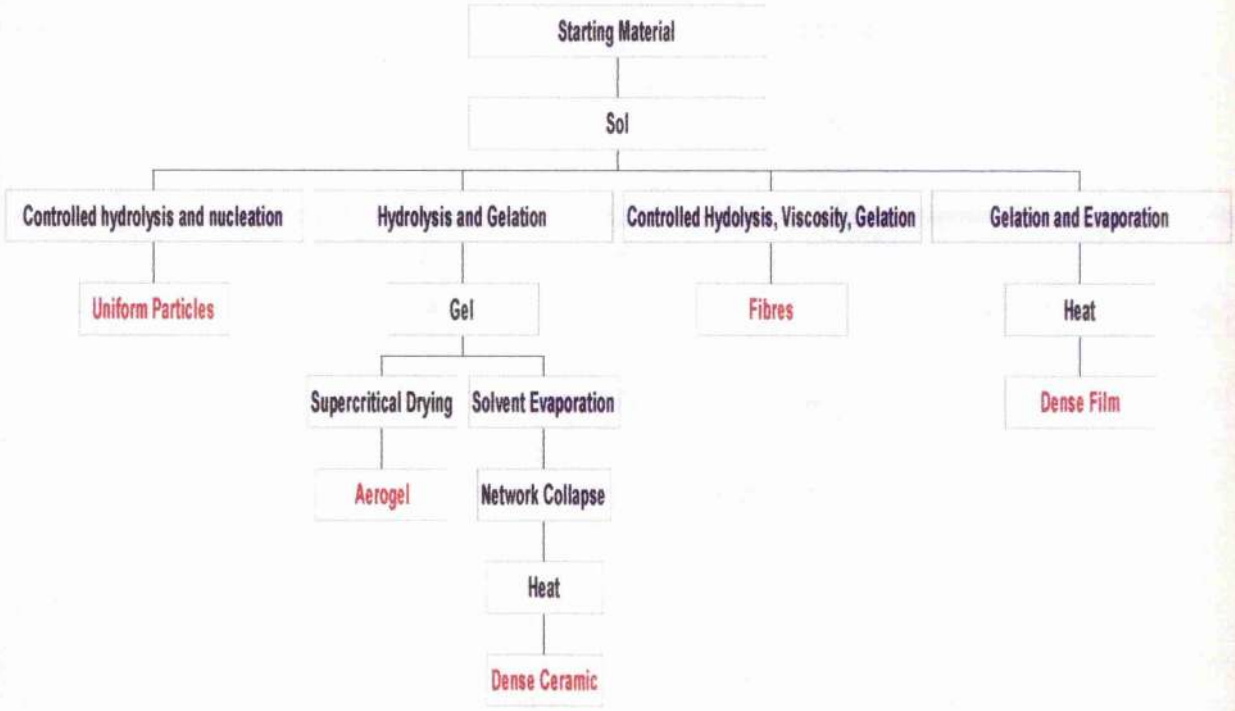

Fig. 1.7 Variation of product type under different sol-gel conditions.

Sol gel processing is divided into two general types:-

A) **The colloidal route**: the peptidization of a water soluble precursor (also known as colloidal processing)

B) **The alkoxide route**: the controlled hydrolysis and condensation of a hydrolytically unstable precursor (usually based upon a metal alkoxide species) soluble in non-aqueous solvents.

There are four principal advantages to using sol-gel processing techniques over traditional methods:-

A) Purity of the final product. As the process uses molecular precursors rather than bulk materials standard purification techniques such as distillation, sublimation, chromatography and recrystallization can be applied.

B) Greater stoichiometric control. The use of molecular precursors, sol-gel processing allows precise amounts of starting materials to be mixed together in solution with control of the exact stoichiometry and thus the desired final properties upon calcination. This aspect of the technique is particularly important for the production of complex oxides such as the materials used for high T_c superconductors.

C) Low temperature synthesis: Due to the homogeneity of the dried powder/gel product and the smaller particle size when compared to grind and

fire methods, nucleation and growth of crystalline phases can occur at lower temperatures. This also allows the synthesis of metastable phases and the inclusion of organic or other compounds with low thermal stability into the final product. Volatile materials are no longer lost and amorphous phases can be formed.

D) Control of ceramic properties through control of parameters. Variation of the reaction conditions affects product morphologies and bulk properties. Variation of pH, temperature, concentration and chemical control of the rates of hydrolysis and condensation dramatically affect the final product. The complexity of the reactions involved often precludes a complete mechanistic understanding but the use of computer simulation and mathematical models to predict the behaviour of the precursors under different conditions allows an insight into how the reaction might proceed and thus how the nature of the final product can be controlled.

1.4.1Reactions and the partial charge model

Sol-gel processing techniques have not been widely applied to the platinum group metals, however some work has been done on using base catalysed hydrolysis of ruthenium and titanium alkoxide (and also in some cases iridium) mixtures as a route to the mixed oxide of these metals. The tendency for the various precursors to hydrolyze may be predicted by the partial charge model.

The partial charge model was developed by Livage and coworkers[58] in an

attempt to explain the nature of precursors in aqueous solution. It was observed that there are three possible types of ligand bound to the metal center:-

$M\text{-}(OH_2)$	M-OH	M=O
Aqua	Hydroxo	Oxo

The number of each of these ligands attached to the metal center was found to be dependent upon both the charge on the metal and on the pH of the solution (Fig. 1.8)

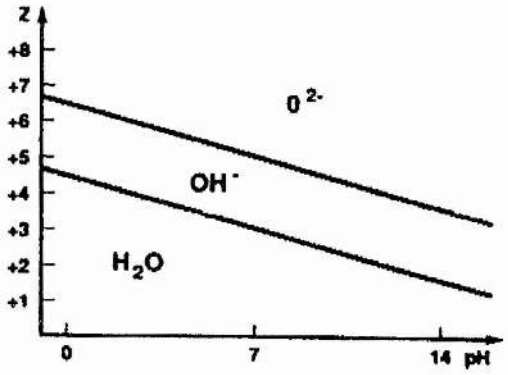

Fig. 1.8: Charge vs pH diagram indicating the "aqua", "hydroxo" and "oxo" domains.

The relative ratios of these different ligands affects the reactivity of the precursor. For example, most of the condensation mechanisms require the presence of at least one M-OH group. The partial charge model allows calculation of the partial charge distribution within a complex and thus a measure of its hydrolytic stability can

be determined.

When two atoms combine, a partial electron transfer occurs and each atom acquires either a positive or negative charge δ_i. It is usually assumed that the electronegativity of an atom changes linearly with charge

$$\chi_i = \chi_i^0 + \eta_i\delta_i \qquad (1.9)$$

where χ_i^0 is the electronegativity of the neutral atom and η_i is the "hardness" which may be defined as

$$\eta_i = k\sqrt{\chi_i^o} \qquad (1.10)$$

where k is a constant that depends on the electronegativity scale (either Pauling or Allred Rochow) being used. According to the principle of electronegativity equalization the charge transfer should stop when the electronegativities of all the constituent atoms become equal to the mean electronegativity given by

$$\chi = \frac{\Sigma_i\ p_i\sqrt{\chi_i^0} + kz}{\Sigma_i\ (p_i/\sqrt{\chi_i^0})} \qquad (1.11)$$

Where p_i corresponds to the stoichiometry of the ith atom in the compound and z is the total charge of the ionic species. Electronegativity actually corresponds to electronic chemical potential and electronegativity equalization is actually chemical potential equalization in the equilibrium state. The partial charge on each component

atom can be deduced from 1.9,1.10 and 1.11 leading to

$$\delta_i = (\bar{\chi} - \chi_i^0)/ k\sqrt{\chi_i^0} \qquad (1.12)$$

Thus the partial charge δ_i can be determined from readily available data, namely the electronegativity of all the neutral species involved, the stoichiometry of the precursor and its overall charge. This model can be applied to both aqueous and non-aqueous precursor systems. For example, the principle of electronegativity equalisation dictates that at equilibrium the electronegativity of a partially hydrolysed cation must equal that of water. Using this principle and the partial charge model Reeves[59] has been able to determine the predominant species present in aqueous Fe(III) solutions at any given pH.

1.4.2 Mechanisms

Hydrolysis of an aqueous metal precursor occurs on changing the pH of the precursor solution. Hydrolysis of an alkoxide occurs upon adding water or a water alcohol solution and a three step mechanism is usually proposed[58].This reaction is favoured when:-

i) The nucleophilic character of the entering molecule is high.

ii) The leaving group has a positive partial charge making it favourable for it to leave the positively charged metal center.

Condensation occurs by one of three mechanisms:-

i) Oxolation: reaction between two M-OH species to give an oxo bridge and water

$$M\text{-}OH + MOH \rightarrow M\text{-}OH\text{---}M\text{-}OH \rightarrow M\text{-}O\text{-}M\text{---}HOH \rightarrow M\text{-}O\text{-}M + HOH \quad (1.13)$$

ii) Alcoxolation: reaction between M-OH and an alkoxide resulting in an oxo bridge and alcohol.

$$M\text{-}OH + MOR \rightarrow M\text{-}OH\text{---}M\text{-}OR \rightarrow M\text{-}O\text{-}M\text{---}HOR \rightarrow M\text{-}O\text{-}M + ROH \quad (1.14)$$

iii) Olation: when the full coordination of the metal is not fully satisfied (when there is coordinated water or solvent) a hydroxo bridge can be formed.

$$M\text{-}OH + M\text{-}(HOR) \rightarrow M\text{-}OH\text{-}M + ROH \quad (1.15)$$

$$M\text{-}OH + M\text{-}(HOH) \rightarrow M\text{-}OH\text{-}M + HOH \quad (1.16)$$

The nature of the condensation process depends on a number of factors for metal alkoxide and colloidal sol-gel processing in different ways which will be discussed below.

1.4.3 Metal alkoxides

The alkoxo group is a hard π-donor which prefers to bind to early transition metals, and the stability of the species $M(OR)_n$ decreases from left to right across the periodic table. Electronegative alkoxide groups make the metal highly prone to nucleophilic attack.

Metal alkoxides differ from their silicon analogues in that they can increase their coordination number which leads to faster hydrolysis. Alcoxolation should be the preferred method of condensation. Partial charge studies have shown that there is a partial positive charge on coordinated alcohol molecules making them better leaving groups than coordinated water, which has a partial negative charge.

The rate of hydrolysis decreases with increasing size of the alkyl group: partial positive charge on both the metal and on the transferring hydrogen atom decreases as the size of the chain increases. Steric factors must also be taken into account as differences in the rate of hydrolysis have been observed for tertiary, secondary and primary butoxides of titanium[60] arising from the ease with which the incoming water molecule can reach the metal centre. Condensation is affected by the size of the alkyl group as is the nature of the final product (morphology, surface area, particle size and phase are all affected by the length and nature of the chain).

Often the oxidation state of the metal is less than its normal coordination number and oligomerization tends to occur via vacant d orbitals on the metal and lone pairs on the nucleophilic ligand to achieve coordinative saturation. This oligomerization is

essentially nucleophilic addition of an OR group and is called alcolation. It is possible for coordination of solvent to occur and this may become the dominant form of coordination expansion under dilute conditions and may also be the dominant form if oligomerization is sterically unfavourable. Alkoxo bridges appear more stable to hydrolysis than solvent bonds although compounds achieving coordinative saturation by solvent addition are still less reactive than coordinatively unsaturated compounds. For example gelation rather than precipitation occurs for $Zr(O^iPr)_4$ dissolved in cyclohexane rather than propanol[61] as in the latter solvent solvent addition can occur. It has also been observed that hydrolysis is faster in monomeric $Ti(O^iPr)_4$ than in oligomeric $Ti(OEt)_4$[62].

The extent of condensation for a condensed species with a given number of M-O-M links can be determined from two factors:-

$$1/n = 1/a - 1/h \qquad (1.17)$$

where n is the average degree of polymerization, a is the extent of oligomerization in the precursor and h is the hydrolysis ratio given by

$$h = [H_2O]/[M(OR)_x] \qquad (1.18)$$

For example Bradley et al[63] showed that for trimeric titanium tetraethoxide containing 4 M-O-M bonds that the experimental data obtained on adding water to the system gave a straight line with a gradient and intercept close to the values predicted

by equation 1.17.

Three main domains can be said to exist. Firstly, if h<1 condensation is governed mainly by alcolation and alkoxolation. Condensation has been shown to occur between well-defined oligomeric units for many transition metal systems with the extent of oligomerization dependent upon the hydrolysis ratio[64]. Gelation and precipitation cannot occur as long as h is well controlled. The second region 1<h<z (z being the charge on the metal atom) is where there is competition between alkoxolation and oxolation. The extent to which hydrolysis occurs is dependent upon the partial charges in the molecule. It is relatively straightforward to hydrolyse the first group but as the extent of hydrolysis increases so does the positive charge on the OR group, making proton transfer from the attacking water molecule less favorable. In the third region is where h>z it is probable that olation rather than oxolation occurs.

The relative rates of hydrolysis and condensation determine the nature of the final product (Table 1.1). A further way of controlling the hydrolysis and condensation is by adjusting the pH of the water/alcohol solution used for hydrolysis. Use of an acid catalyst allows for the protonation of the OR groups allowing the hydrolysis of all these groups, an outcome which is not generally possible in neutral conditions due to the partial charge distribution in partially hydrolysed alkoxides. The effect is to speed up the rate of hydrolysis but acid catalysis can also slow down the rate of condensation. Yoldas[65] showed that by introducing an acid concentration of at least 0.014 mol per mol alkoxide using HCl or HNO_3 precipitation of titania (caused by fast condensation of hydrolyzed $Ti(OEt)_4$) can be avoided and gels formed. A ratio of 0.075 HNO_3/Ti was used by Bartlett and Woolfrey[66] to produce titania gels from $Ti(O^iPr)_4$. The pathway for condensation is also affected with acid catalysts tending to

give linear polymers with less branching, especially if substoichiometric hydrolysis ratios are used. Base catalysis can slow down the rate of hydrolysis, because OH^- groups reduce the positive partial charge on the metal. Base can also deprotonate OH groups on the metal center favoring olation and speeding up the rate of condensation.

HYDROLYSIS RATE	**CONDENSATION RATE**	**RESULT**
SLOW	SLOW	COLLOIDS/SOLS
FAST	SLOW	POLYMERIC GELS
SLOW	FAST	CONTROLLED PRECIPITATION
FAST	FAST	COLLOIDAL GEL OR GELATINOUS PRECIPITATE

Table 1.1: Variation of product nature with relative rates of hydrolysis and condensation reproduced for Livage et al, *Prog. Solid State Chem.*, 1988, **18(4)**.

Three other parameters are important. Dilution can separate the hydrolysis and condensation reactions if high hydrolytic ratios and acid catalysts are used. It can also prevent growth by agglomeration. Solvents having a high dielectric constant can induce different pathways for hydrolysis and condensation. Finally the rates can be varied by simply varying the temperature of the reaction.

Chemical modification of the metal alkoxide precursors can dramatically affect the nature of the final product. Most additives are nucleophilic XOH molecules that react with the alkoxide to give a different molecular precursor, which will react differently with respect to hydrolysis and condensation by changing the distribution of charge. Modification decouples hydrolysis and condensation with different groups undergoing different reactions and this leads to anisotropic growth which favors gel formation. Modification can be performed in several ways. Firstly, mixed alkoxides can be made which have groups which hydrolyze and condense at different rates. Secondly, metal chloride alkoxides can also be used as gel precursors; for example, it has been shown that niobium chloroalkoxides can lead to gels for niobium whereas the pentachloro and pentaalkoxo species give powders[67]. Thirdly, stable metal alkoxo acetates can be formed by the addition of acetic acid. In general, the coordination number of the metal is increased by nucleophilic addition of the acetate group which is not immediately removed during hydrolysis or condensation. Diketones such as acetylacetone are also known to stabilize the precursor and increase gelation times for transition metal alkoxides. Finally, hydrogen peroxide has been used as a chemical modifier to give gels. Peroxide ions (O_2^{2-}) are strongly chelating and increase the coordination number of the metal. But the peroxy groups are not removed as easily as the alkoxide groups so the functionality of the precursor is reduced.

1.4.4 Metal Oxo-Alkoxides and Non-Hydrolytic Sol-Gel Processing.

1.4.4.1 Non-hydrolytic sol-gel processing

The first non-hydrolytic condensation reaction was reported in 1956[20,68]. Silica was obtained by reaction of silicon chloride and some tetraalkoxy silanes in sealed vials:-

$$SiCl_4 + Si(OR)_4 \rightarrow 2SiO_2 + 4RCl \qquad (1.19)$$

The mechanism is thought to involve coordination of the oxygen atom of an alkoxy group to silicon tetrachloride followed by nucleophilic attack of a halogen at the carbon centre of the alkoxy group resulting in a monolithic gel. The process depends on the ability of the O-R bond to split and is hence governed by the nature of the carbon group and the halide involved. Likewise condensation between metal acetates and alkoxides[69] and even metal halides by themselves, via etherolysis (equation 1.20) and non-hydrolytic condensation[70], also allows the formation of gels. Corriu et al applied these techniques to producing gels of Al_2O_3 and TiO_2 with gels times ranging from twenty hours for the former to eight days for the latter.

$$M\text{-}X + R_2O \rightarrow M\text{-}O\text{-}R + RX \qquad (1.20)$$

It is in the production of mixed metal oxides that non-hydrolytic techniques are most useful. In ordinary hydrolytic sol-gel processing of mixed metal oxides the different reactivities of the precursors involved can lead to homocondensation and thus problems in obtaining homogenous gels[69]. This problem is generally overcome by synthesizing mixed alkoxide precursors or by prehydrolysing the less reactive precursor to make it more reactive but in many cases the hydrolytic reactions are in

part reversible and homocondensation can still occur. In the case of non-hydrolytic processing the byproduct of a reaction is an alkyl halide or an ester, the nucleophilic character of which is virtually non-existent. Thus reactions are not reversible and even if they were the byproduct is often volatile enough to be removed during a reaction. Work on production of mixed oxides has not yet been widely reported as the field is relatively new but to date mixed SiO_2-ZrO_2 and SiO_2-TiO_2 and zirconium titanate gels have been synthesized[70, 71].

1.4.4.2 Metal oxo alkoxides

There is much interest in the mechanism of hydrolysis in sol gel reactions and it has long been known that hydrolysis and condensation are not the only reactions that can occur and that metal alkoxides can be converted to oxo alkoxides by a number of alternative pathways, the elimination of ether for example:

$$\text{M-OR} + \text{M-OR} \rightarrow \text{M-O-M} + R_2O \qquad (1.21)$$

Oxo-alkoxides are thus partially condensed species and represent a new class of sol gel precursors. These species are oligomeric and can be either homometallic or heterometallic. In many cases the oxo bridges produced in these compounds are multiply bridging. An alkoxide of yttrium, postulated initially as a trisisopropoxide, was found to correspond to $Y_5O(OPr^i)_{13}$ and contain μ_3-OPr^i and a μ_5-O bond with the bridging oxygen at the base of a square pyramid of 5 yttrium atoms[72]. The formation of the oxo species is thought to result from structural modification induced by removal of

Pr-^{i}OH ligands in order to achieve the most favoured coordination number of six for yttrium atoms in alkoxide species[73]. Isolation of compounds with similar multiply bridging oxygen atoms has been observed by the reaction of metals with the appropriate phenol or alcohol, with, in some cases,[74] reaction with solvent molecules producing compounds vastly different from the simple binary alkoxides expected.

As in the simple alkoxide systems, the nature of the solvent used has consequences for the final product obtained. It was found that in reactions between $Sn(O\text{-}^{t}Bu)_4$ and $Sn(OAc)_4$, as well as with Me_3SiOAc, in a refluxing hydrocarbon solvent, elimination of tert-butyl acetate occurs resulting in Sn-O-Sn and Sn-O-Si derivatives. This ester elimination is thought to arise from a mechanism similar to acid catalysed esterification with the coordinatively unsaturated tin atom acting as a Lewis acid facilitating transfer of an alkoxide group onto an acetate carbonyl carbon[75]. If a coordinating solvent such as pyridine or the parent alcohol is used the rate of ester formation is reduced dramatically and it was found that with no vacant coordination sites precursors remain monomeric with ligand exchange the only process observed.

Both homometallic and heterometallic oxo-alkoxides can be produced by partial hydrolysis of metal alkoxide precursors via dehydroxylation and dealkoxolation of metal hydroxo alkoxides. The crystal structures of a number of polynuclear titanium oxo alkoxides have been elucidated by Schmid et al[76] with these structures having evolved by the slow addition of small amounts of water to $Ti(OEt)_4$. Further to this single metal niobium, zirconium, tin and lithium along with bimetallic titanium/lithium, titanium/barium, zirconium/barium and zirconium/copper polynuclear oxo alkoxides have all been isolated and characterized[73].

Single metal and mixed metal oxo alkoxides can also be prepared by reaction

between metal halides, oxy halides and alkali metal alkoxides. In the presence of a proton accepting base, reaction of $UO_2Cl_2(Ph_3PO)_2$ in thf with K-O^{t}Bu results in $UO^2(O\text{-}^tBu)_2(Ph_3PO)_2$[77]. Likewise, reaction of $VOCl_3$ with a number of bulky and chiral alcohols such as adamantanol and norborneol ,in the presence of base to scavenge the HCl produced and thus shift the equilibrium in favour of alkoxide formation, results in the formation of stable, reduction-resistant oxovanadium alkoxides[78]. The synthesis of mixed heterometallic oxo alkoxides is generally performed by reaction of a mixed alkali metal/transition metal alkoxide and a transition metal halide. One exception to this is the mixed sodium/iron oxoalkoxide $Na_2Fe_6O(OMe)_{18}$ which is prepared by reaction of a suspension of anhydrous $FeCl_3$ in methanol with an excess of 2M NaOMe[79].

1.4.5 Sols and Gels of Metal Oxides from Aqueous Solution

The formation of gels of metal oxides from aqueous solutions is less straightforward than for metal alkoxides but the relative ease and cheapness of the process has sustained interest in these routes.

As shown earlier the nature of the metal and the pH of the solution affect the nature of the ligand bound to a metal centre and this will affect the condensation pathway. For low valent metals at low or intermediate pH the aqua ion tends to be a mixed hydroxo-aquo species with the principle method of condensation being olation. The mechanism is basically nucleophilic substitution in which M-OH is the nucleophile and H_2O the leaving group. Several types of bridges can be formed after condensation as is shown in figure 1.9.

In all cases an aquo ligand must be removed and the rate of reaction thus depends upon the charge, size, electronegativity and electronic configuration of the M-OH_2 bond.

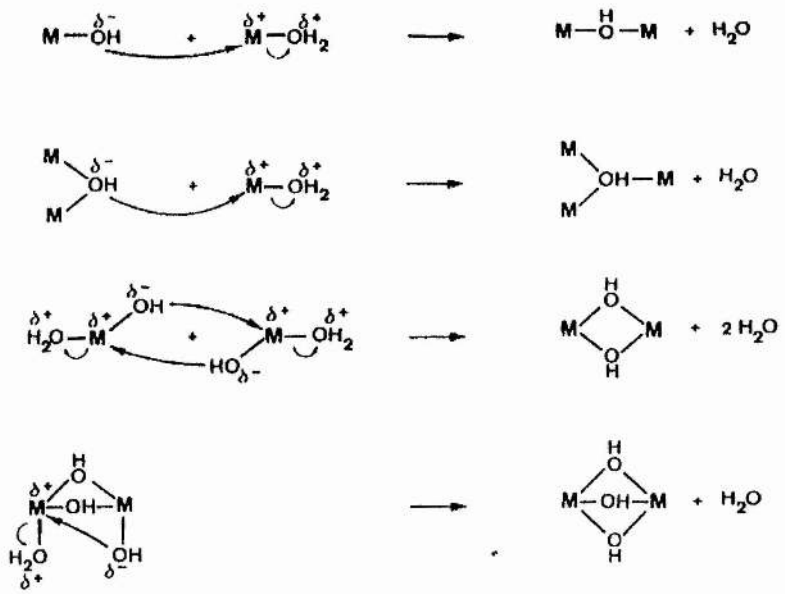

Figure 1.9: Mechanisms and types of OH bridge formation in aqueous solution, reproduced from Livage et al, *Prog. Solid State Chem.*, 1988, **18(4)**.

Oxolation occurs in aqueous solutions when there is no coordinated aquo group i.e either in higher valent metals or in solutions at higher pH. Two basic oxolation mechanisms exist. Firstly, if the metal coordination is not fully satisfied then rapid nucleophilic addition can occur in order to achieve saturation. If the metal coordination is fully satisfied a two step mechanism involving nucleophilic addition of an OH group leading to an unstable M-OH-M bond followed by β-elimination of a water molecule.

The first step in this mechanism is catalysed by base which can remove a proton from the attacking M-OH group to give a highly nucleophilic M-O$^-$ group. Conversely, the second step can be acid catalysed as OH groups bound to the unstable intermediate can be protonated facilitating the elimination of the leaving group.

It has been shown from partial charge calculations[58] that the nature of the counterion is of importance as well as the nature of the oxygen species bound to the metal centre as, at certain pH values, these counterions will become bound to the metal affecting its reactivity. The counterion can also compete for protons with the metal aqua species and thus affect whether the metal has bound aquo, hydroxo or oxo ligands. For example, it has been shown that sols of cobalt can only be produced in the presence of an acetate counterion[80].

Crystal field effects must also be considered in colloidal sol-gel processing: gels of cobalt (III), a d^6 low spin species, can be made easily from cobalt sulphate, chloride, nitrate or acetate whereas iron (III) tends to give gelatinous precipitates due to rapid olation arising from the d^5 high spin electron configuration. Gels of tetravalent metals are also hard to obtain due to rapid olation. This problem has been overcome for manganese by using reduction routes to dioxide species from $KMnO_4$, with gels of birnessite[81] ($K_{0.28}MnO_{1.96}$) and cryptomelane[82] ($K_{0.125}MnO_2(H_2O)_{0.09}$) being obtained by addition of solutions of $KMnO_4$ to concentrated solutions of glucose or sucrose and fumaric acid respectively. Extraction of potassium ions can be achieved by soaking the gels in solutions of potassium nitrate to leave gels of manganese dioxide.

For higher valent oxides such as vanadium and tungsten, the presence of solute compact polyanions can prevent condensation[83,84] with acidification via ion-exchange chromatography required to sufficiently neutralize the species involved to allow the

formation of a solid phase. Vanadium oxides produced from aqueous solutions condense via two mechanisms with the presence of bound water molecules allowing condensation by both olation and oxolation[83]. Tungsten on the other hand can only condense via oxolation as the high charge on the metal centre allows only the formation of hydroxo groups[84].

1.5 Sol-Gel Derived Ceramic Materials

The use of sol-gel processing techniques has become extremely important in the production of advanced materials. The variety and flexibility of the techniques available allows for tailoring of materials with very specific properties. For example, the production of vanadia-silica aerogels by sol-gel processing followed by supercritical drying[85] gives a high surface area material highly desired for its use as a heterogenous catalyst.

The discovery of high Tc superconductors in the late 1980s led to the need to produce homogenous pure complex metal oxide species, a need that could be met by the use of sol-gel techniques. The first sol-gel routes to YBCO (yttrium barium copper oxide involved coprecipitation[58] but more recently routes based on the hydrolysis and condensation of yttrium and barium alkoxides with copper methoxyethoxide have been developed. It is found that the hydrolysis ratio used in the production of the gel can affect the temperature of the onset of Tc and the sharpness of the transition to superconductivity[57].

Titanate materials are important as sensors, capacitors and ferroelectric materials. Ferroelectric materials have an electric dipole in the absence of a magnetic

field due to positive and negative centres of charge not coinciding. A crystal has two or more states of polarization, which can be switched between by applying an electric field. The syntheis of these materials once required the use of very high temperatures to give coarse inhomogenous materials with poor electrical properties due to impurities. Now lead titanate can be simply prepared from mixtures of lead acetate and titanium alkoxides[86] by sol-gel processing and a simple mixed alkoxide[87] of barium and titanium has been reported allowing the preparation of homogenous gels with the correct stoichiometry. Lithium niobates are also used as ferroelectric materials and are prepared from $Li(Nb(OC_2H_5)_6)$ or from niobium ethoxide and lithium nitrate[88].

There is much interest in electrochromic materials for use in smart windows mirrors or even sunglasses. Such materials are generally amorphous and low temperature routes such as sol-gel processing are cheap and effective. Vanadium and tungsten oxides are potential electrochromic materials and sol-gel routes to these materials have been extensively explored. Recently,[89] a new technique involving laser drying has been developed for tungsten oxide gels with changes in laser power densities giving different properties. Lee has produced electrochromic films of Nb_2O_5 using sol-gel techniques[90].

Sol-gel processing is an important technique for the production of catalysts. Chromium oxides gels, for example, are effective catalysts for the dehydro-cyclization of paraffin[57]. Birnessite has potential catalytic applications and has been produced cheaply by reduction of $KMnO_4$ with solutions of sucrose, gelation occuring within thirty seconds[81]. Lanthanum oxide is a good catalyst for methane coupling and can be prepared by hydrolysis and condensation of lanthanum isopropoxide[91].

1.6 Aims of Project and Thesis Summary

The overall aim of this project is to prepare and characterize gels and powders of ruthenium and iridium dioxides and any new precursors produced by sol-gel processing techniques. The possible applications of sol-gel processed RuO_2 and IrO_2 are given in Table 1.3 and the advantages of using sol-gel processing are summarised in Table 1.4.

Application	Material
Capacitors	RuO_2
Resistors	RuO_2
Metal Contacts	RuO_2
Electrode Coatings	RuO_2, IrO_2
Electrocatalytic Materials	RuO_2, IrO_2
Electrochromic films	IrO_2

Table 1.3: Possible uses of sol-gel processed RuO_2 and IrO_2.

Chapters 2 and 3 will concentrate on aqueous sol-gel routes to RuO_2 and attempts to characterize the $[Ru_4O_6^{4+}]$ aqua ion firstly by trying to grow crystals suitable for single crystal X-ray diffraction and secondly by the use of EXAFS spectroscopy. The results of attempts to produce gels of RuO_2 from the aqua ion by changing the pH of solutions are presented and discussed.

Problems with Current fabrication methods	Advantages of sol-gel Processing
Inhomogeneity in painted films and in 'grind and fire' synthesis	Molecular mixing of precursors and therefore final product
Impurities in painted films and in 'grind and fire' synthesis and in films produced by CVD	Fewer impurities due to simple precursors which can be purified before use
High Temperatures required for solid state synthesis and in calcining painted films	Low Temperature synthesis, better mixing allows lower calcination temperatures
Little control of product morphology in traditional methods	Control of precursors/drying conditions allows control of particle size and surface area

Table 1.4: Advantages of using sol-gel processing over current methods

Chapters 4 and 5 present the results of attempts to produce gels of RuO_2 and IrO_2 by mainly non-aqueous methods. The results of extensive characterization by thermal, X-ray and microscopic methods of gels obtained from different precursor systems are reported. Attempts to isolate and characterize new precursors are discussed and some

partial charge calculations for theoretical ruthenium and iridium alkoxides are presented.

Chapter 6 deals with attempts to determine the electrocatalytic properties of the gels and powders produced by studying the rates of oxygen evolution and the rate of consumption of cerium (IV) ions added to suspensions of the dried gels in perchloric acid.

1.7 References

1) V. N. Pitchkov, *Platinum Metals Rev.*, 1996, **40**, 181.

2) F. R. Hartley (Ed), *Chemistry of the platinum group metals: Recent developements*,Vol.1, Elsevier, Amsterdam, 1991, Ch. 2.

3) Z. Yuan and R. J. Puddephatt, *Chem. Mater.*, 1993, **5**, 908.; M. L. Green, M. E. Gross, L. E. Papa, K. J. Schnoes and D. Brasen, *J. Electrochem. Soc.*, 1985, **132**, 2677.

4) S. Y. Mar, C. S. Chen, Y. S. Huang and K. K. Tiong, *Appl. Surface Sci.*, 1995, **90**, 497.; A. Yoshida, Y. Watanabe, N. Yoshiike, M. Ikeda and A. Hishino, *J. Electrochem. Soc.*, 1995, **142**, 3165.

5) E. W. Tsai and K. Rajeshwar, *Electrochim. Acta*, 1991, 36(1), 27.

6) J. P. Zheng, and T. R. Jow, *Journal of Power Sources*, 1996, **6**, 155.

7) J. G. Lee, S. K. Min and S. H. Choh, *Jap. J. App. Phys P1*, 1994, **33**, 7080

8) J. P. Zheng, P. J. Cygan and T. R. Jow, *J. Electrochem. Soc.*, 1995, **142,** 2699.

9) K. I. Arshak, D. Collins and F. Ansari, *Int. J. Eelectronics*, 1994, **77**, 387.

10) M. Vukovic, D. Cukman, M. Milun, L. D. Atanasoska and R. T. Atanasoski, *J. Electroanal. Chem.*, 1992, **330**, 663

11) A. Mills, *Chem. Soc. Rev.*, 1989, **18**, 285.

12) M. Spiro and A. B. Ravno, *J. Chem Soc.*, 1965, 78.

13) S. Trasatti, *Electrochim. Acta*, 1991, **36**, 225

14) A. Mills and D. Worsley, *J. Chem. Soc. Faraday Trans.*, 1991, **87**, 3275.

15) A. Mills and M. L. Zeeman, *J. Chem. Soc., Chem. Commun.*, 1981, 948.

16) A. Mills, *J. Chem. Soc., Dalton Trans.*, 1982, 1213.

17) A. Mills, C. Lawrence and R. Enos, *J. Chem. Soc., Chem. Commun.*, 1984, 1436.

18) A. Mills, S. Giddings, and I. Patel, *J. Chem Soc., Faraday Trans. 1*, 1987, **83**, 2317

19) A. Mills, S. Giddings, I. Patel and C. Lawrence, *J. Chem. Soc., Faraday Trans. 1*, 1987, **83**, 2331.

20) A. Mills and T. Russell, *J. Chem. Soc., Faraday Trans.*, 1991, **87**, 1245.

21) K. Kameyama, S. Shohji, S. Onuoe, K. Nishimura, K. Yahikozawa and Y. Takasu, *J. Electrochem. Soc.*, 1993, **140**, 1034

22) A. Harriman, J. M. Thomas and G. R. Millward, *New J. Chem.*, 1987, **11**, 757.

23) G. W. Jang and K. Rajeshwar, *J. Electrochem. Soc.*, 1987, **134**, 1830.

24) S. Daolio, J. Kristof, C. Piccirillo, C. Pagura and A De Battisti, *J. Mater. Chem.*, 1996, **4** 567

25) R. Kotz and S. Stucki, *Electrochim. Acta*, 1986, **31**, 1311.

26) D. T. Richens, *The Chemistry of Aqua ions*, Wiley, Chichester, 1997

27) P. Werner and J. C. Hindman, *J. Am. Chem. Soc.*, 1950, **72**, 3911.

28) L. W. Niedrach and A. D. Tevebaugh, *J. Am. Chem. Soc.*, 1951, **73**, 2385.

29) D. K. Atwood and T. De Vries, *J. Am. Chem. Soc.*, 1962, **84**, 2659.

30) R. M. Wallace and R. C. Propst, *J. Am. Chem. Soc.*, 1969, **91**, 3779.

31) J. Schauwers, F. Meuris, L. Heerman and W. D'Olieslager, *Electrochim. Acta*, 1981, **26**, 1065.

32) A. Patel, Ph.D Thesis, University of Stirling, 1988.

33) D. T. Richens and A. Patel, *Inorg. Chem.*, 1991, **30**, 3789.

34) D. T. Richens, C. Helm, P. Pittet, A. E. Merbach, F. Nicolo and G. Chapuis, *Inorg. Chem.*, 1989, **28**, 1394.

35) J. M. Power, K. Evertz, L. Henling, R. Marsh, W. P. Schaefer, J. A. Labinger and J. E. Bercaw, *Inorg. Chem.*, 1990, **29**, 5058; W. Klaui, *Z. Naturforsch*, 1979, **34b**, 1403.

36) K. Wieghardt, U. Bossek and W. Gebert, *Angew. Chem. Int. Ed. Eng.*, 1983, **22**, 328.

37) E. A. Seddon and K. R. Seddon, *The Chemistry of Ruthenium*, Elsevier, Amsterdam, 1984.

38) M. Guglielmi, P. Columbo, V. Rigato, G. Battaglin, A. Boscolo-Boscoletto and A. De Battisti, *J. Electrochem Soc.*, 1992,**139**, 1655.

39) K. E. Swider, C. I. Merzbacher, P. L. Hagans and D. R. Rolison, *Chem Mater.*, 1997, **9**, 1248.

40) P. Legzdins, R. W. Mitchell, G. L. Rempel, J. D. Ruddick and G. Wilkinson, *J. Chem. Soc. A*, 1970, 3322; A. Spencer and G. Wilkinson, *J. Chem. Soc. Dalton Trans.*, 1972, 1570.

41) F. P. Dwyer and E. Gyarfas, *J. Proc. R. Soc. NSW.*, 1950, **84**, 122; P Desideri and F. Pantani, *Ric. Sci. pt 2:Ser. A.*, 1961, **1**, 265.

42) M. A. Hepworth, P. L. Robinson and G. J. Westland, *J. Chem. Soc.*, 1954, 4269; P. L. Robinson and G. J. Westland, *J. Chem. Soc.*, 1956, 4481.

43) K. Isobe, P. M. Bailey and P. M. Maitlis, *J. Chem. Soc. Chem. Commun.*, 1981, 808; T. M. Gilbert and R. G. Bergmann, *Organometallics*, 1983, **2**, 1458; K. Isobe, A. Vasquez De Miguel, A. Nutton and P. M. Maitlis, *J. Chem. Soc. Dalton Trans.*, 1984, **12**, 929.

44) S. E. Castillo-Blum, D. T. Richens and G. Sykes, *Inorg. Chem.*, 1989, **28**, 954.

45) S. J. Crimp, L. Spiccia, H. R. Krouse and T. W. Swaddle, *Inorg. Chem.*, 1994, **33**, 465 and references therein.

46) J. Springborg, *Adv. Inorg. Radiochem.*, 1988, **32**, 55.

47) R. Cervini, G. D. Fallon and L. Spiccia, *Inorg. Chem.*, 1991, **30**, 831.

48) M. C. Read, J. Glaser, M. Sandstrom and I. Toth, *Inorg. Chem.*, 1992, **31**, 4155.

49) W. Gamsjager and P. Beutler, *J. Chem. Soc. Dalton Trans.*, 1979, **7**, 1415.

50) M. Ardon, A. Bino and K. Michelson, *J. Am. Chem. Soc.*, 1987, **109**, 1986.

51) A. Osaka, T. Takatsuna and Y. Miura, *J. Non-Cryst. Solids*, 1994, **178**, 313.

52) S. Uemura, A. Spencer and G. Wilkinson, *J. Chem. Soc., Dalton Trans.*, 1973, 2565.

53) O. Almog, A. Bino and D. Garfinkel-Shweky, *Inorg. Chim. Acta*, 1993, **213**, 99.

54) Lord Rayleigh, *Philos. Mag.*, 1919, **38**, 738.

55) H. B. Weiser and W.D. Milligan, "*Advances in Colloid Science*", Ed. E. Kraemer, Interscience, New York, 1942, vol. 1, 227.

56) W. Gerrard and K. D. Kilburn, *J. Chem. Soc.*, 1956, 1536.

57) G. R. Lee and J. A. Crayston, *Adv. Mater*, 1993, **5**, 434.

58) J. Livage, M. Henry and C. Sanchez, *Prog. Solid State Chem.*, 1988, **18**,1.

59) N. Reeves, PhD Thesis, University of Bath, 1995.

60) G. Winter, *J. Oil and Colour Chemists Association*, 1953, **34**, 30.

61) D. Kundu and D. Ganguli, *J. Mater. Sci. Lett.*, 1986, **5**, 293.

62) E. A. Barringer and H. K. Bowen, *Langmuir*, 1985, **1**, 414.

63) D. C. Bradley, *Coordin. Chem. Rev.*, 1967, **2**, 299.

64) D. C. Bradley, W. Wardlaw and R. C. Mehrotra, *Metal Alkoxides*, Academic

Press, London, 1978.

65) B. D. Yoldas, *J. Mater. Sci.*, 1986, **21**, 1087.

66) *Chemical Processing of Advanced Materials*, L. L. Hench and J. K. West Eds, Wiley, New York, 1992.

67) G. Alquier, M. T. Vandenborre and M. Henry, *J. Non-Cryst. Solids*, 1986, **79**, 383.

68) R. J. P. Corriu, D. Leclercq, P. Lefevre, P. H. Mutin and A. Vioux, *J. Mater. Chem.*, 1992, **2**, 673.

69) M. Jansen and E. Guenther, *Chem. Mater*, 1995, **7**, 2110.

70) M. Andrianainarivelo, R. Corriu, D. Leclercq, P. H. Mutin and A. Vioux, *J. Mater. Chem.*, 1996, 6, 1665.

71) M. Andrianainarivelo, R. Corriu, D. Leclercq, P. H. Mutin and A. Vioux, *J. Mater. Chem.*, 1997, **7**, 279.

72) O. Poncelet, W. J. Sartain, L. G. Hubert-Pfalzgraf, K. Folting and K. G. Caulton, *Inorg. Chem.*, 1989, **28**, 263.

73) R. C. Mehrotra and A. Singh, *Chem. Soc. Rev.*, 1996, **25**, 1.

74) K. G. Caulton, M. H. Chisholm, S. R. Drake and K. Folting, *J. Chem. Soc. Chem. Commun.*, 1990, 1349.

75) J. Caruso, R. F. Schwartfeger, M. J. Hampden-Smith, A. L. Rheingold and G. Yap, *Inorg. Chem.*, 1995, **34**, 449.

76) R. Schmid, A. Mosset and J. Gady, *J. Chem. Soc. Dalton Trans.* 1991, 1999.

77) C. J. Burns, D. C. Smith, A. P. Sattelberger, and H. B. Gray, *Inorg. Chem.*, 1991, **31**, 3724.

78) D. C. Crans, H. Clem and R. A. Felty, *J. Am. Chem. Soc.*, 1992, **114**, 4543.

79) K. Hegetschweiler, H. W. Schmalle, H. M. Streit, V. Gramlich, H. Hund and I. Erni, *Inorg. Chem.*, 1992, **31**, 1299.

80) T. Sugimoto and E. Matijevic, *J. Inorg. Nucl. Chem.*, 1979, **41**, 165.

81) S, Ching, J. Landrigan, M. L. Jourgenson, N. Duan, S. L. Suib and C. O'Young, *Chem. Mater.*, 1995, **7**, 1604.

82) S. Ching, J. L. Roark, N. Duan and S. L. Suib, *Chem. Mater.*, 1997, **9**, 750.

83) J. Livage, *Solid State Ionics*, 1996, **86-88**, 935.

84) J. Livage and G. Guzman, *Solid State Ionics*, 1996, **84**, 205.

85) D. C. M. Dutoit, M. Schneider, P. Fabrizioli and A. Baiker, *Chem. Mater.*, 1996, **8**, 734

86) S. D. Ramamurthi and D. A. Payne, *J. Am. Ceram. Soc.*, 1990, **73**, 2547.

87) V. W. Day, T. A. Eberspacher, W. G. Klemperer and S. Liang, *Chem. Mater.*, 1995, **7**, 1607

88) H. C. Zeng and S. K. Tung, *Chem. Mater.*, 1996, **8**, 2667.

89) D. J. Taylor, J. P. Cronin, L. F. Allard Jr. and D. P. Birnie III, *Chem. Mater.*, 1996, **8**, 1396.

90) G. R. Lee, Ph.D Thesis, University of St. Andrews, 1992.

91) F. Ali, M. E. Smith, S. Steuernagel and H. J. Whitfield, *J. Mater. Chem.*, 1996, **6**, 261.

CHAPTER 2

Synthesis and Sol-Gel Reactions of Derivatives of the Tetrameric $Ru_4O_6^{4+}$ Aqua Ion

2.1 Introduction

The structure of the core of the tetrameric ruthenium (IV) aqua ion remains unknown despite numerous attempts to elucidate it. A number of investigations[1-3] have shown that the formula of the core is $Ru_4O_6^{4+}$ and that the structure is one of two possibilities: either an adamantanoid or a stacked dimer (Fig. 2.1).

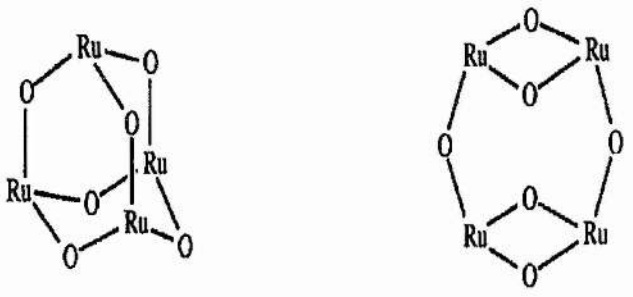

Fig. 2.1: The two possible structures for the core of the tetrameric ruthenium (IV) aqua ion, $Ru_4O_6^{4+}$ (aq). Each ruthenium atom has 3 coordinated water molecules.

Although previous attempts at obtaining a crystal structure of derivatives of the aqua ion have failed not every possibility had been tried. This chapter describes attempts to produce single crystals of the derivatives of aqua ion with a variety of new

ligands and fresh attempts to obtain crystals with ligands used previously.

$RuCl_3.nH_2O$ has been used as a sol-gel precursor in producing powders of RuO_2 by Jow and Zheng[4]. The Ru (IV) aqua ion represents a ready made sol-gel precursor in the correct +4 oxidation state and partially hydrolysed. As a result attempts to produce gels of RuO_2 by hydrolysis of this ion are also subsequently reported.

2.2 Instrumentation

UV-Visible spectra were run on a Perkin-Elmer Lambda 5 or Lambda 14 spectrophotometer using samples in 0.1 or 1.0 cm quartz cuvettes.

NMR spectra in $CDCl_3$ were run on either a Brucker AM-300 or a Varian 300 spectrometer.

Infra-red spectra were run on a Perkin-Elmer 1710 Fourier-Transform instrument and data manipulated using the Perkin-Elmer Data manager (IRDM) software for the IBM PC.

CHN analysis was carried out by the microanalysis service of the School of Chemistry, University of St. Andrews.

FAB mass spectra were recorded at the EPSRC National Mass spectrometry Service Centre at the University of Wales at Swansea.

2.3 Preparation and derivatization of the $Ru_4O_6^{4+}$ Aqua Ion

2.3.1 Preparation of solutions of the Aqua Ion

2.3.1.1 Experimental

RuO_4, $HClO_4$ and CCl_4 are all highly hazardous and the following procedure was carried out in a well ventilated fume cupboard.

The method used to prepare the $Ru_4O_6^{4+}$ aqua ion was that of Patel[1]. $RuCl_3$ (Johnson Matthey 0.5g) was added to industrial grade sodium hypochlorite NaOCl (B.D.H 200 cm^3) in a 600 cm^3 round bottomed flask and the yellow/brown solution stirred for 1 hour. Carbon tetrachloride (200 cm^3) was added to extract the green yellow RuO_4 and stirring was continued for another half hour. The mixture was separated in a large separating funnel and the aqueous layer drained and retained for further reaction. The CCl_4 layer was washed (H_2O) and after each washing a small sample was tested with silver nitrate to determine whether any residual chloride ions remained in the solution. When no precipitate due to silver chloride was observed, the solution was washed a further two times and drained into a flask containing $HClO_4$ (100cm^3) and H_2O_2 (30% w/v 3 cm^3). The mixture was rigourously stirred for one hour during which time the $HClO_4/H_2O_2$ layer became red/brown. These procedures were repeated until no more RuO_4 could be extracted into the organic layer from the hypochlorite solution.

An alternative route to RuO_4 involves oxidation of RuO_2 using sodium periodate and is found to give a better yield of the tetroxide than oxidation of the trichloride.

This method also has the advantage of containing less halide ions which react with the tetrameric aqua ion to give ruthenium oxo halides. RuO_2 is generated by refluxing $RuCl_3.nH_2O$ in NaOH for two to three hours. The RuO_2 product is filtered or centrifuged and washed with water to remove sodium chloride impurities. The RuO_2 product is then added to a solution of excess sodium periodate, $NaIO_4$, and stirred. The aqua ion is generated in the same way as for the hypochlorite oxidation by extraction into CCl_4 and reduction, by washing with $HClO_4/H_2O_2$. It is also possible to generate the aqua ion by bubbling N_2 through the reaction vessel to sweep the RuO_4 generated into a flask containing the $HClO_4/H_2O_2$ mixture. This diffusion method is found to give no better yield than the standard extraction preparation but is found to facilitate the generation of derivatives of the aqua ion which cannot be produced by either reduction with acidic H_2O_2 or by cation-exchange chromatography.

After setting aside samples of the aqua ion for attempted purification using gel filtration methods (see discussion), and after waiting long enough to ensure that any residual peroxide present had decomposed, the remainder of the $Ru_4O_6^{4+}$ solution was diluted 10 times and loaded onto a column of Dowex 50W-X2 200-400 mesh. The column was washed with 0.5M $HClO_4$ (100 cm^3) followed by 2M $HClO_4$ (100 cm^3) to remove lower charged species.

$La(ClO_4)_3$ was prepared by saturation of 2M $HClO_4$ (500cm^3) with La_2O_3 (Aldrich). The resulting solution was loaded onto a column of Dowex 50W-X8 (H^+ form) and the displaced H^+ ions titrated against 0.1M NaOH. This allowed determination of the concentration of La^{3+} and a standard solution of 0.1M La^{3+} in 0.1M $HClO_4$ was prepared. This was carefully added to the saturated 50W-X2 column onto which the aqua ion had been transferred and allowed to drip through very slowly.

Fractions of the eluted $Ru_4O_6^{4+}$ tetramer were collected and tested for the presence of La^{3+} using 0.5M sodium oxalate.

It was subsequently found that by changing the ion exchange resin to Dowex 50W-X2 50-100, mesh the aqua ion could be eluted directly with $HClO_4$ in reasonable yields rather than requiring the La^{3+} solutions. It was found that both 2M perchloric acid and 2M nitric acid could be used to elute the aqua ion from the column.

The resulting red/brown solution eluted with $HClO_4$ had a UV-Vis spectrum with the peaks at 487 and 302 nm characteristic of the $Ru_4O_6^{4+}$ aqua ion.

2.3.1.2 Discussion.of synthesis and purification of the $Ru_4O_6^{4+}$ aqua ion

Some problems were encountered when altering the conditions for the synthesis of the aqua ion. Firstly when RuO_4 is reduced in 0.1M $HClO_4$ a black precipitate of $RuO_2.nH_2O$ is produced. When 1M acid is used again a black precipitate of $RuO_2.nH_2O$ is obtained, this time so fine that it cannot be filtered or centrifuged.

When 2M $HClO_4$ solutions that are not properly free of Cl^- are used a red rather than red/brown solution is obtained with a UV-Vis spectrum characteristic of the $[Ru(OH)_2Cl_2(OH_2)_2]$ species postulated by Werner and Hindman[5]. The Cl^- arises from the $RuCl_3.nH_2O$ starting materialand possibly also from the hypochlorite. Testing for Cl^- with using $AgNO_3$ showed that 5-7 washings with water are required before the CCl_4 extracts of RuO_4 are completely chloride free.

Reducing the RuO_4 with H_2O_2 in 2M $HClO_4$ after testing with $AgNO_3$ to confirm the absence of chlorides, results in a red brown solution with a UV-Vis spectrum characteristic of the $Ru_4O_6^{4+}$ aqua ion[1]. A small amount of black $RuO_2.nH_2O$ precipitate

was produced during the washing and reduction stages.

Previously methods of purification of the $Ru_4O_6^{4+}$ ion have involved diluting the solution after the residual peroxide has been allowed to decompose and loading it onto a Dowex 50W-X2 200-400 mesh cation exchange column. Although this has the advantage of concentrating the solution, previous studies[3] showed that the ion can only be eluted from such a column using a solution of a highly charged cation such as Th^{4+} or more recently La^{3+} in the required acid. This technique is not able to remove all the $Ru_4O_6^{4+}$ ion from the column and also has the added disadvantage of contaminating much of the Ru (IV) product with displacing cation. Indeed it has proved impossible in all experiments performed to get a reasonable amount of Ru (IV) product from such column separation without some contamination from La^{3+}.

For this reason it was decided to experiment with the use of Sephadex gel filtration with loading and elution with 0.5M $HClO_4$. To this end 4 test columns of Sephadex resins were prepared (7 cm by 0.5 cm) with the following pore sizes: 10-120, LH20-100, 25-120, 25-150. In all cases a broad pink band was produced when impure solutions of the tetramer in $HClO_4$ diluted to 0.5M were loaded onto the column. Elution occurred very quickly as indicated by pink band moving extremely rapidly down the column. Although some separation did seem to be occurring with the finer gels, it proved impossible to collect fractions containing separate components. It was therefore decided to return to the use of Dowex cation exchange chromatography to purify the final $Ru_4O_6^{4+}$ solutions.

A number of different Dowex 50W resins were investigated. Eventually it was discovered that if a more coarse mesh type of Dowex 50W resin was used i.e a 20-100 mesh then elution of $Ru_4O_6^{4+}$ could be performed directly using 2M or even 1M $HClO_4$

without the need for elution with a highly charged cation. The results suggest that the inability of acid to remove the aqua ion from the finer 200-400 μm resin may be linked to hydrolytic polymerization of the ion as a result of the closer proximity of the tetramer units on the resin. The formation of these species can be thought of as a first step in the hydrolytic polymerization of the aqua ion to RuO_2 and must be accompanied by a degree of protonation. This protonation must be reversible at higher pH ($\geq$ 1), to explain elution by cation displacement, but not by strong acid, from the fine mesh resin beads. Within the coarser mesh size resin it is thought that the individual $Ru_4O_6^{4+}$ units are more dispersed and thus that condensation is less favourable and allowing direct elution with acid giving reasonable concentrations of up to 10 mM.

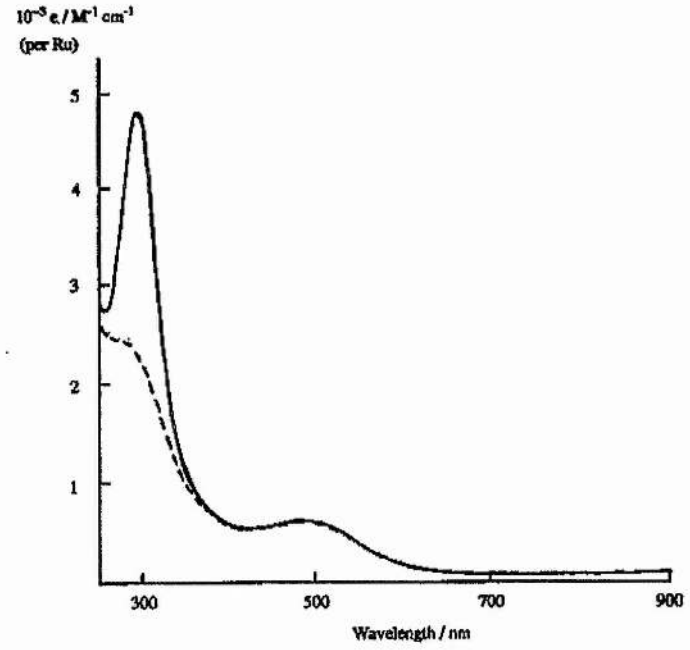

Fig. 2.2 UV-Vis spectrum of the tetrameric $Ru_4O_6^{4+}$ aqua ion in 2M nitric acid.

An interesting feature was noticed when examination of the UV-Vis spectrum of the aqua ion eluted with 2M nitric acid (Fig 2.2) was performed. An intense UV absorption maximum is apparent at 330 nm (ε = 4910 M^{-1} cm^{-1}) which is absent in $HClO_4$ solutions and indicative of strong ion pair or inner sphere coordination of nitrate ions to the tetrameric cation. Partial charge calculations[6] and experimental observations have shown that coordination of highly electronegative anions such as nitrate can occur under highly acidic conditions and it would seem that this is what is occuring with the Ru(IV) aqua ion, although it would appear that the conditions are not acidic enough to allow coordination of perchlorate.

2.3.2 Attempted Preparation of a Tosylate (pts) salt of the $Ru_4O_6^{4+}$(aq) Aqua Ion

Single crystals of p-toluenesulphonate salts of a number of oligomeric aqua ions have been isolated at low temperature (-30 °C) from frozen Hpts solutions and structurally characterised. One such example is the triangular species $[Mo_3O_4(OH_2)_9](pts)_4.13H_2O$[7]. It was for this reason that samples of $Ru_4O_6^{4+}$ (aq) were eluted from a Dowex 50W X2 50-100 mesh column with 2M Hpts and subjected to crystallization at -30 °C.

2.3.2.1 Experimental

$RuCl_3$ (Johnson Matthey 2g) was converted to the $Ru_4O_6^{4+}$ aqua ion in 2M

$HClO_4$ following the method described above in section 2.3.1.1.

100cm^3 of the $Ru_4O_6^{4+}$ (aq) solution of the aqua ion were loaded onto a Dowex 50W-X2 50-100 mesh column (H^+ form) and lower charged species were removed using 0.5M p-toluene sulphonic acid (Hpts) (100cm^3) followed by 1.0M Hpts. Elution of the tetramer was carried out using a solution of 0.25M La^{3+} in 1M Hpts (standardized as for $La(ClO_4)_3$ above) and eluted fractions were tested for the presence of La^{3+} using 0.5M sodium oxalate. In subsequent experiments it was found that elution from the column could be performed using 2M Hpts.

Upon addition of La^{3+} a deep red brown solution eluted off the column. La^{3+} free samples were kept separate from those that were contaminated and the pure solutions evaporated and dried under vacuum. Characterization was performed using UV-Visible spectrophotometry (λ_{max} at 478 and 327 nm) and attempts were made to recrystallize the product from a number of different solvents.

2.3.2.2 Results and Discussion

Cooling to –30 °C or slow evaporation failed to yield crystals so extraction of the residue (after evaporation to dryness) was tried using a number of solvents. The use of ethanol or acetone led to the extraction of a red solution leaving behind a white residue. The UV-Vis spectrum of the acetone solution showed similarities to that of the aqua ion with a band at around 487 nm.

After 6 days of slow evaporation pale pink/white crystals were precipitated from the acetone solutions containing $Ru_4O_6^{4+}$. These were dried under vacuum and the presence of $Ru_4O_6^{4+}$confirmed by UV-Vis spectrophotometry. CHN values gave C

37.74%, H 3.89% N 0% (the expected values for $Ru_4O_6(H_2O)_{12}(pts)_4$ are C 24.00%, H 3.71% N 0%) which suggests the presence of Hpts (soluble in acetone) in the crystals as the data can be fitted for 9 molecules of Hpts for every molecule of a tosyl salt containing no coordinated water i.e. $Ru_4O_6(pts)_4(Hpts)_9$.(Anal Calcd C 37.6, H 3.61, N 0) Due to the Hpts contamination these crystals were unsuitable for further examination

2.3.3 Attempted Preparation of a Complex of $Ru_4O_6^{4+}$ with Tris(3,5-Dimethylpyrazolyl)Borate (2)

Tris (1-pyrazolyl)borate (Fig 2.3) is an attractive tripodal coordinating ligand at the three facially coordinating sites on the $Ru_4O_6^{4+}$ core. It has previously been shown to react with the $Ru_4O_6^{4+}$ aqua ion in nitric acid, produced by eluting the tetramer from the column with lanthanum nitrate, to give a purple powder[3]. FAB mass spectrometry has shown that $Ru_4O_6^{4+}$ units were present in the isolated complex. Since the 3,5-dimethyl derivative was available and has been shown to give crystalline derivatives in other cases wherein the unsubstituted ligand has not, a complexation experiment was performed using this ligand.

2.3.3.1 Experimental

A solution of the $Ru_4O_6^{4+}$ aqua ion was prepared as before in 2M $HClO_4$ but in this instance the ion was eluted off the column with a 0.2M solution of lanthanum nitrate. This gave a solution at around pH 1. Further neutralization was performed with

$NaHCO_3$ to raise the pH to 2. A 1:1 stoichiometric amount per Ru atom of solid tris(3,5-dimethylpyrazolyl)borate ($K[HB(Me_2pz)_3]^3$) was slowly added and the pH adjusted back to within the range 2-2.5 after each addition. The resultant deep red solution was left to evaporate slowly.

2.3.3.2 Results and Discussion

The expected purple precipitate was not obtained, however, suggesting that the ligand was not coordinating. This may be a result of steric factors, due to the presence of the methyl groups on the aromatic rings making coordination unfavorable.

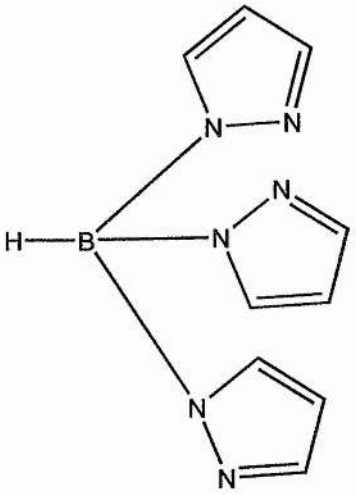

Fig. 2.3 Basic structure of tris (1-Pyrazolyl)borate

2.3.4 Attempted Preparation of a Complex of $Ru_4O_6^{4+}$ Ion with Methyliminodiacetate (MIDA) (3)

2.3.4.1 Experimental

A solution of the $Ru_4O_6^{4+}$ aqua ion in 2M $HClO_4$ was prepared as before and loaded onto a column of Dowex 50W-X2 ion exchange resin. The column was then soaked in 0.2M MIDA for two hours before elution with more 0.2M MIDA. A deep red solution was obtained and this was allowed to evaporate in the presence of tetramethylammonium tetrafluoroborate (Me_4NBF_4:Ru ratio of 1:1) in the hope that a suitable crystalline salt for X-ray analysis could be obtained. A sample of the $Ru_4O_6^{4+}$ MIDA complex was also left on the column to investigate whether colour (and thus coordination) changes would occur over time, as has been observed previously[1]. Recrystallization was also attempted by slow diffusion of methanol into a portion of the $Ru_4O_6^{4+}$-MIDA solution.

Crystals obtained from this synthesis were washed with water and dried under a vacuum. The product was then characterized by UV-Visible spectrophotometry and microanalysis.

2.3.4.2 Results and Discussion

The UV-Visible spectrum of the complex contained bands corresponding to the $Ru_4O_6^{4+}$ ion at 487 nm. Crystals of this derivative were obtained via both slow evaporation and diffusion of methanol into an aqueous solution of the derivative. Microanalysis of the red crystals obtained by diffusion gave values of C 31.99%, H 7.17% and N 8.41%. The carbon value suggest that the compound is more than the simple $Ru_4O_6(MIDA)_2$ complex and the ratio of C:N suggests that there is some Me_4N present. The best fit for these is $(Me_4N)_4H_4Ru_4O_6(MIDA)_6$ (C 33.05%, H 5.63%, N

8.38%). The IR spectrum confirms the spectrum of MIDA in the crystals but peaks that may indicate the presence of Me_4N are obscured. The crystals obtained from slow evaporation are colorless, however, which may indicate a different product.

2.3.5 Attempted Preparation of a Complex of the $Ru_4O_6^{4+}$ Ion with Triazacyclononane (TACN) (5)

The cyclic amine1,4,7,-triazacyclononane has been shown to give rise to a $Mn_4O_6^{4+}$ complex having an adamantanoid arrangement[8]. Thus it was decided to attempt to prepare a derivative of $Ru_4O_6^{4+}$ using this ligand. Because of the nature of the tacn ligand which is likely to protonate in aqueous solution at the pH values at which the $Ru_4O_6^{4+}$ is stable, reaction of the tacn was carried out on a sample of the tosylate salt in ethanol.

2.3.5.1 Experimental

The tosylate salt of the $Ru_4O_6^{4+}$ (aq) ion was prepared as previously described in section 2.4.2 and dried under vacuum.

At low values of pH triazacyclononane will protonate raising the pH. As a consequence of this it is impossible to use tacn at pH levels at which the $Ru_4O_6^{4+}$ aqua ion is stable in solution. Thus it was decided to dissolve the tosylate salt in ethanol in order to carry out the complexation reaction.

A sample of the tosylate salt (0.2 mmol) of the Ru (IV) aqua ion was dissolved in anhydrous ethanol (50 cm^3) (pure ethanol was used to prevent dissolution of as little

of the lanthanum tosylate impurity present as possible) and triazacyclononane (prepared by T Clifford, 0.32g 0.2 mmol) was added. The resulting brown solution was stirred for two hours before being left to evaporate slowly.

The final product was characterized using UV-Vis spectrophotometry and ^{1}H-NMR spectroscopy.

2.3.5.2 Results and Discussion

When the tosylate salt was dissolved in ethanol prior to adding tacn it was noticed that a copious amount of white precipitate (probably a lanthanum tosylate species) was left. On evaporation of the red ethanol solution and redissolution in water the peaks in the UV-Vis spectrum shifted to 341.6 and 472.0 nm different to those expected (302 and 487 nm) and upon evaporation prior to adding tacn, a brown precipitate (compound **4**), rather than the red one observed on evaporating the aqueous tosylate salt to dryness, was obtained. Thus it was postulated that the tosyl derivative was reacting with the ethanol to give an ethoxide, which may then hydrolyze to a hydroxide. Alternatively, ethanol may be coordinating to the tetrameric ion.

When the tacn derivative of $Ru_4O_6^{4+}$ (compound **5**) was evaporated down a brown precipitate, this time also containing a lighter precipitate, was obtained, similar to that of the starting material. The UV-Vis spectrum of the tacn derivative was almost exactly that of the solution of the tosyl derivative in ethanol. For the expected product, $Ru_4O_6(tacn)_4(pts)_4$ the theoretical CHN values are C 36.71%, H 5.18%, N 9.88%. Microanalysis gave the results C 44.00%, H 5.21%, N 0% thus revealing that the attempted derivative complex contained no nitrogen and thus could not have any tacn

coordinated. This was checked using ^{1}H-NMR on solutions in $CDCl_3$ of the $Ru_4O_6^{4+}$

Compound **4**

PEAK/ppm	RELATIVE INTENSITY	TYPE
1.2	7.5	overlapping peaks
2.2	6.67	singlet
2.4	8.33	singlet
3.8	3.58	broad singlet
4.1	1	quartet
7.2,7.75	7.92	AB quartet
10.2	6.67	broad

Compound **5**

PEAK/ppm	RELATIVE INTENSITY	TYPE
1.2	3.25	triplet
2.2	5.31	singlet
2.4	1	singlet
3.6	2.62	broad singlet
3.8	2.62	quartet
7.2	3.19	singlet
7.2,7.7	1	AB quartet

Table 2.1: ^{1}H-NMR data for new $Ru_4O_6^{4+}$ derivatives in $CDCl_3$.

tosyl salt after evaporation of an ethanolic solution and the attempted tacn derivative (Table 2.1) and comparing the results to those for other metal alkoxide species and p-toluene sulphonic acid from the Aldrich library[9].

Peaks at 2.2 ppm in both cases correspond to an acetone impurity and can be ignored as can the single peak at 7.2 ppm in the spectrum of compound **5** which corresponds to $CHCl_3$. The peak at 1.2 ppm in the spectrum of compound **4** corresponds to the methyl groups in the ethanol. The peak is also a simple triplet in the spectrum of compound **5.** The peaks in both spectra at about 2.4 ppm correspond to the methyl group in the tosyl group and the AB quartets correspond to the benzene ring protons. As ruthenium is in the +4 state the spectrum of $Ge(OEt)_4$ was examined and found to contain a quartet at 3.9 ppm and a triplet at 1.3 ppm which correlates with the values obtained from the spectra of both the derivatives above. The peaks at 3.8 ppm in both spectra are also shifted downfield slightly from those of free ethanol suggesting coordination is occurring. Further to this the shape of the peak is found to be very similar to the shape of a peak in that region of the ^{1}H-NMR spectrum of $Nb(OEt)_5$. Were there to be coordinated tacn a peak corresponding to the proton bound to the nitrogen atom at 7.4 ppm and a singlet corresponding to the methylene protons at 2.8 ppm on the tacn molecule would be expected to be observed in the spectrum of compound **5**, in addition to the peaks seen for the tosyl derivative. It is noticable that the size of the tosyl group peaks is smaller relative to the ethanol/ethoxide peaks which suggests that tosyl groups are being removed from the $Ru_4O_6^{4+}$ ion. An ethoxide derivative might however be expected to hydrolyse. Nevertheless there is likely to be only one ethoxide group bound to each ruthenium to balance the charge which may lead to there being a positive partial charge on the ethoxide group making hydrolysis harder. The IR spectrum of the tacn derivative confirms the NMR results as there is clear evidence from this spectrum that tosyl species are present. The IR spectrum also confirms the absence of coordinated tacn. No peaks are seen corresponding to ethoxide

but it is possible that these are hidden by other peaks.

The NMR spectra clearly shows that tacn did not react and is not present in compound 5. It is possible that this derivative if it turns out to be an ethoxide, may have some application as a sol-gel precursor for the production of RuO_2, certainly the fact the $Ru_4O_6^{4+}$ derivatives are soluble in organic solvents open up new sol-gel possibilities. However the spectra obtained contain large numbers of unassigned peaks and no firm conclusion can be drawn.

2.3.6 Attempted Preparation of a Complex of the $Ru_4O_6^{4+}$ Aqua Ion with the Anionic Tripod Ligand $^5\eta$-cyclopentadienyltris(diethylphosphito)cobalt (L_{OEt}) (6)

2.3.6.1 Experimental

A solution of the $Ru_4O_6^{4+}$ aqua ion in nitric acid was prepared and purified as described in section 2.3.1. The solution was concentrated to 0.015 M by rotary evaporation and the pH was raised to 1 by addition of solid $NaHCO_3$ (Aldrich). To $20cm^3$ of this solution was added 0.16g (0.29 mmol) of NaL_{OEt}[10] to give a ratio of ruthenium to L_{OEt} of 1:1. The solution was stirred overnight and shortly after addition of the ligand a red/purple precipitate was observed and the solution turned yellow. The precipitate was filtered, washed with cold distilled water (2 x $5cm^3$) and dried under vacuum.

The final product was analysed by ^{1}H-NMR ($CDCl_3$): δ 5.35 (s, H_2O), 5.10 (s C_5H_5), 4.9 (m OCH_2CH_3), 1.8 (s), 1.2 (m OCH_2CH_3). The sample was also analysed by UV-Vis spectrophotometry (λmax 487 and 332 nm), FAB mass spectrometry (discussed below) and microanalysis: Anal Calcd. (for 4 L_{OEt} ligands complexing the aqua ion) C,

30.91; H, 5.30; N, 0. Found C, 23.83; H, 4.55, N, 2.36.

2.3.6.2 Results and Discussion

The anionic tripod ligand NaL_{OEt}, where L_{OEt} is $[CpCo\{(EtO)_2P=O\}_3]^-$ has been shown to form a ruthenium di-μ-oxo bridged dimer complex[10] (Fig 2.4).

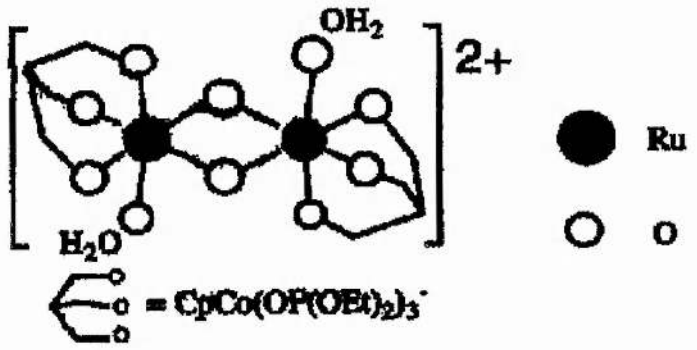

Fig 2.4 The μ-oxo bridged ruthenium (IV) dimer containing the ligand L_{OEt} reported by Power et al.

The red/purple compound was insoluble in water but soluble in ethanol. The UV-Vis spectrum of this derivative is found to contain the band at 487 nm characteristic of the tetramer and there is no evidence of a peak at 632 nm suggesting that none of the dimeric ruthenium species obtained by Power et al[10] (Fig. 2.5) has been formed.

The ^{1}H-NMR spectrum of the compound shows shifts downfield from the peaks of the free ligand suggesting that the ligand is coordinated to the aqua ion although the spectrum obtained was not very clear. However, the solution from which the derivative

was isolated retains yellow colour of the ligand and microanalysis of the compound revealed that nitrogen is present in the sample.

Further to this the FAB mass spectrum suggests that less than 1 ligand per ruthenium is coordinating to the core (Fig 2.5). The highest value found for a cluster is m/z = 2382 rather than at the expected value of 2640 for a derivative of the aqua ion containing 4 L_{OEt} ligands. Other clusters are found at m/z = 2363,2197 and 2116. The peak at 2382 could, however correspond to a species containing 3 L_{OEt} ligands, $[Ru_4O_6(H_2O)_{12}]$ $(L_{OEt})_3NO_3$, which are acting as counterions (although the calculated CHN values for this compound do not fit the values found: C 25.69; H, 5.41; N, 0.54). It seems likely then, that steric hindrance is preventing full coordination of the ligand. It would also seem likely that nitrate coordination is occuring to give the precipitate and that it is this process that is responsible for the nitrogen found in the microanalysis of the sample.

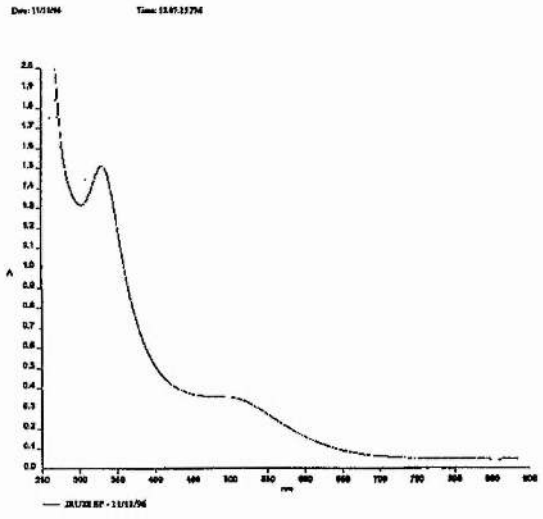

Fig. 2.5 UV-Vis spectrum of the complex of the $Ru_4O_6^{4+}$ aqua ion with the Anionic tripod ligand $^5\eta$-cyclopentadienyltris(diethylphosphito)cobalt (L_{OEt}).

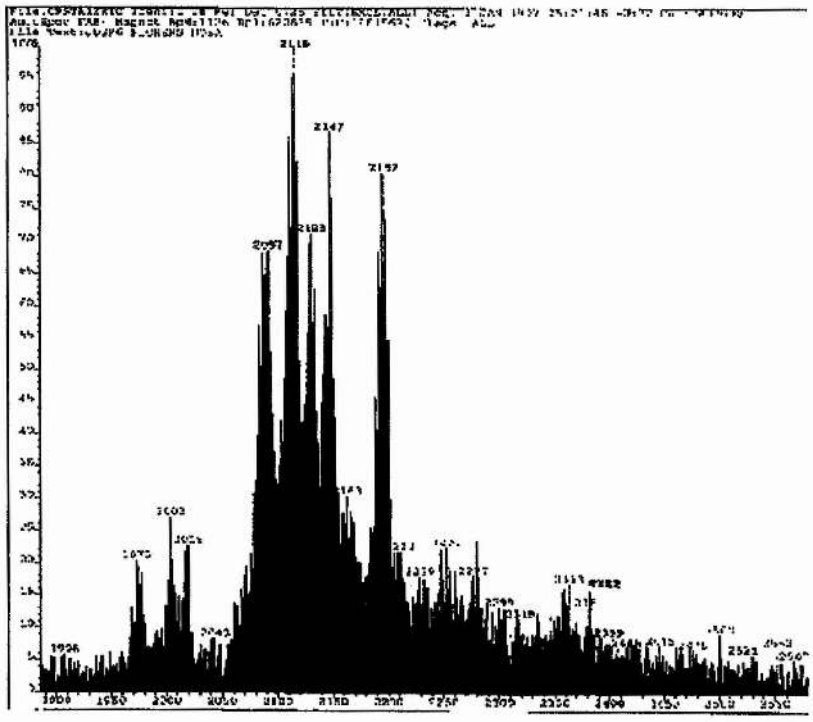

Fig 2.6: Part of the FAB mass spectrum of the L_{OEt} derivative of the Ru (IV) aqua ion produced from aqueous acidic solution.

Like the other derivatives of the aqua ion that were prepared, however, attempts to recrystallize this compound from a number of solvents did not result in a crystal suitable for single crystal X-ray diffraction.

2.3.7 Attempted Preparation of an Acetate complex of the $Ru_4O_6^{4+}$ Aqua ion(7)

The dimeric ruthenium compound $[Ru_2O_6(py)_4].3.5H_2O$ has been prepared by diffusion of RuO_4 into a solution containing the ligand[11]. It was thought that, as the $Ru_4O_6^{4+}$ aqua ion could not be eluted from a Dowex column using acetic acid, an

acetate derivative might be obtained by this method.

2.3.7.1 Experimental

RuO_2 (Johnson Matthey, 0.75g, 5.5 mmol) was placed in a flask containing $20cm^3$ of distilled water and 2.5g (11.7 mmol) of $NaIO_4$. The RuO_4 produced was flushed with nitrogen into a flask containing $15cm^3$ of 4M acetic acid and $9cm^3$ of H_2O_2. The experiment was continued for 5 hours. The solution goes green on initial addition of RuO_4 and a black powder precipitates after approximately one hour.

2.3.7.2 Results and Discussion

On sweeping a RuO_4 into a 4M solution of acetic acid a green colour is initially observed. This, however, rapidly converts to a black colloid as more RuO_4 is swept in. These results suggest that the acetic acid is not strong enough to allow stable derivatives of the aqua ion to be formed and that RuO_2 is being produced through hydrolytic polymerization. Although this procedure has not yielded the desired complex it might have applications as a route to RuO_2.

2.4 Sol-gel processing of RuO_2 using the $Ru_4O_6^{4+}$ aqua ion

2.4.1 Experimental

100 cm^3 of a 0.016M solution of the $Ru_4O_6^{4+}$ aqua ion in $HClO_4$ were placed in a

beaker. 114.6 cm^3 of 1M aqueous NaOH was added dropwise until the pH of the solution reached 4.5 after which the solution was left overnight to see whether gelation would occur. The experiment was repeated using $NaHCO_3$ as the base and also using solutions of the aqua ion in nitric acid.

2.4.2 Results and Discussion

The pH of solutions of the $Ru_4O_6^{4+}$ aqua ion in perchloric or nitric acid was raised by slowly adding sodium hydroxide or sodium hydrogen carbonate. When the pH is raised to 4 the solution turns brown and there is some evidence of precipitation of small black particles. Addition of more NaOH is accompanied by a rapid rise in pH to around 5. After leaving the solution for two days to allow it time to gel the pH dropped from 4 to 3.73 and it is found that the sample did not gel.

There are several possible reasons for why precipitation rather than gelation is occuring in this system. Partial charge calculations performed using the method of both Livage[6] and Reeves[12] indicate that at pH 4 the aqua ion precursor is a mixed hydroxo-aquo species. It has been suggested[6] that sols of a number of tetravalent metal oxide sols condense via rapid olation and that as a consequence gels are difficult to obtain and it would seem sensible to assume that ruthenium is no different. Further to this the samples undergoing hydrolysis and condensation are dilute (of the order of tens of mM even after concentration of samples) and that formation of a gel network at these concentrations is not possible. Finally it is possible, especially in the case of condensed solutions of the aqua ion in perchloric acid, that the counterion is inappropriate for gel formation: if a less electronegative counterion were used this

might coordinate to the metal changing the nature of the precursor and allow gel formation.

2.5 Conclusions

The Ru(IV) aqua ion has been prepared, characterized and derivatized with a number of different ligands although none have produced crystals of suitable quality for analysis by single crystal X-ray diffraction. It is clear that another means of determining the structure of the core is needed as will be reported in chapter 3.

The attempts to obtain crystals have not been totally unsuccessful, however. It was previously thought that La^{3+} salts were necessary to remove the aqua ion from a Dowex ion exchange column. In the course of this work three alternative ways to elution by ionic displacement have been developed. The first, confirming the initial work of Patel, involves soaking the purification column with a solution of a ligand designed to reduce the overall charge on the atom, in this case using MIDA. There is also evidence that dissolution of the tosyl derivative of the aqua ion in an organic solvent might remove lanthanum impurities. However, these techniques were not developed further as by far the most successful of the new elution methods was simply to change the ion exchange resin used to purify the solutions. By changing to a coarse mesh resin hydrolytic condensation within the beads as a result of the close proximity of the $Ru_4O_6^{4+}$ units is prevented allowing direct elution with solutions of a number of 2M acids and, in the case of the aqua ion in nitric acid, there is also some evidence of ion pair formation as shown by UV-Vis spectrophotometry.

Attempts at producing RuO_2 by controlled hydrolysis and condensation of the

Ru (IV) aqua ion with different bases has been unsuccessful in as much as gels were not obtained. The product is a powder in all cases, this probably arising due to rapid condensation of the precursor by olation or as a consequence of the low concentration of the sample. RuO_2 has been produced, however, and further manipulation of the experimental conditions might allow gel formation and the powder product already obtained might find uses.

2.6 References

1) A. Patel and D. T. Richens, *Inorg. Chem.*, 1991, **30**, 3789.

2) R. M. Wallace and R. C. Propst, *J. Am Chem. Soc.*, 1969, **91**, 3779.

3) A.Patel, PhD Thesis, University of Stirling, 1988.

4) J. P. Zheng and T. R. Jow, *J. Electrochem. Soc.*, 1995, **142**, L6

5) P. Werner and J. C. Hindmann, *J. Phys. Chem.*, 1952, **56**, 10.

6) J. Livage, M. Henry and C. Sanchez, *Prog. Solid State Chem.*, 1988, **18(4)**, 1. And references therein

7) D. T. Richens, C. Helm, P. Pittet, A. E. Merbach, F. Nicolo and G. Chapuis, *Inorg. Chem.*, 1989, **28**, 1394.

8) K. Wieghardt, U. Bossek and W. Gebert, Angew. Chem. Int. Ed. Eng., 1983, **22**, 328.

9) The Aldrich Library Of ^{13}C And ^{1}H FT NMR Spectra, The Aldrich Chemical Company, 1993.

10) J. M. Power, K. Evertz, L. Henling, R. Marsh, W. P. Schaefer, J. A. Labinger and J. E. Bercaw, Inorg. Chem., 1990, **29**, 5058; W. Klaui, Z. Natorforsch, 1979, **34b**, 1403.

11) A. C. Dengel, A. M. El-Hendawy, W. P. Griffith, C. A. O'Mahoney and D. J. Williams, J. Chem. Soc. Dalton Trans., 1990, 737.

12) N. Reeves, PhD Thesis, University of Bath, 1995.

CHAPTER 3

The Tetrameric Ruthenium (IV) Aqua Ion $Ru_4O_6^{4+}{}_{(aq)}$: Probing Its Structure in Solution Using Extended X-Ray Absorption Fine Structure (EXAFS) Spectroscopy

3.1 Introduction

Repeated attempts to obtain suitable crystals of the $Ru_4O_6^{4+}(aq)$ cation or of a suitable derivative complex for single crystal X-ray analysis have thus far resulted in failure.

Attention was turned therefore to other probes which could shed light on the structure of this tetrameric cation. Previous studies[1] indicated one of two structures for the $Ru_4O_6^{4+}$ core, adamantanoid or stacked dimer (Scheme 1 on page 10) and ,since this species is relatively simple in terms of the nature of the backscattering atoms, it was viewed as an excellent candidate for structural study in solution using extended X-ray absorption fine structure spectroscopy (EXAFS) at the ruthenium K edge. This technique has already been shown to be useful in determining local structure around aqueous molybdenum aqua cluster ions[2]. A number of polynuclear oxo-bridged model complexes as both solids and solution species were also examined in the hope of yielding further structural information on the nature of the aqueous tetrameric cation. This study contributes the first detailed K edge EXAFS study on a range of oxo-bridged ruthenium species and has yielded definitive structural results on the tetrameric cation for the first time and it is these results that will be reported in this

chapter.

3.1.1 X-Ray Absorption Spectroscopy (XAS)

X-ray absorption spectroscopy is a powerful probe for determining local structure[3]. The technique is based upon the process by which an atom can absorb an X-ray of a particular energy and a photoelectron is ejected from the metal core with an energy equal to that of the photoelectron, minus the energy required to eject it (eq. 3.1)

$$E_f = h\nu - E_b \qquad (3.1)$$

Where E_f is the energy of the ejected photoelectron, $h\nu$ is the energy of the incident X-ray and E_b is the binding energy. The structural information is then derived from the interaction between the photoelectron wave and the atoms surrounding the absorbing atom. The absorption edges for each element are at different frequencies and as these X-rays are only absorbed over a narrow range the technique is element specific.

The X-ray absorption spectrum can be split up into 3 regions: pre-edge, XANES and EXAFS (Fig 3.1). The pre-edge spectrum, as the name implies, concerns events occurring at frequencies just before the absorption edge (2-10 eV). This feature arises from localized transitions involving atomic or molecular orbital energy levels and are determined in part by the symmetry of the ligands surrounding the absorber. If a pre-edge structure is observed in a spectrum it can give information on the oxidation state

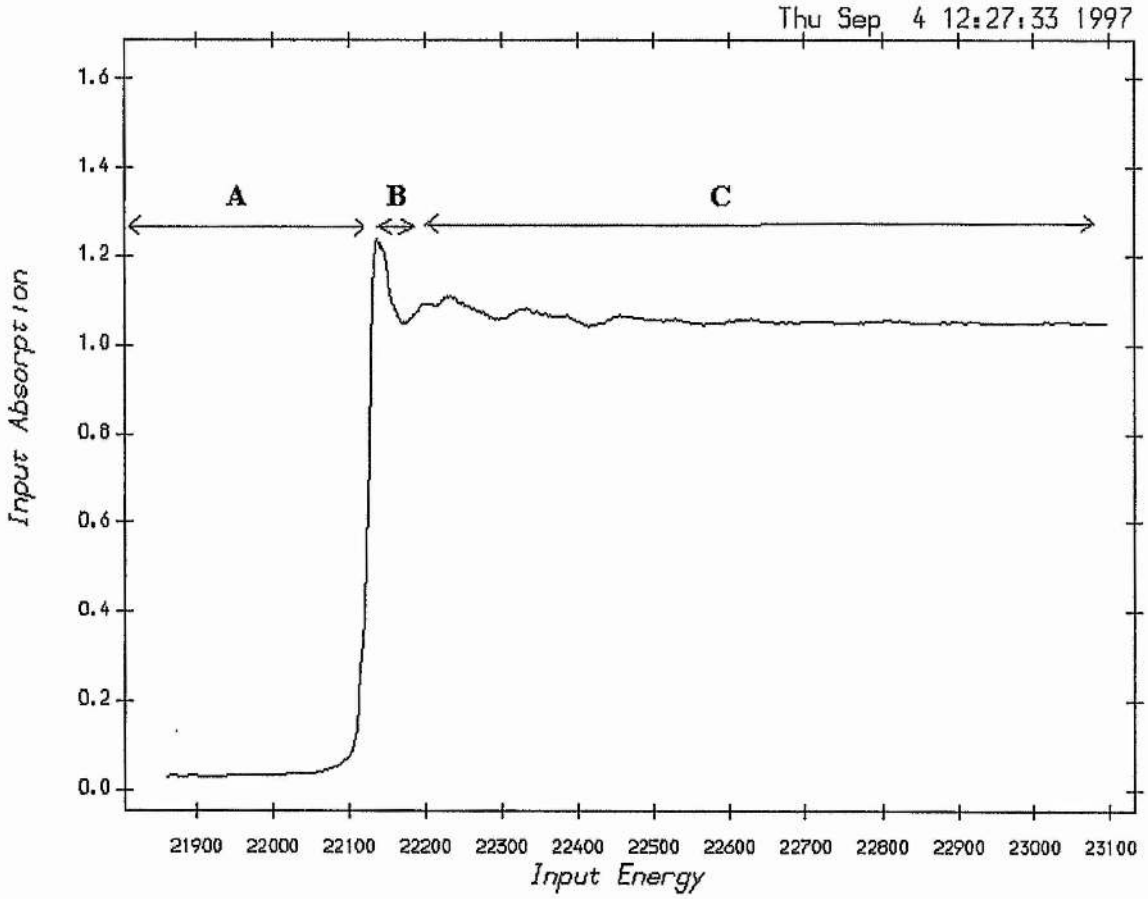

Fig.3.1: A typical X-ray absorption spectrum. Region A is the preedge spectrum, B is the XANES and C the EXAFS region.

of the absorber, the site geometry and information about the absorber ligand bonding.

The next region in the spectrum is called the X-ray Absorption Near Edge Structure or XANES (also sometimes referred to as NEXAFS or Near Edge X-ray Aborption Fine Structure). This part of the spectrum concerns the region just after the absorption edge and thus a region where the ejected photoelectrons have low kinetic energies. This leads to multiple scatterings of the ejected photoelectron by neighbouring atoms making this technique is extremely sensitive to the geometrical arrangement of atoms around the absorbing atom. From the XANES spectrum information on site geometry, bond angles and distance information.

The final region of the spectrum is the Extended X-ray Absorption Fine Structure or EXAFS region. This region of the spectrum begins at about 50 eV above the absorption edge. The spectrum arises from single scattering events of photoelectrons of relatively high kinetic energy. The photoelectron wave moves out from the excited atom and when it encounters a neighbouring atom it is reflected back causing interference with the outgoing wave. Thus, depending on the distance between the excited and the reflecting atoms the interference will be constructive or destructive. As the X-ray energy varies, the wavelength of the photoelectron varies and the interference will pass through cycles of being constructive or destructive. These cycles lead to oscillations in the absorption coefficient μ. The frequency of the oscillations is determined by the distance from the absorbing atom to the backscatterer and the amplitude is determined by the number of backscatterers present hence the EXAFS spectrum can give information on both interatomic distances and bond lengths and also on the coordination number of the absorber.

3.1.2 Experimental Methods

3.1.2.1 Data Collection

The nature of X-ray absorption spectroscopy requires that the incident X-ray beam meets a number of criteria. The beam must be tunable so X-rays of the required frequency for the element under investigation can be obtained, it must be monochromatic to avoid absorption by other elements and finally the intensity should be as high as possible to obtain sufficient information to give an acceptable signal to noise ratio allowing reliable structure determination. To this end synchrotron radiation is now the most commonly used source of X-rays for XAS.

Synchrotron radiation is produced by fast moving elementary particles. These particles are contained within a high vacuum storage ring with the radiation emitted being transmitted down beam lines tangential to the curved sections of the ring which are placed within a magnetic field. The ring also contains a number of devices to increase the energy of the particles in the ring and the intensity of the beam. The emitted X-ray beam must be monochromated before the spectrum can be measured. This is done using two parallel crystals each cut parallel to the same hkl plane, the first to monochromatize the incoming beam and the second to keep the outgoing beam parallel to the incoming one.

Two principle detection methods are used for XAS: fluorescence and transmission. Transmission is use for high concentration samples (> 2 wt% of absorber) whereas fluorescence is used for less concentrated samples. Both methods

use gas filled ion chambers to detect the spectrum but use different methods for doing so: the transmission method detects the difference in energy of the beam before and after it passes through the sample, whereas fluorescence measurements involve measuring the intensities of X-rays emitted from the sample due to the de-excitation of the core hole produced by the incident beam.

3.1.2.2 Data Processing of EXAFS spectra

The dataset obtained in an EXAFS experiment is a list of the values of various detectors collected at each point in the spectrum[4]. Thus a number of steps must be taken to convert this data into a spectrum from which useful information can be obtained. The first step involves conversion of the signal detector values to energy values. Secondly E_0 (the absorption edge) must be defined and the background must be subtracted to give

the EXAFS spectrum of the sample. Fourier transformation of this spectrum gives a quasi-radial distribution function, although this does not contain phase shift information. From this Fourier transform the spectrum can be refined using a least squares method and compared to theoretical models or crystallographic data giving information on the local structure around the excited atom.

3.2 Instrumentation

EXAFS spectra were collected on station 9.2 at the synchrotron radiation source at the CCLRC Daresbury laboratory operating at 2GeV and 200mA using

transmission and fluorescence detection methods for solid and solution samples respectively. Analysis was performed at the ruthenium K edge using a harmonic rejecting double Si (220) monochromator. The X-ray absorption was measured using gas filled ion chambers. The detector gases for I_t (transmitted X-ray intensity) and I_0 (incident X-ray intensity) were Ar + He and Ar respectively. Solid samples were of ≈1mm thickness and were diluted with boron nitride to allow sufficient X-rays through to record a spectrum. Aqueous acidic, ethanol or CH_2Cl_2 solution samples of ≈2mm thickness were measured in specially constructed perspex cells with mylar windows (Fig. 3.2). For the fluorescence measurements a thirteen element (TlI/NaI) detector was employed.

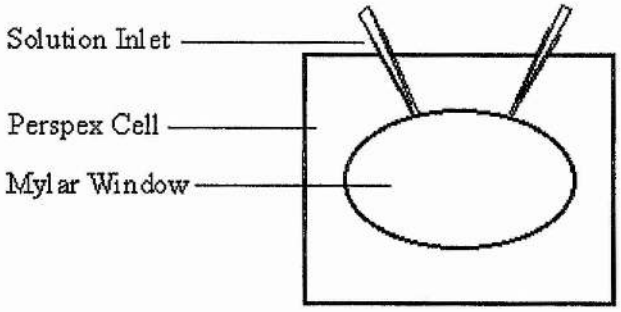

Fig. 3.2: Schematic representation of the perspex cell used for measurement of EXAFS spectrum of solution samples.

The EXAFS data was extracted as follows: the raw data were corrected for dark currents and converted to energy values using the EXCALIB[5] program. The position of the absorption edge was determined from the derivative of the spectrum using EXBACK[5]. This program was also used to extract an EXAFS function $\chi(k)$ by first

order polynomial removal of the pre-edge data and second or third order polynomial removal of post edge data. The raw EXAFS oscillations in k space was obtained by subtracting the background, converting the x-axis from energy to k-space and multiplying by k^3 to enlarge the oscillations at large k. These oscillations ($k^3\chi(k)$) were Fourier transformed to give a quasi-radial distribution function.

Fitting of the two structural models for the $Ru_4O_6^{4+}$ core, adamantanoid (model A) and stacked dimer (model B) was carried out with the EXCURV92[6] program using curved wave theory with the help of either Xalpha or Hedin Lindquist ground states and Xalpha or Von Barth exchange potentials. This program was also used to calculate potentials and phaseshifts. Peaks were fitted using standard Ru-O bond lengths and Ru-Ru distances from crystallographic data.

Infra red, UV-Vis, NMR, mass spectrometric and microanalysis were obtained using the methods described in chapter 2.

3.3 Results and Discussion

3.3.1 Solutions of the $Ru_4O_6^{4+}$ aqua ion in 2.0M perchloric acid

The EXAFS spectrum and quasi-radial distribution function obtained from solutions of the $Ru_4O_6^{4+}$ aqua ion in 2M perchloric acid, calculated using Xalpha ground states and exchange potentials, are shown in Fig.3.3 along with the results of a fit of the spectrum to model A. The quality of the fit of the experimental to the theoretical model is reported in terms of to the discrepancy index R and the fit index FI[7]. A value of 23.6951 is obtained for R and 0.00036 for FI, of the calculated to the

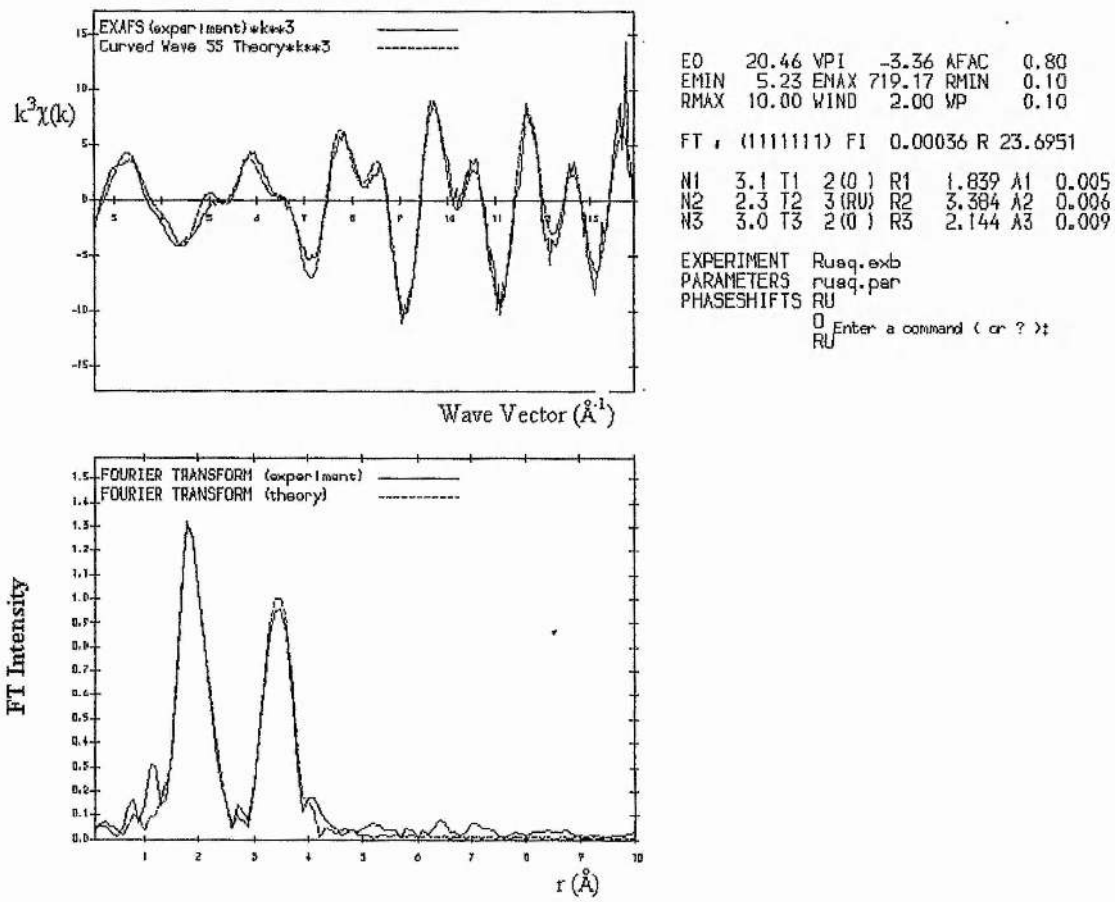

Fig. 3.3. Refined EXAFS spectrum (top) and quasi-radial distribution function (bottom) obtained for solutions of $Ru_4O_6^{4+}$(aq) in 2M perchloric acid calculated using Xalpha ground states and exchange potentials. Fit is for an adamantanoid structure.

experimental spectrum of model A using an amplitude reduction factor (AFAC) of 0.8. Two ruthenium oxygen shells are fitted corresponding to two different ruthenium oxygen distances. The first, with a Ru-O distance of 1.839Å and an occupancy number (N) of 3.1 is assigned to the ruthenium to bridging oxygen bond and the second, with a Ru-O distance of 2.144Å and an N value of 3.0, is assigned to the bond between ruthenium and the oxygen atom of the coordinated water molecules. Both these values correlate well with values for Ru-(μ)O-Ru and Ru-OH_2 bond lengths typically found in the Literature[8-11]. The ruthenium to ruthenium distance is calculated as 3.384Å with an N value of 2.3. The number of atoms in each shell varies from the values of three, three and three postulated for this model with the ruthenium shell containing closer to two nearest neighbours.

If Hedin-Lindquist ground states and Von Barth exchange potentials are used a similar refinement is obtained for model A as is shown in figure 3.4. These ground states and exchange potentials, used to calculate phaseshifts, contain real and imaginary parts whereas Xalpha contains only real parts. The AFAC is 0.8, the same as for the Xalpha ground states and exchange potentials and within the expected value of 0.8-1.0 for the complex potentials used. The fit improves slightly having an R value of 20.4744 and an FI value of 0.00032. Results using Hedin-Lindquist and Von Barth ground states and exchange potentials are considered to be more accurate than those obtained using Xalpha hence subsequent models for the two postulated structures of the aqua ion were built and refined using these algorithms. The results for these models are shown in Table 3.1.

Model A is fitted using three shells, corresponding to only one ruthenium-ruthenium distance whereas model B has four shells corresponding to two ruthenium-

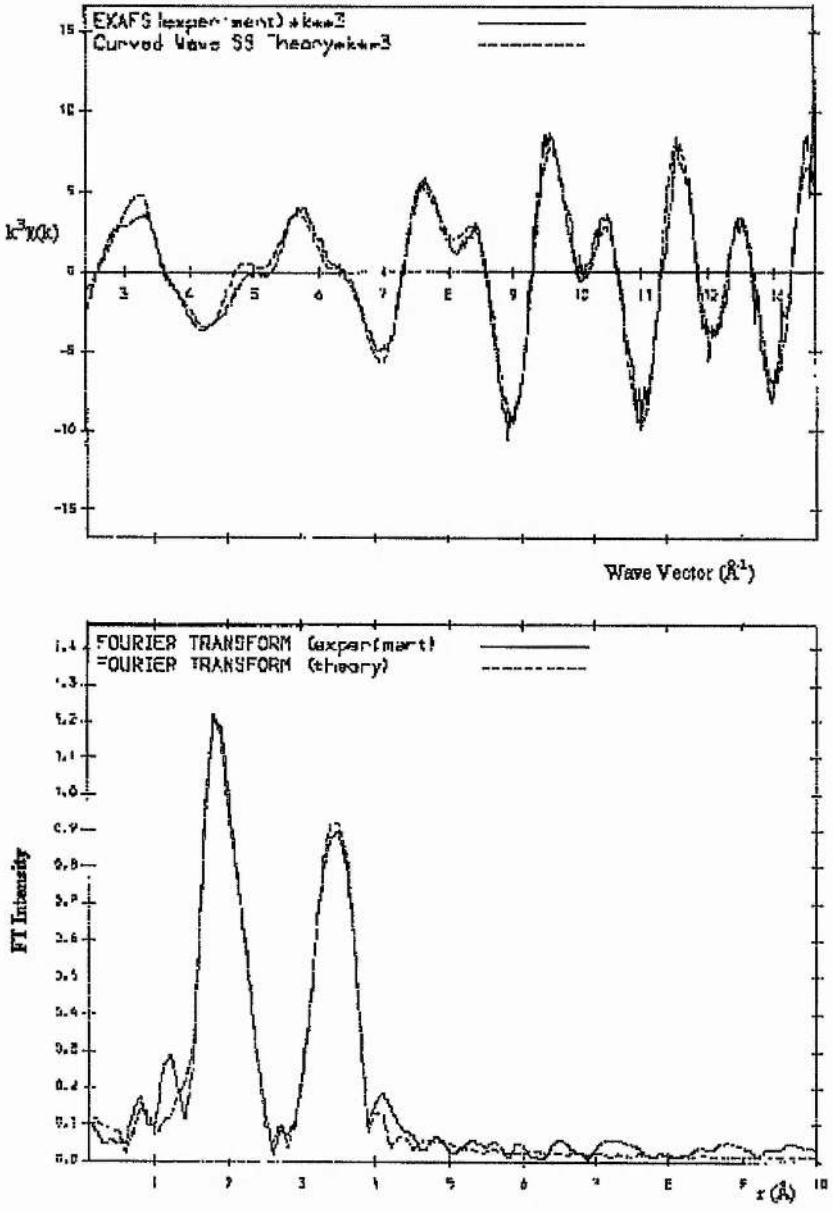

Fig. 3.4. Refined EXAFS spectrum (top) and quasi-radial distribution function (bottom) obtained for solutions of $Ru_4O_6^{4+}{}_{(aq)}$ in 2M perchloric acid calculated using Hedin Lindquist ground states and Von Barth exchange potentials.

ruthenium distances. The latter model should actually be fitted for 6 shells as the distances from the absorbing ruthenium atom to the adjacent ruthenium atoms will be different, due to one being mono oxo and the other being di-oxo bridged. The ruthenium oxygen distances for the two types of bridging oxygen will also be different. The results obtained using a six shell model have proved unsatisfactory as the Debye Waller factors obtained are always negative (and thus unacceptable) whichever parameters are used and in all cases the values for the number of atoms in each shell is too high. The distances to the first two backscattering ruthenium atoms, although different, are very similar, likewise the distances to the different types of bridging oxygen atoms, and the unsatisfactory results obtained may be due to the resolution of the spectrometer being insufficient to differentiate between the two.

The stacked dimer (B) model, although giving the best fit (R=19.7061, FI=0.00022), is unsatisfactory in many respects: the number of atoms in the third shell is closer to three than to the value of two expected and the value for the fourth shell is much lower than the expected value of one. Although the values obtained for higher shells tend to be less accurate than for the first shell the error values calculated when the data are correlated are not large enough to suggest that the results are inaccurate. The refinement of the data must also be considered: The initial N values for the third and fourth shells in model B are two and one respectively and on iteration the value for the third shell iterates upwards towards three and that of the fourth down towards zero. It may be the case that this model is actually refining to the adamantane model (A) and that the fourth shell is modelling a different interaction possibly with oxygen shells further from the absorbing atom or perhaps an artifact arising from imperfect fitting of the background. Further evidence for this refinement towards the adamantane model

Model A (adamantanoid) AFAC = 0.8

Species		**N**	**D,Å**	**A,Å^2**	**R,%**	**FI**
$Ru(IV)_{(aq)}$	Ru-O(μ)	3.10(7)	1.833(2)	0.003	20.4744	0.00032
2M $HClO_4$	$Ru-OH_2$	2.70(1)	2.163(3)	0.003		
	Ru-Ru	3.00(7)	3.401(2)	0.004		

Model B (stacked dimer) AFAC = 0.8

Species		**N**	**D,Å**	**A,Å^2**	**R,%**	**FI**
$Ru(IV)_{(aq)}$	Ru-O(μ)	3.00(5)	1.833(2)	0.003	19.7061	0.00022
2M $HClO_4$	$Ru-OH_2$	2.60(8)	2.167(2)	0.003		
	Ru-Ru (near)	2.40(5)	3.402(1)	0.002		
	Ru-Ru (distal)	0.50(1)	4.436(1)	0.004		

Table 3.1: EXAFS results for adamantane and stacked dimer models of the $Ru_4O_6^{4+}$ aqua ion in 2M perchloric acid where N = Number of atoms in shell; D = Distance of shell from absorbing atom; A = Debye Waller factor; R = Discrepancy Factor and FI = Fit index

(A) can be found in the obtained Debye Waller factors, A: It is expected that the A values for shells further from the absorbing atom should be higher than for nearer

shells. This is not the case for the stacked dimer model (B) with the third shell having a lower value than the first two. The value for the third shell, although within acceptable limits, is lower than expected and increases as the number of atoms in this shell is iterated upwards.

In general, the overall fit improves as the number of shells fitted is increased. The significance of a shell, that is to say the extent to which a particular shell improves the fit, can be tested using a statistical package built into EXCURV92. The program calculates a probability level at which a shell becomes significant by comparing the fit with and without that shell fitted. Low values of this probability level indicate that a shell is important. This package was used to test the significance of the fourth shell in the stacked dimer model. The results showed that the fourth shell is significant at a 5% probability level suggesting that this shell does contribute significantly to the fit.

The adamantanoid model (A) also fits very well with sensible N and bond distances. However, the fitted model is superior to the stacked dimer model (B) in many respects. Firstly the N value in each shell is close to that expected with only the second shell containing 2.7 oxygen atoms deviating from the value of three expected. More importantly the N value for the third shell, containing three identical ruthenium atoms is exactly the value of three expected for this model. Secondly the values for the Debye Waller factors increase as the shells move further form the absorbing metal centre.

3.3.2 Solutions of the $Ru_4O_6^{4+}$ aqua ion in 2.0M Nitric acid

A similar refinement of the observed EXAFS spectrum (Fig. 3.5) for solutions

of $Ru_4O_6^{4+}$ (aq) in 2.0M HNO_3 as is shown in Table 3.2. Again it is found that the fit is slightly better for Model B (R = 24.7971 as opposed to 25.5070 for the Model A) and that both models have bond lengths and distances at comparable values to those in the literature.

Model A (adamantanoid) AFAC = 0.8

Species		**N**	**D,Å**	**A,Å²**	**R,%**	**FI**
$Ru(IV)_{(aq)}$	Ru-O(μ)	3.10(7)	1.837(2)	0.003	25.5070	0.00037
2M HNO_3	$Ru-OH_2$	3.00(1)	2.163(3)	0.004		
	Ru-Ru	2.90(7)	3.406(2)	0.004		

Model B (stacked dimer) AFAC = 0.8

Species		**N**	**D,Å**	**A,Å²**	**R,%**	**FI**
$Ru(IV)_{(aq)}$	Ru-O(μ)	3.20(7)	1.831(2)	0.004	24.7971	0.00033
2M HNO_3	$Ru-OH_2$	2.60(1)	2.166(3)	0.002		
	Ru-Ru (near)	2.60(7)	3.405(2)	0.003		
	Ru-Ru (distal)	0.30(2)	4.420(3)	0.006		

Table 3.2: EXAFS results for adamantane and stacked dimer models of the $Ru_4O_6^{4+}$ aqua ion in 2M nitric acid where N = Number of atoms in shell; D = Distance of shell from absorbing atom; A = Debye Waller factor; R = Discrepancy Factor and FI = Fit Index.

As with solutions of the aqua ion in 2.0M perchloric acid, however, taken together the occupancy number (N) and Debye Waller factors for each bond distance to neighbouring backscatterers are more indicative of the adamantanoid structure, model (A). This model has almost exactly the expected values for the number of atoms in each shell and Debye Waller factors that increase as the distance from the absorbing atom increases. Fitting for model (B) leads to the third shell having more atoms than expected, in this case the value of the occupancy N for shell three is 2.6, refining closer to the value expected for model (A). The fourth shell is found to contain 0.3 atoms suggesting that this is refining towards zero. The Debye Waller factors for the second and third shells of model (B) are once again are somewhat lower than expected. The overall fit for both models of the aqua ion in nitric acid is slightly inferior to that for the ion in 2M perchloric acid. This may be a consequence of the nature of the species bound to the ruthenium atoms: the UV-Visible spectrum of the $Ru_4O_6^{4+}(aq)$ ion in 2M Nitric acid shows a sharp peak in the UV region at around 300nm (ε = 5628 M^{-1} cm^{-1}) suggesting that inner sphere coordination of the nitrate counterion may be occurring replacing coordinated water. EXAFS can not distinguish between oxygen and nitrogen (thus the second shell is fitted for three oxygen atoms for convenience) but the bound counterion may affect the final fit. Alternatively the poorer fit obtained for the aqua ion in nitric acid may however simply arise from inferior data or from imperfect background subtraction. For example, artefacts are seen in the Fourier transform of the nitric acid solution at short distances (Fig. 3.5)which cannot correspond to any interatomic interactions.

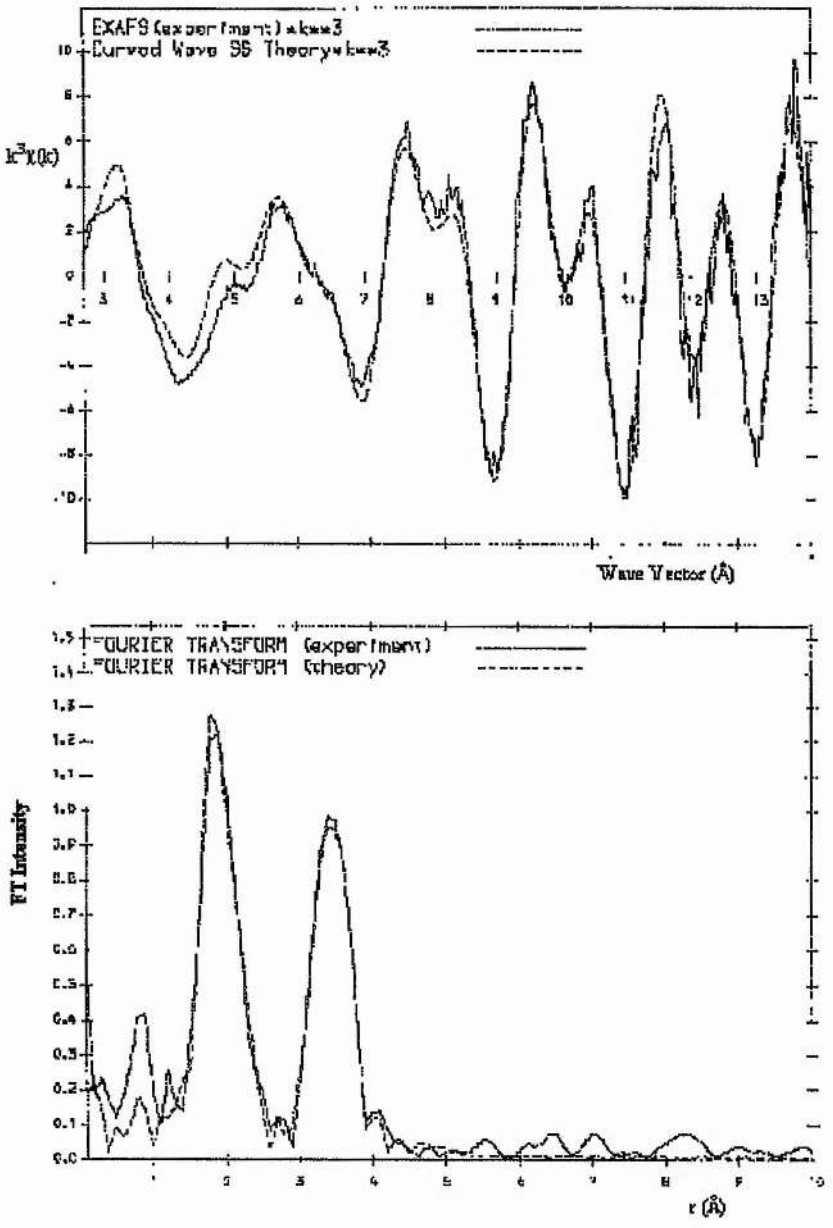

Fig. 3.5: Refined EXAFS spectrum (top) and quasi-radial distribution function (bottom) obtained for solutions of $Ru_4O_6^{4+}$(aq) in 2M nitric acid calculated using Hedin Lindquist ground states and Von Barth exchange potentials.

Having established that the adamantanoid model (A) for the $Ru_4O_6^{4+}$ core fits the EXAFS data better one has to consider the alternative symmetrical three shell model based on a cuboidal arrangement, 'Ru_4O_4'. It should be possible to distinguish between the two arrangements based upon the successfully fitted Ru-O(μ) and Ru-Ru distances which allow a calculated estimate of the angle subtended at the bridging oxygen atoms. The M-O-M angle in an adamantanoid arrangement is typically around 125-140°[12-16] in compounds and is typically around 100°[18] for cuboidal structures (Fig. 3.6).

The best fitted Ru-Ru and Ru-O distances obtained from the EXAFS spectra can only be accommodated by an adamantanoid arrangement which allows for a Ru-O-Ru angle of 135.8°: this angle is clearly too large to be accommodated within a cuboidal arrangement. A cuboidal arrangement would also have a first oxygen shell containing two atoms and a second containing four rather than the two three atom shells fitted using EXCURV92. Indeed the evidence suggests that the second shell contains less than 3 atoms rather than more. An adamantane $Ru_4O_6^{4+}$ core is moreover the only one able to explain the ion exchange behaviour (+4 charge see chapter 2) and is present in one form of the $HBpz_3$ complex as indicated by mass spectroscopic studies[1]. Multiple scattering techniques within EXCURV92 were used in an attempt to obtain an accurate figure for the Ru-O-Ru bond angle in the aqua ion. These techniques involve defining units of atoms and further parameters corresponding to the polar coordinates and bond angles. These coordinates and angles are refined along with the interatomic distances and numbers of atoms in each shell allowing some geometry determination. Certain bond lengths can be restrained if desired. These techniques were, however,

unsuccessful in obtaining useful bond angle data for solutions of the aqua ion in perchloric acid: although a sensible value of 121.7° was obtained for the adamantane model, the values for the bond length from the second shell oxygen to the third shell ruthenium atoms iterated to an unacceptably high value, even when restrained. Multiple scattering also failed to give any further insight into whether $Ru_4O_6^{4+}$ (aq) has an adamantanoid or stacked dimer structure.

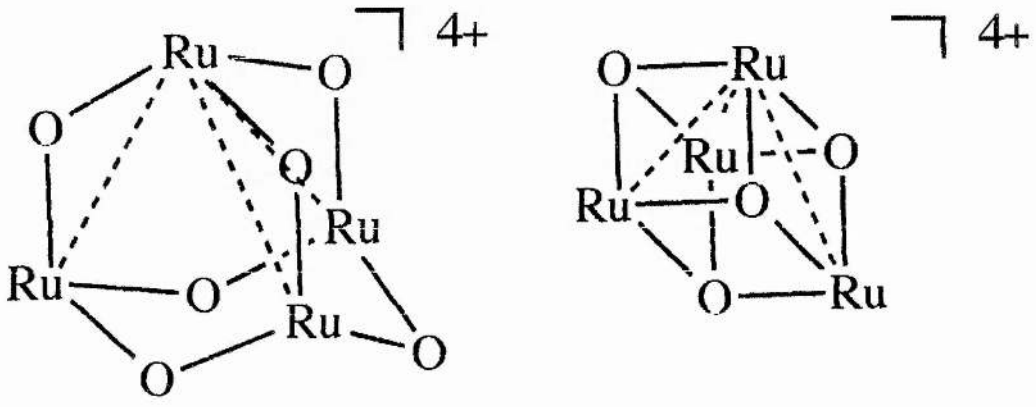

Fig. 3.6: Adamantane and cuboidal models for the core of the Ru(IV) aqua ion.

3.3.3 EXAFS studies on attempted derivative complexes of the $Ru_4O_6^{4+}$ ion

3.3.3.1 Pyrazol-1-yl borate derivatives

The Fourier transform and backscattered EXAFS oscillations for the tris-pyrazolyl borate derivative of the $Ru_4O_6^{4+}$ ion in solutions of CH_2Cl_2 are shown in Fig. 3.7 and the bond lengths, shell occupancies and Debye Waller factors in Table 3.3.

The values given in Table 3.3 are for a multiple scattering model. Modelling the tris-pyrazolyl borate derivative is made more complicated due to the five membered pyrazole rings in the coordinated ligand as, although the ruthenium atom is bound through only one nitrogen atom, the other atoms in the ring are at distances comparable to the Ru-Ru distance and hence must be included in the final model. These rings are inherently inflexible and their bond lengths angles and number of atoms must be restrained to get an accurate model for the molecule. To this end a five membered ring

Model C: Tris-Pyrazolyl Borate Derivative AFAC = 0.8

Shell	T	N	D, Å	A, Å^2	R %	FI
1	4(N)	3.4	1.785	0.017	23.7308	0.00043
2	2(O)	2.1	1.941	-0.018		
3	2(O)	1.1	2.085	-0.028		
4	3(Ru)	0.9	2.405	0.004		
5	4(N)	3.4	3.638	0.015		
6	4(N)	3.4	3.638	0.015		
7	4(N)	3.4	4.867	0.046		
8	4(N)	3.4	4.867	0.046		

Table 3: EXAFS results for the Tris-Pyrazolyl Borate derivative of Ru(IV) where N = Number of atoms in shell; T = Atom type; D = Distance of shell from absorbing atom; A = Debye Waller factor; R = Discrepancy Factor and FI = Fit Index

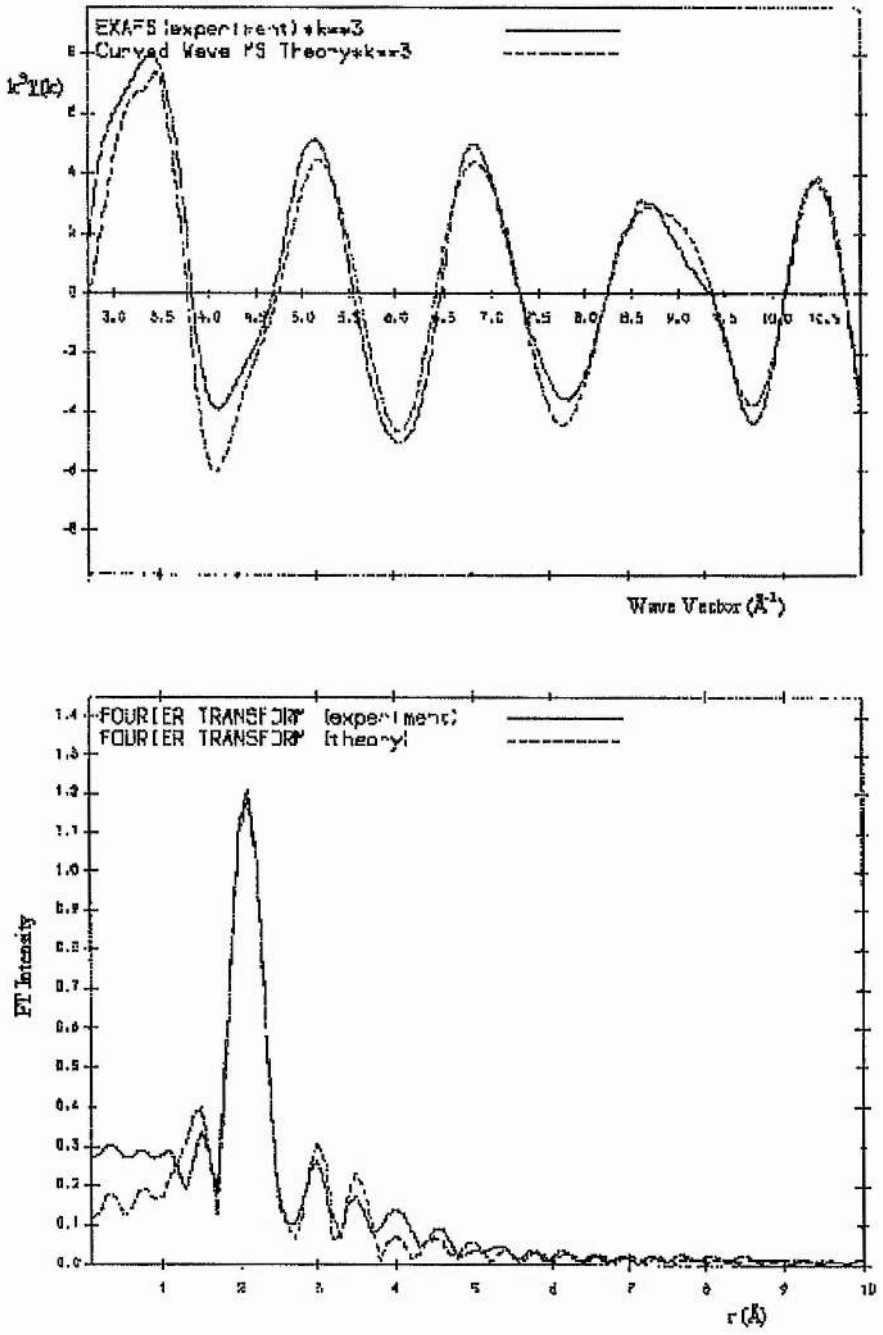

Fig. 3.7: Refined EXAFS spectrum (top) and quasi-radial distribution function (bottom) obtained for the tris-pyrazolyl Borate derivative of the Ru(IV) aqua ion calculated using Hedin Lindquist ground states and Von Barth exchange potentials.

coordinated to a ruthenium atom was built in EXCURV92 and the bond lengths and angles restrained using the multiple scattering program built into the software. The model ring contains only nitrogen atoms as EXAFS would be unable to distinguish between nitrogen and carbon. The interatomic distances from the absorbing ruthenium atoms and certain atoms in the ring are refined together as groups of atoms had to be put in different shells even though they were at the same distance from the absorbing metal centre. The results suggest that the compound is dimeric as the best fit for the model contains only one Ru-Ru distance and it is thought that this compound might have the same core structure as the $^{5}\eta$-cyclopentadienyltris(diethylphosphito)cobalt (L_{OEt}) ruthenium dimer of Power et al[8] (Fig. 3.8).

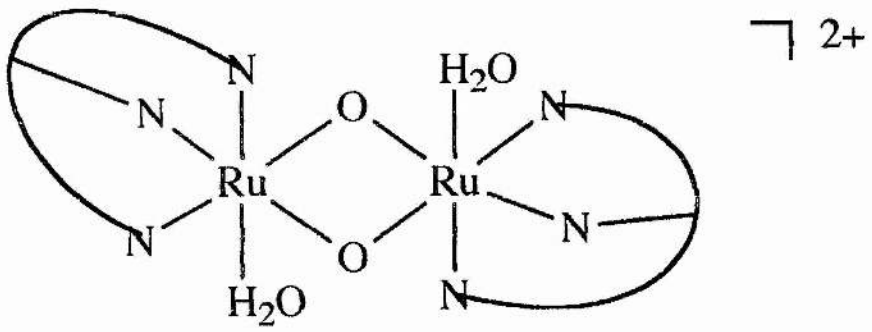

Fig. 3.8: Possible structure for the tris-pyrazolyl derivative of Ru(IV).

The electrospray mass spectrum of this derivative measured after the experiment had been performed also suggests a dimeric structure. The spectrum had a maximum m/z at around 715 which can be fitted for an oxo-bridged dimer containing to tris-pyrazolyl borate ligands. The isotope patterns are also concurrent with those expected

for a compound containing two ruthenium atoms.

Problems exist with the model as it proved impossible to obtain acceptable (positive) Debye Waller factors for several of the shells. Although apparently dimeric in nature i.e the sample did not fit for containing the $Ru_4O_6^{4+}$ core, the spectrum of this derivative if refined satisfactorily may give a useful insight into the pH behaviour of the aqua ion as the compound was prepared at higher pH than other compounds analysed. Problems in the refinement may arise firstly from the nature of the coordinated ligand although the use of multiple scattering techniques should minimize this. It may be that the ruthenium to nitrogen bond lengths are not all equal as studies on a copper dimer with coordinated tris-pyrazolyl borate ligands[19] show that one Cu-N bond is longer than the other two. Attempts to model a longer Ru-N bond have been unsuccessful as again the Debye Waller factors have unacceptable negative values with one possibility for this being that the resolution of the spectrometer is insufficient to resolve so many simliar bond lengths.

3.3.3.2 Derivative with methyliminodiacetate (MIDA)

The spectrum of the MIDA derivative of the $Ru_4O_6^{4+}$ aqua ion in a solution of 0.2M MIDA in water was also refined however no sensible structure could be obtained after it became clear that refinement to either of the postulated adamantanoid or stacked dimer structures was not possible. It is clear though that whatever species is eluted off a column by the MIDA solutions does not contain the $Ru_4O_6^{4+}$ core even though the UV-Visible spectrum contains the expected bands. It is clear that a reaction is occuring on the purification/derivatization column and that it is for this reason that

elution from the column was possible without the use of lanthanum salts.

3.3.3.3 $^{5}\eta$-cyclopentadienyltris(diethylphosphito)cobalt (LOEt) ruthenium dimer, $[L_{OEt}(H_2O)Ru(\mu\text{-}O)_2Ru(H_2O)L_{OEt}][PF_6]_2$

The Fourier transform and backscattered EXAFS spectrum of the solid dimeric oxo-bridged compound $[L_{OEt}(H_2O)Ru(\mu\text{-}O)_2Ru(H_2O)L_{OEt}][PF_6]_2$ (model D) is shown in Fig. 3.9. Of the four model compounds analysed this proved the least difficult to fit (indeed this was the only compound that could be refined to even approximately the structure expected) as it was the only compound which did not contain aromatic rings for which multiple scattering analysis would be necessary. Modelling of the bridging oxygens is found to be compromised by a large artifact which could not be removed during background subtraction although the number of atoms in the shell is almost modelled correctly (Table 3.4). As for the tris-pyrazolyl borate derivative of the tetramer, a number of the atoms of the bound ligand are located at distances comparable to the Ru-Ru distance and thus has to be included and resolved in an attempt to get a decent fit. In this case the phosphorous atoms of the L_{OEt} ligand are modelled and refined and although the results of the modelling of the interatomic distances is gives satisfactory results, the shell occupancy values are far lower than expected.

In the light of the satisfactory fits obtained for the $Ru_4O_6^{4+}$ (aq) ion in perchloric and nitric acid it was decided not to attempt further involved refinement these results in the time available.

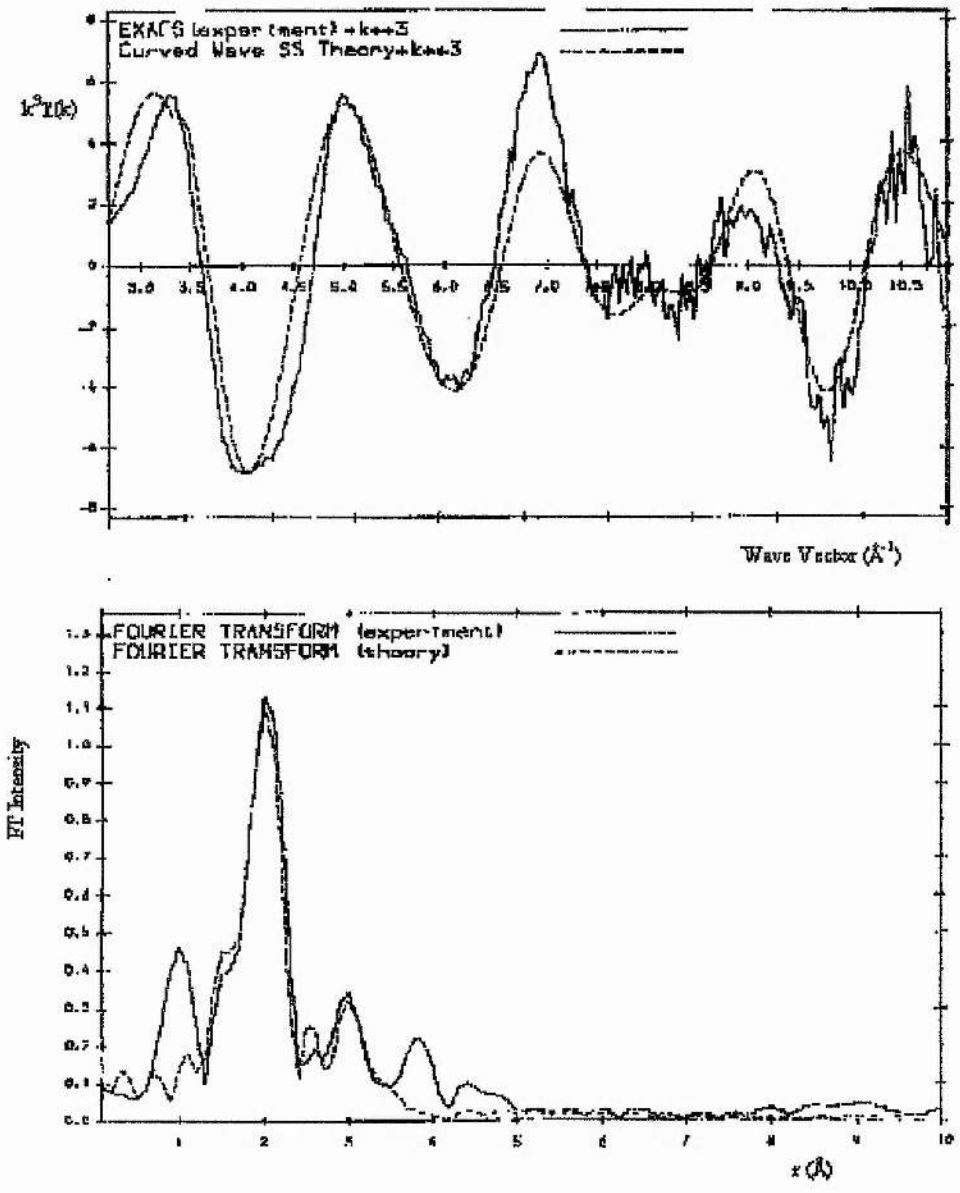

Fig. 3.9: Refined EXAFS spectrum (top) and quasi-radial distribution function (bottom) obtained for $[L_{OEt}(H_2O)Ru(\mu\text{-}O)_2Ru(H_2O)L_{OEt}][PF_6]_2$ calculated using Hedin Lindquist ground states and Von Barth exchange potentials.

Model D: $[L_{OEt}(H_2O)Ru(\mu\text{-}O)_2Ru(H_2O)L_{OEt}][PF_6]_2$, AFAC = 0.8

Shell	T	N	D, Å	A, Å^2	R %	FI
1	2(O)	1.9	1.840	0.004	37.3228	0.00090
2	2(O)	3.8	2.014	0.000		
3	3(Ru)	1.5	2.417	0.025		
4	4(P)	1.6	3.184	0.005		

Table 3.4: EXAFS results for $[L_{OEt}(H_2O)Ru(\mu\text{-}O)_2Ru(H_2O)L_{OEt}][PF_6]_2$ where N = Number of atoms in shell; T = Atom type; D = Distance of shell from absorbing atom; A = Debye Waller factor; R = Discrepancy Index and FI = Fit Index.

3.4 Conclusions

EXAFS spectroscopy has been shown to be a useful and highly successful tool for determining the structure of the tetrameric $Ru_4O_6^{4+}$ aqua ion. The refined results suggest that the $Ru_4O_6^{4+}$ core of the aqua ion in 2M perchloric or nitric acid has an adamantanoid structure with ruthenium oxygen bond lengths of 1.83Å for the bond to bridging oxygen and 2.13Å for the bond to the oxygen atom of the coordinated water molecules. The ruthenium-ruthenium distance is found to be 3.40Å (Fig. 3.10).

Previously postulated stacked dimer and cuboidal models for the core of the aqua ion can now be rejected on the grounds of unsatisfactory refinement and geometric grounds respectively. The Tris-pyrazolyl borate and MIDA derivatives studied were found not to contain the $Ru_4O_6^{4+}$ core.

The refinement of model oxo-bridged ruthenium compounds has been much less successful due to the complicated nature of the compounds concerned. Although successful refinement of the spectra of these compounds would have produced firmer evidence that the refinement of the aqua ion derivatives was giving an accurate representation of these species, the quality of the spectra obtained means that a comparison to known compounds is not necessary.

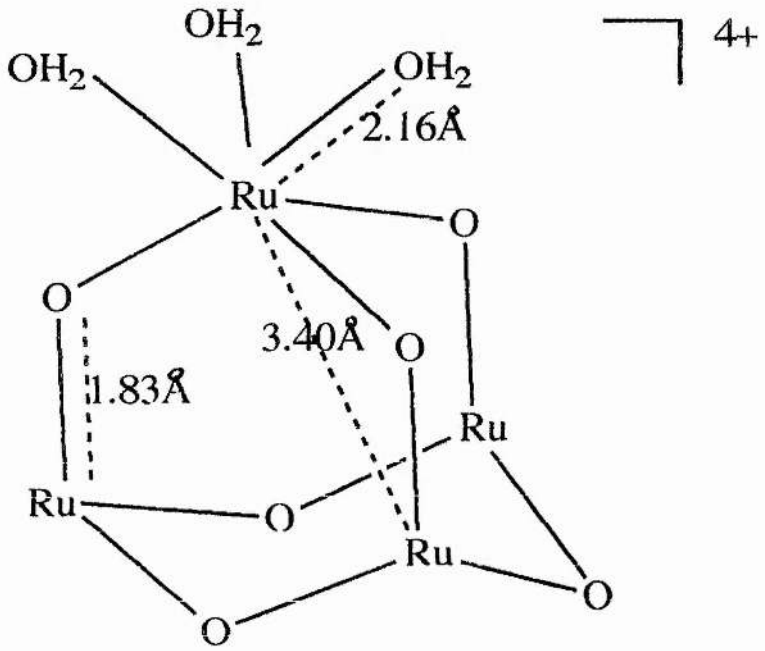

Fig. 3.10: Postulated adamantanoid structure for the core of the tetrameric $Ru_4O_6^{4+}$ aqua ion derived from EXAFS data.

3.5 Experimental Section

3.5.1: Attempted Preparation of derivatives of the tetrameric $Ru_4O_6^{4+}$ aqua ion

Two complexes of the $Ru_4O_6^{4+}$ aqua ion were synthesized for EXAFS studies in addition to the solutions prepared in perchloric and nitric acids. For synthetic details see chapter 2. All complexes prepared showed the characteristic band in the UV-Vis spectrum at 487 nm.

3.5.2: Preparation of μ-oxobis(bis-(2,2-bipyridine)aquaruthenium (III)) perchlorate hydrate $[(bipy)_2(OH_2)RuORu(H_2O)(bipy)_2](ClO_4)_4.2H_2O$.

This compound (Fig. 3.11) was synthesized using the procedure of Gilbert et al[10]. Commercial Ruthenium trichloride, $RuCl_3$ (Johnson Matthey, 2g, 7.5mmol), bipyridine (Aldrich, 15mmol) and LiCl (Aldrich, 2g, 5mmol) were dissolved in DMF ($50cm^3$) and refluxed for 8 hrs with stirring. The solution was cooled to room temperature and the volume of DMF reduced to ≈20 cm^3 on a rotary evaporator. 50 cm^3 of acetone were added and the solution left overnight after which a green/black precipitate was produced. The precipitate was filtered and washed 3 times with cold distilled water and 3 times with cold diethyl ether. The product, *cis*-$(bpy)_2RuCl_2.2H_2O$ was dried under vacuum.

1.2g of *cis*-$(bpy)_2RuCl_2.2H_2O$ were dissolved in $30cm^3$ of water and heated under reflux with stirring. $AgNO_3$ (0.92g, 5.4mmol)was added and the solution refluxed for a further 30 mins. The AgCl produced was filtered off and the filtrate

heated at reflux for a further 30 mins. Saturated $NaClO_4$ (≈20cm^3) was added and the total volume reduced to 30cm^3 on a rotary evaporator. After refrigeration for 8 hrs the solid product was collected by filtration, washed with 10cm^3 of saturated $NaClO_4$ followed by 5cm^3 of ice cold water. The product was recrystallized by dissolving it in warm water and adding saturated $NaClO_4$ until precipitation just began to occur. The solution was filtered and kept at room temperature before filtering and drying of the final crystalline product.

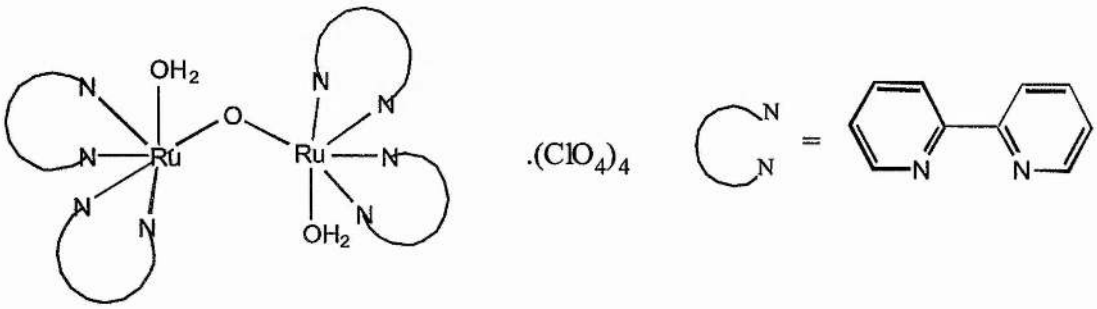

Fig. 3.11: Molecular Structure of $[(bipy)_2(OH_2)RuORu(H_2O)(bipy)_2](ClO_4).2H_2O$.

The final product, $[(bipy)_2(OH_2)RuORu(H_2O)(bipy)_2](ClO_4).2H_2O$ possessed the UV-Vis peaks at 660,410,284 and 244nm in MeCN in agreement with the literature values of 660 nm, ε = 25000; 410 nm, ε = 9500; 284 nm, ε = 53000; 244, ε = 38000. Anal. Calcd C, 36.60; H, 3.07; N, 8.53. Found C, 35.86; H, 2.61; N, 8.62.

3.5.3: Preparation of di-μ-oxobis(bis(pyridine)oxoruthenium (VI)) heptaahemihydrate, $[Ru_2O_6(py)_4].3.5H_2O$

This compound (Fig. 3.12) was synthesized via the method of Dengel[9]. 0.75g (5.5 mmol) of $RuO_2.2H_2O$ was added to a solution of $NaIO_4$ (2.5g, 11.7 mmol) in water (20 cm^3) and nitrogen gas bubbled through the solution to sweep out the RuO_4 generated. The RuO_4 was passed into a flask containing ice cold pyridine (0.75g, 9.5 mmol) in water (10 cm^3). After 24 hrs the dark red crystals obtained were filtered off. The crystals obtained were stored under the vapour pressure of their mother liquor to prevent decomposition. A brown powder was obtained if the crystals were dried.

Anal. Calcd.C, 35.45; H, 3.99; N, 8.27. Found C, 31.07; H 3.34; N 7.08. The UV-Vis spectrum showed a weak band at 257 nm and bands at 420 and 720 nm in agreement with the published results.

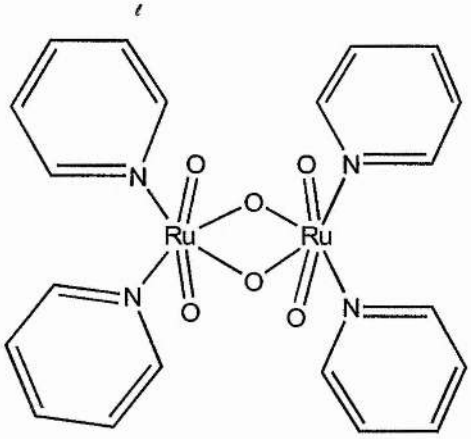

Fig. 3.12: Molecular structure of $[Ru_2O_6(py)_4$. The compound has 3.5 coordinated water molecules of crystallization.

3.5.4: Preparation of di-μ-acetato-μ-oxobis(tris(pyridine)ruthenium(III)) hexaflurophosphate, $[Ru_2(\mu\text{-}O)(\mu\text{-}CH_3COO)_2(py)_6][PF6]_2$

The method used to produce this compound (Fig. 3.13) was that of Sasaki[11]. 0.5g (2 mmol) of $RuCl_3.nH_2O$ (Johnson Matthey) were dissolved in a mixture of water (60 cm^3), acetic acid (40 cm^3) and ethanol (20 cm^3) and heated to 70 °C for 10 minutes. During this time the colour changed from brown to red. Pyridine (Aldrich, 3 cm^3, 40 mmol) was added and the mixture refluxed for one hour. After cooling to room temperature 2g (12 mmol) of NH_4PF_6 was added and the volume reduced to 20 cm^3 on a rotary evaporator. A blue precipitate was obtained. A further 20 cm^3 of water were added to the solution before placing it in a refrigerator. The precipitate obtained was filtered and washed with water.

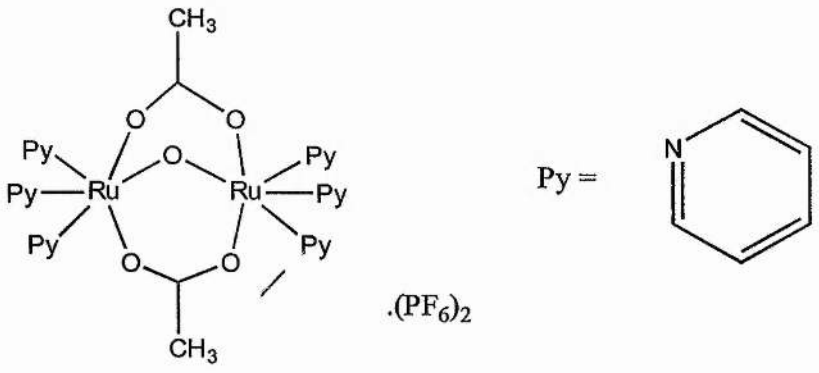

Fig. 3.13: Molecular structure of $[Ru_2(\mu\text{-}O)(\mu\text{-}CH_3COO)_2(py)_6][PF6]_2$

The blue precipitate was dissolved in acetonitrile containing a small amount of

pyridine and heated to 80 °C for 20 minutes. An amount of water equal to the amount of acetonitrile used was added and the solution refrigerated. The blue precipitate obtained was filtered, washed three times with distilled water and recrystallized from CH_2Cl_2.

The crystals obtained gave peaks in the UV-vis spectrum at 582, 326 and 250 nm. These are slightly displaced from the literature values but the peak sizes are in the correct ratio indicating that the desired product has been obtained. Anal. Calcd.C, 37.10; H, 3.30; N, 7.63. Found C, 36.96; H, 3.12; N, 7.64.

3.5.5: Synthesis of di-μ-oxobis(η^5cyclopentadienylcobaltbis(diethylphosphito)aqua ruthenium(IV)) hexaflurophosphate, $[L_{OEt}(H_2O)Ru(\mu\text{-}O)_2Ru(H_2O)L_{OEt}][PF_6]_2$

L_{OEt} is the anionic tripod ligand $[\{(\eta\text{-}C_5H_5)Co\{(CH_3CH_2O)_2P{=}O\}]$ (Fig.3.14). The structure of the μ-oxo bridged ruthenium dimer is shown in chapter 2, Fig. 2.4.

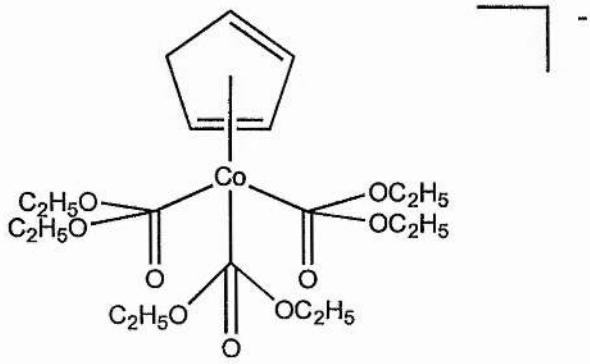

Fig.3.14: The anionic tripod ligand $[[(\eta\text{-}C_5H_5)Co\{(CH_3CH_2O)_2P{=}O\}]$ where R is CH_3CH_2O

This preparation was a slight modification of the procedure of Power et al[8]. A CCl_4 solution of RuO_4 (51.5 cm^3 of a 0.017M solution, 0.9 mmol) was added dropwise to a solution of NaL_{OEt} (0.6 g, 1.1 mmol)[8] in 1% H_2SO_4 (10 cm^3, 1.1 mmol) at 0°C. The mixture was stirred at 0 °C for 30 minutes then at room temperature for three hours. The aqueous layer was separated from the CCl_4 layer and was found to be of a red brown colour rather than the olive green reported[8]. After cooling to 0°C ≈2 cm^3 of saturated KPF_6 (Aldrich) were added to the aqueous layer and a red brown precipitate was observed. After 15 minutes this product was filtered, washed twice with water and dried under vacuum.

Anal. Calcd.C, 25.04; H, 4.57; N, 0. Found C, 23.63; H,4.52; N 0. Uv-Vis shows peaks shows expected peaks at 340 and 632 nm but also shows presence of unexpected peak at 500 nm. IR (KBr disk): ν_{max} 3425 (br), 1101 (s), 1032 (br), 956 (s), 949 (s), 846 (vs), 776 (m), 618 (m), 558 (m). ^{1}H-NMR ($CDCl_3$): δ 5.25 (s, H_2O, 2H) 5.17 (s, C_5H_5 5H), 4.49 (m OCH_2CH_3, 2H), 4.23 (OCH_2CH_3, 4H), 4.11 (OCH_2CH_3, 4H), 3.82 (OCH_2CH_3, 2H), 1.46 (t, OCH_2CH_3, 6H), 1.29 (t, OCH_2CH_3, 6H). ^{31}P-NMR ppm 119.9 to 131.6 (m, $P(O)(OCH_2CH_3)_2$).

3.6 References

1) D. T. Richens and A. Patel, *Inorg. Chem.*, 1991, **30**, 3789.

2) S. P. Cramer, P. K. Eidem, M. T. Paffett, J. R. Winkler, Z. Dori and H. P. Gray, *J. Am. Chem. Soc.*, 1983, **105**, 799

3) *Spectroscopic Methods in Mineralogy and Geology,* F. C. Hawthorne Ed., 1988.

4) A. J. Dent and J. F. W. Mosselmans, *"An Introduction to EXAFS Data Analysis."*, EPSRC Daresbury Laboratory, 1996.

5) EPSRC Daresbury Program Library, 1991.

6) N. Binsted, J. W. Campbell, S. J. Gurman, P. L. Stephenson, EPSRC Daresbury Program Library 1992.

7) N. Binsted, J. Evans, N. G. Greaves and R. J. Price, *Organometallics*, 1989, **8,** 613.

8) J. M. Power, K. Evertz, L. Henling, R. Marsh, W. P. Schaefer, J. A. Labinger and J. E. Bercaw, *Inorg. Chem.*, 1990, **29**, 5058.

9) A. C. Dengel, A. M. El-Hendawy, W. P. Griffith, C. A. O'Mahoney and D. J. Williams, *J. Chem. Soc. Dalton Trans.*, 1990, 737.

10) J. A. Gilbert, D. S. Eggleton, W. R. Murphy Jr., D. A. Geselowitz, S. W. Gerston, D. J. Hodgson and T. J. Meyer, *J. Am. Chem. Soc.*, 1985, **107**, 3855.

11) Y. Sasaki, M. Suzuki, A. Nagasawa, A. Tokiwa, M. Ebihara, T. Yamaguchi, C. Kabuto, Y. Ochi and T. Ito, *Inorg. Chem.*, 1991, **30(26)**, 4903.

12) J. Sala-Pala, J. E. Geurchais and A. E. Edwards, *Angew. Chem. Int. Ed. Engl.*, 1982, **21**, 870.

13) K. Wieghardt, U. Bossek and W Gebert, *Angew. Chem. Int. Ed. Engl.*, 1983, **22**, 328.

14) K. Wieghardt, D. Ventur, Y. H. Tsai and C. Kruger, *Inorg. Chim. Acta*, 1985, **99**, L25

15) D. Wormsbacher, K. M. Nicholas and A. L. Rheingold, *J. Chem. Soc. Chem. Commun.*, 1985, 721.

16) J. Glerup, H. Weihe, P. A. Goodson and D. J. Hodgson, *Inorg. Chim. Acta*,1993, **212**, 281.

17) K. Wieghardt, M. Kleine-Boymann, B. Nuber and J. Weiss, *Inorg. Chem.*, 1986, **25**, 1654.

18) R. O. Gould, C. L. Jones, D. R. Robertson and T. A. Stephenson, *J. Chem. Soc. Chem. Commun.*, 1977, 222.

19) A. Murphy, B. J. Hathaway and T. D. King, *J. Chem. Soc. Dalton Trans.*, 1979, 1646.

CHAPTER 4

Non-Aqueous Sol-Gel Processing of RuO_2 and RuO_2-TiO_2 Mixed Oxides

4.1 Introduction

Sol-gel processing involving the hydrolysis and condensation of metal alkoxides to metal oxides is well characterized for early transition metals[1]. Later transition metals such as the platinum group metals have been less extensively studied and, in cases where they have, problems have arisen due to the lack of suitable well-defined alkoxide precursors. Most of the work[2-5] involved sol-gel routes to powders or to films without evidence for intermediate gelation. Only one paper[6] has reported work on producing mixed oxide gels of which RuO_2 is a component. In much of the reported literature the starting material is commercial ruthenium trichloride, $RuCl_3.nH_2O$ which is very poorly defined, being a mixture of Ru(III) and Ru(IV) chlorides, oxides and nitrates. The groups of Guglielmi[2] and Merzbacher[6] have studied other precursors, namely $Ru(acac)_3$ and anhydrous $RuCl_3$, the latter having recently produced gels of a mixed RuO_2-TiO_2 oxide.

Alessio et al have synthesized a range of well defined chloride-dimethyl sulfoxide-Ru(III) complexes, $[RuCl_x(DMSO)_{6-x}]$, for antitumour applications[7]. These complexes could be useful precursors for RuO_2 production as it is possible that ethoxide groups could replace the coordinated chloride allowing subsequent controlled hydrolysis and condensation, and finally oxidation to Ru(IV). In addition, the compounds contain no coordinated water, unlike commercial $RuCl_3$. The Ru(IV) compound $(Et_4N)[RuCl_5MeCN]$ prepared by Dehand and Rose[8] is another well-defined

ruthenium starting material.

Outlined in this chapter are attempts to produce gels of RuO_2 and a mixed RuO_2-TiO_2 system via the alkoxide route along with partial charge calculations on a number of ruthenium alkoxide species. We began with attempts to prepare mixed RuO_2-TiO_2 systems since TiO_2 gels are known to be straightforward to prepare and indeed RuO_2-TiO_2 gels had been reported earlier by Kameyama et al[3].

4.2 Instrumentation

Many of the instrumental techniques are described in chapter 2. In addition thermal analysis was performed using a TA instruments SDT 2960 simultaneous is thermogravimetric analysis (TGA) and is differential thermal analysis (DTA) machine.

Powder X-ray Diffraction (XRD) analysis was performed using a Siemens D-500 diffractometer using the powder method with Cu K_a (Ni filtered) source. The scan range used was 2θ_=_10-90° with a step size of 0.02° . The scan rate was 0.5° 2θ per minute continuous scan. The patterns were compared to RuO_2 and TiO_2 data (JCPDS 21-1172 and JCPDS 21-21-1272, respectively). Some analysis was performed on a STOE STADI X-Ray diffractometer.

For XPS (X-ray photoelectron spectroscopy) analysis the six samples were mounted on specimen stubs using double sided adhesive tape and analysed using $MgK\alpha$ radiation at 170 W using 7.5 mm slits and 80/40 eV pass energies.

Transmission electron microscopy (TEM) analysis was performed using a Philips EM400T electron microscope (100 kV, a C2 aperture of 50 μm and a diffraction aperture of 30 μm). For scanning electron microscopy (SEM) analysis the samples were dispersed in methyl isobutyl ketone (MiBK) and drops of this dispersion

were placed on clean aluminium stubs. When dry these were coated with gold . Typical features were analysed by energy dispersive analysis of X-rays (EDX).

4.3 Results and Discussion

We begin with an account of our attempts to prepare mixed RuO_2-TiO_2 gels by sol-gel processing. We start with an account of the synthetic procedure followed

4.3.1 Attempted Sol-Gel Studies on RuO_2-TiO_2 Mixed Oxides

In non-aqueous sol-gel processing we require alcohol soluble precursors, preferably alkoxides. Following the method of Kameyama[3] we attempted to generate ruthenium alkoxides *in situ* from $RuCl_3.nH_2O$ and sodium alkoxide (1:3) ratio (equation 4.1)

$$RuCl_3 + 3NaOR \rightarrow Ru(OR)_3 + 3NaCl \qquad (4.1)$$

Thus six RuO_2-TiO_2 mixed oxides were prepared by generating solutions of ruthenium alkoxides from commercial $RuCl_3$ and sodium ethoxide solution (Table 4.1) under reflux in anhydrous alcohol. After cooling the solution was mixed with $Ti(OEt)_4$ and then hydrolysed using water with acid, base or no catalyst. Hydrogen peroxide, H_2O_2, was then added to all samples to oxidize Ru (III) to Ru (IV). The gels or powders obtained were dried under vacuum to remove residual solvent. The ruthenium to titanium ratio was kept at 4:1 at all times to investigate the effects of different catalysts on the final product.

Hydrolysis of the precursors using NH_3 (sample 1) and water (samples 2 and 3) gave powders in agreement with the previous work of Kameyama et al[3]. Hydrolysis of the ruthenium alkoxides using HNO_3 as a catalyst gave a mixture of gel and powder almost instantaneously which dispersed and then re-gelled upon addition of hydrogen peroxide. Hydrolysis using HNO_3 in a large volume gave a black sol and ultimately gave brown powders after several days. This is in contrast to the other experiments which gave black products. Hydrolysis of the isopropoxide precursor gave a gel within 10 minutes of the commencement of hydrolysis. Upon addition of peroxide, however, black particles were obtained.

Sample[a]	ruthenium alkoxide	[Ru][b]	hydrolysis catalyst
1	ethoxide	0.16M	$NH_{3(EtOH)}$
2	ethoxide	0.16M	none
3	ethoxide	0.32M	none
4	ethoxide	0.16M	$HNO_{3(aq)}$
5	ethoxide	0.04M	$HNO_{3(aq)}$
6	isopropoxide	0.16M	$HNO_{3(aq)}$

a) Typically water, catalyst and hydrogen peroxide (100 volumes) are added to 4mmol Ru and 1 mmol Ti (after 12mmol NaOR added to generate ruthenium ethoxide) in alcohol to give final ratio H_2O:M:H^+ = 5:1:0.1. b) Initial concentration of ruthenium before addition of NaOR,

Table 4.1: Ruthenium precursors and catalysts used in production of RuO_2-TiO_2 mixed oxides.

It is not in any way surprising that hydrolysis using base or neutral conditions gives powders, as according to Livage et al[1], these conditions will not lead to gels unless the alkoxide precursor is chemically modified due to fast condensation. Use of acid catalysts with ethoxide precursors would appear to give a gel as long as the conditions are not too dilute. In the case of the high dilution experiment it would appear that the concentration of the precursors ($\approx$ 0.05M) is too low for them to be able to form a continuous network and that the powders obtained are a mixture of partially condensed hydroxide species. The brown colour of the final product does suggest that it is not the same as that produced by hydrolysis and condensation using base or neutral conditions which give black powders. The addition of peroxide, which can speed up the rates of both hydrolysis and condensation, may then increase the rates of both reactions to the extent that the formation of particles is favoured over gelation. It is also possible from the long time taken to produce any precipitation that the solution may be too dilute. A further consideration must be the catalytic decomposition of H_2O_2 by $RuO_2.2H_2O$. If the RuO_2 is hydrated then this decomposition will raise the hydrolysis ratio (the ratio of water to metal) of the mixture and also the temperature of the solution and thus the nature of the final product will be affected.

In the case of the isopropoxide precursor the fast gel time relative to the ethoxide precursor suggests two possible explanations. i) The ruthenium ethoxide precursor may be oligomeric, like $Ti(OEt)_4$, and the isopropoxide is monomeric. The oxidation state of metal alkoxides are generally less than their normal coordination numbers leading to oligomerization or, in the case of bulky groups, such as isopropoxide, for which oligomerization cannot occur, solvent coordination. ii) Alternatively, after $Ti(OEt)_4$ addition to $Ru(O^iPr)_3$ mixed precursors are produced containing OEt and O^iPr groups which hydrolyse and condense at different rates. Supercritical drying of the

gel prepared without addition of peroxide led to a collapse of the gel network and a powder product. Replacement of ethanol with methanol normally allows supercritical drying but this in itself led to a collapse of the gel. This may be due to either: i) water in the methanol solution further hydrolysing the product; or ii) alcohol exchange of ethanol for methanol, giving bound methoxide groups, which will hydrolyse and condense more quickly than ethoxides.

4.3.2 Thermal Analysis of the RuO_2-TiO_2 Mixed Oxide system

Four of the samples produced have been studied by thermogravimetric analysis (TGA) and differential thermal analysis (DTA) (Figs 4.1-4.5). The ethoxide precursors, hydrolysed using NH_3, H_2O and HNO_3, were heated at 10 °C min^{-1} to 450 °C under O_2, the HNO_3 hydrolysed ethoxide was heated to 450 °C under N_2 and the HNO_3 hydrolysed isopropoxide was heated to 700 °C under O_2. Samples heated in oxygen generally contained three peaks: one endothermic peak at around 100 °C (although this peak was not present in the ammonia hydrolysed sample (1)) corresponding to desorption of adsorbed water (the size of these peaks may depend upon how long the sample is dried and the temperature of the oven), one exothermic peak between 190 and 275 °C and one exothermic peak close to 400 °C on the DTA trace. In the case of ammonia hydrolysis this was a sharp peak at 196 °C (Fig. 4.1) whereas all other cases showed a broad peak between 250and 275 °C with some evidence of a shoulder at lower temperatures (very noticeable in the case of the hydrolysed isopropoxide). Moreno et al[9] studied the DTA/TGA traces of metal titanates and assigned peaks in this area to the combustion of residual organic material. This seems to be a reasonable assignment for the RuO_2-TiO_2 samples as these peaks

coincide in all cases with sharp drops in weight in the TGA trace. Further evidence that this is the case arises from the heating trace under nitrogen (Fig. 4.4) where the peak becomes much smaller and less broad. This transition may in fact correspond to a different process altogether as it occurs at a lower temperature and may be responsible for the shoulder observed in the traces recorded under oxygen, this could be explained by further condensation of residual OH or OR groups in the sample. This reaction has been postulated as the reason why RuO_2 becomes more corrosion resistant after heat treatment, albeit at lower temperatures[10] than those observed in this work, as this condensation removes surface defects at which ruthenium oxidation can occur. Previous samples[10] that had been thermally activated for oxygen evolution were prepared from precursors with no organic components leading to condensation between OH groups, rather than between residual OR and OH groups or OR and OR groups.

The peak at around 400 °C also disappears when a sample is heated under nitrogen. This peak at 400 °C has been assigned by other workers[5] to the crystallization of rutile phase RuO_2 and in this case it would appear sensible to assign this transition to crystallization of either this phase or a mixed RuO_2-TiO_2 phase. Certainly there appears to be no transition at higher temperatures that could correspond to crystallization. Crystallization is, however, normally an endothermic process and the peak seen in the analysis of this sample is exothermic. Indeed, weight loss is observed during this transition, a feature not expected during cystallization. The precursors were generated from $RuCl_3$ and the possibility exists that not all the bound chloride is substituted by OEt^- or O^iPr^- during the generation of the alkoxide precursor and that the transition at 400 °C represents oxidative removal of these chloride atoms by the oxygen atmosphere. This oxidation could also explain why the peak at 400 °C is

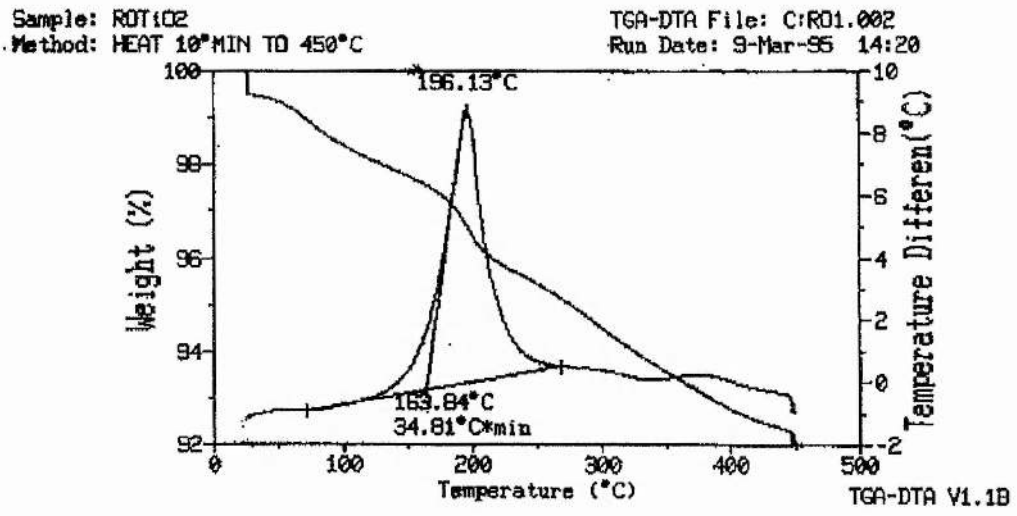

Figure 4.1: DTA/TGA pattern under oxygen for the RuO_2-TiO_2 sample (1) obtained from ethoxide solution with ammonia catalysis.

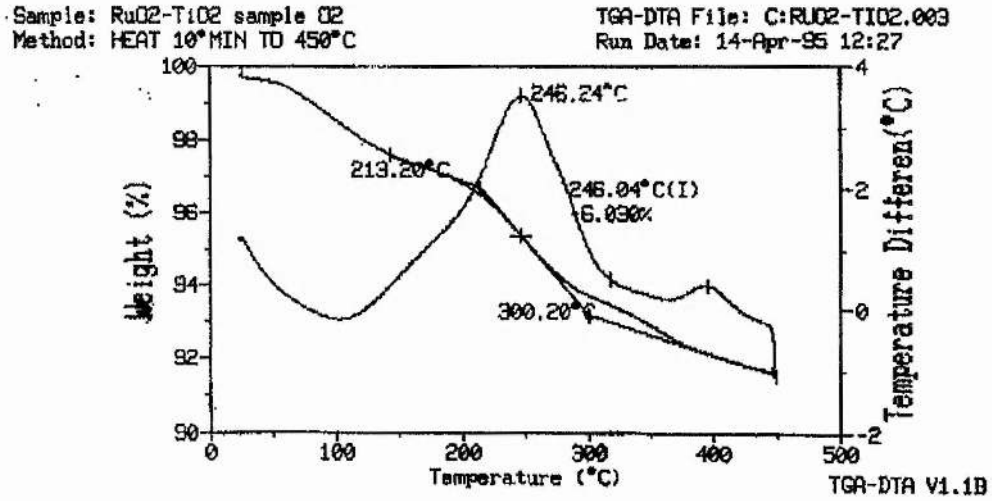

Figure 4.2: DTA/TGA pattern under oxygen for the RuO_2-TiO_2 sample (2) obtained from ethoxide solution without catalyst.

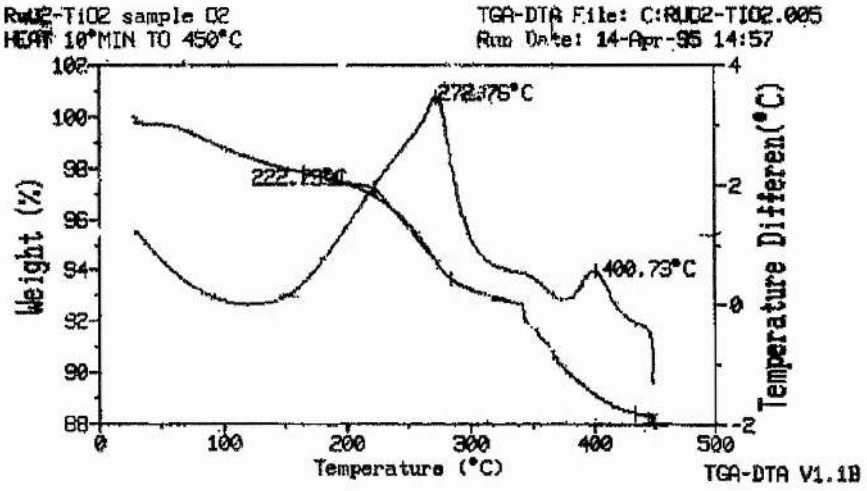

Figure 4.3: DTA/TGA pattern under oxygen for the RuO_2-TiO_2 sample (4) obtained from ethoxide solution with acid catalysis.

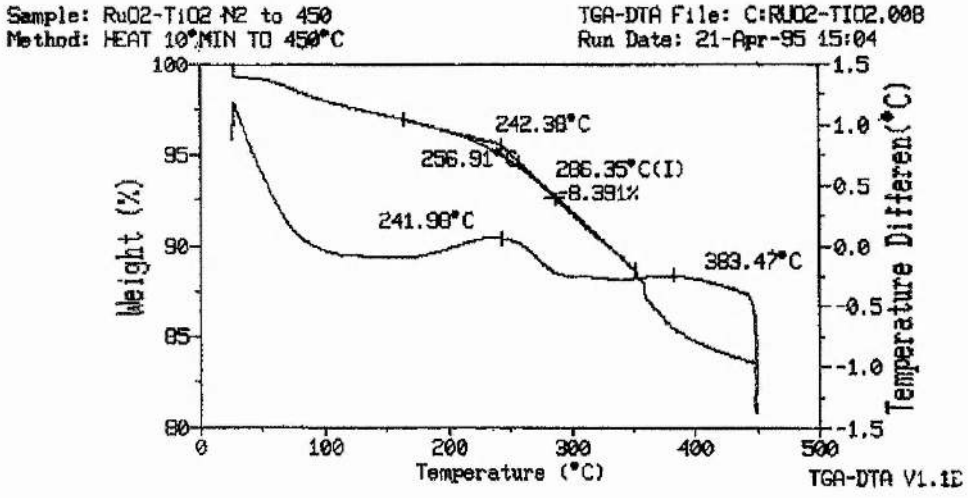

Figure 4.4: DTA/TGA pattern under nitrogen for the RuO_2-TiO_2 sample (4) obtained from ethoxide solution with acid catalysis.

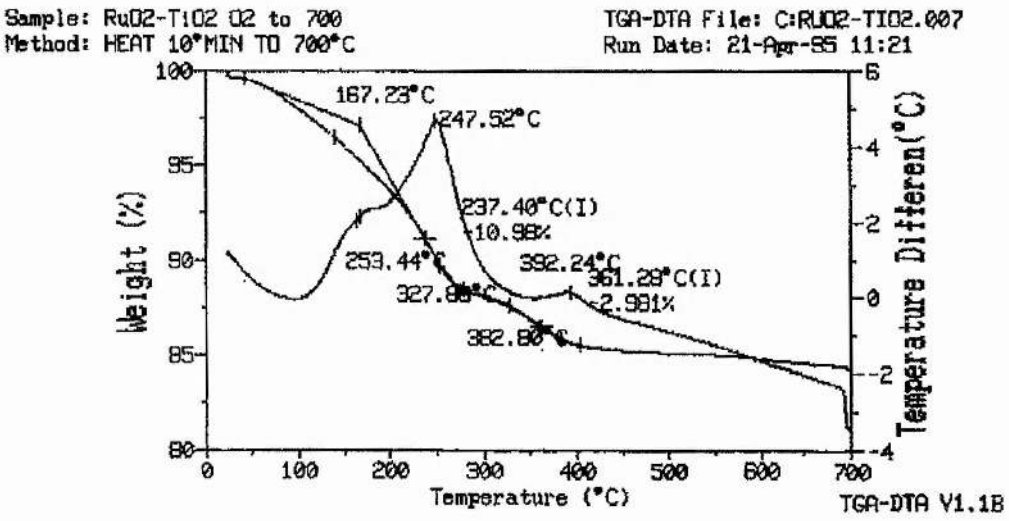

Figure 4.5: DTA/TGA pattern under oxygen for the RuO_2-TiO_2 sample (6) obtained from isopropoxide solution with acid catalysis.

absent in the sample heated under nitrogen. Although assigning this transition to oxidative removal of chloride implies that there is no crystallization occurring it is likely that the crystallinity observed in the samples examined by X-ray diffraction (section 4.3.4) arises from the calcination time and the temperature program used (3 h at 250 °C to burn off organic material, followed by 3 h at 450 °C).

The TGA traces were different depending on whether hydrolysis was performed under basic, neutral or acidic conditions. Basic or neutral hydrolysis gave curves with one sharp area of weight loss, coinciding with the peaks corresponding to the combustion of residual organic material, whereas acid hydrolysed samples have a second area of weight loss starting at around 330 °C. This leads to overall weight losses of around 12% up to 450 °C for acid hydrolysed samples compared to about 8% for base or neutrally hydrolysed samples. This is a surprising result as acid catalysis is expected to lead to more extensive hydrolysis than base catalysis and thus to less residual organic matter in the final product. These results suggest that hydrolysis of either the ruthenium or the titanium precursor (or both) is not extensive, with alkoxide groups remaining even using the acid catalyst. So in order to account for the elimination of alkoxide groups under basic conditions we propose that condensation is taking place by alkoxolation (equation 4.2)

$$\equiv\text{M-OR} + \text{HO-M}\equiv \rightarrow \text{M-O-M} + \text{ROH} \qquad (4.2)$$

4.3.3 XRF Analysis of the Uncalcined RuO_2-TiO_2 Mixed Oxide System

X-Ray Fluorescence (XRF) is a convenient method for determining the bulk composition of insoluble solid samples. The composition is normally reported as wt %

by this technique and the observed molar ratio of Ru:Ti of the samples is calculated by taking the wt % data and dividing by the relative atomic masses of the elements (Table 4.2).

The values for the ratio of ruthenium to titanium in the final product are vastly different to those of the starting material (Ru:Ti = 4:1). Clearly, the sol-gel conditions selected are using excess ruthenium in terms of the product obtained. This suggests that much of the ruthenium is precipitating out of the system before the titanium precursor is added (precipitation of a black solid is observed during preparation of the ruthenium alkoxides).

Problems, however, arise with this argument. If the RuO_2 precipitated before the $Ti(OEt)_4$ was added it would still be present when the final product was centrifuged or dried. A black precipitate does, however, remain attached to the side of the reaction vessel after the product is removed; this precipitate is insoluble in nearly all solvents and is postulated to be RuO_2, or possibly ruthenium metal.

SAMPLE	wt % Ru	wt % Ti	Observed Molar Ratio Ru:Ti
1	27.0	32.8	0.28:0.72 (1:2.57)
2	19.7	32.2	0.22:0.79 (1:3.59)
3	22.0	27.2	0.28:0.72 (1:3.88)
4	23.5	27.0	0.29:0.71 (1:2.45)
5	18.4	25.8	0.25:0.75 (1:3.00)
6	31.8	36.7	0.29:0.71 (1:2.45)

Table 4.2: XRF Results for RuO_2-TiO_2 mixed oxide samples obtained by sol-gel processing

The equivalent oxide content for a metal oxide produced by the sol-gel method is given by the $MO_2/M(OR)_x$ ratio, a measure of the degree of hydrolysis in the product. This ratio is usually obtained from weight loss measurements before and after calcination. Yoldas[11] calculated this ratio for TiO_2 produced by sol-gel methods to determine the effects of hydrolytic polycondensation parameters on the final product. The XRF results also give an indication of the oxide content of the samples providing a measure of the extent of hydrolysis and condensation under the different conditions. The calculated oxide contents of the alkoxide precursors (assuming no oligomerization or solvent coordination) are 58%, 49% and 35% for $Ru(OEt)_3$, $Ru(O^iPr)_3$ and $Ti(OEt)_4$ respectively. The values for the samples given in Table 4.3 are calculated from the ruthenium and titanium values (assuming that Ru and Ti species exist as condensed polymers of RuO_2 and TiO_2 or a mixed oxide) as follows:-

$$\text{Equivalent oxide content} = \left(\frac{M_w\ RuO_2}{A_w\ Ru}\right) * \text{wt \% } RuO_2 + \left(\frac{M_w\ TiO_2}{A_w\ Ti}\right) * \text{wt \% } TiO_2$$

The values in Table 4.3 for the unaccounted mass (i.e mass due to organic material or water) are in good agreement with the results determined by thermogravimetric analysis, with the only exception being the result for the isopropoxide precursor (sample 6). For this sample the TGA trace shows a weight loss corresponding to around 15%. The weight loss observed in the TGA was assigned to loss of coordinated water or solvent and unreacted organic groups. The XRF results show that, for ethoxide precursors, if ammonia is used as catalyst the oxide content is the highest and that this value drops for water and acid catalysts. This conforms with

the accepted principle that base catalysed sol-gel reactions lead to a denser material[1]. Acid catalysis facilitates hydrolysis but retards condensation, whereas the reverse is true for base catalysis. Thus it would appear that the lower oxide contents in the acid hydrolysed ethoxides are due to less extensive condensation and, given that base catalysis would not remove all the alkoxide groups by hydrolysis, that condensation in this system is taking place by alcoxolation or olation rather than oxolation. One factor, though, that must be considered is that the acid-hydrolysed samples are dried gels and may, therefore, be subject to contamination with the sodium chloride produced as a by-product in the preparation of the ruthenium alkoxide species. This remains dissolved in the solvent trapped within the gel network and is deposited when the solvent is evaporated. Thus the proportion of the final product corresponding to RuO_2 and TiO_2 and partially reacted precursors will be lower for gel samples.

Sample	Oxide Content /%	Unaccounted Mass /%
1	93.6	6.4
2	86.6	13.4
3	84.0	16.0
4	84.1	15.9
5	78.5	21.5
6	102.1	-2.1

Table 4.3: XRF Determined Bulk (5-500 μm) Metal Oxide Contents of the RuO_2-TiO_2 Samples obtained by sol-gel techniques.

Sample 6, showing anomalous behaviour, derives from an isopropoxide

precursor which is probably a monomer containing bound solvent molecules, due to the steric hindrance of the bulky isopropoxide groups preventing oligomerization. It is, therefore, more reactive than the oligomeric ethoxide precursors as it has been shown[1] that bound solvent molecules are easier to remove than coordinated alkoxide species. This allows faster, and possibly more extensive, hydrolysis and may explain the high oxide content value for this system.

4.3.4 Powder XRD analysis of the Calcined RuO_2-TiO_2 Mixed Oxide System

The X-ray diffraction patterns for the six samples are shown in Figs 4.6-4.11. The analysis reveals three major features. Firstly, it is clear that the samples are more likely mixtures of RuO_2 and TiO_2 rather than a solid solution of the two. This becomes apparent from the peak positions. The TiO_2 has crystallized in the anatase phase as indicated by clear peaks at around $2\theta = 25.28°$ and 48.05° and the RuO_2 has crystallized in a different, rutile, phase with peaks at values close to $2\theta = 28°$ and 35°. If the products were mixed oxides a single rutile phase should be formed with peaks at 2θ values between the pure RuO_2 and TiO_2 values, depending upon the ratio of the metals, as has been observed in other work on mixed RuO_2-TiO_2 oxide systems[5]. Previous work[3] has suggested that it is hard to obtain mixed oxides in Ti rich systems. The peak values for RuO_2 in all cases do show a slight displacement from the values for pure RuO_2 and it is possible that the precursors do mix to some extent, this being more apparent in the case of the ammonia and water hydrolysed systems (Samples 2 and 3, Figs 4.6-4.8) especially the low volume sample (3, Fig. 4.8), where there is evidence of a shift in the rutile peak at $2\theta = 28.02°$ to a value that would correspond to a mixed oxide (the rutile phase of TiO_2 has major peaks at $2\theta = 27.45°$ and 36.08°).

The second interesting feature of the patterns is the presence of metallic ruthenium in all the samples except the ammonia hydrolysed sample (1). Osaka et al[12] examined the application of sol-gel techniques for the production of iridium dioxide and found that with ethoxide precursors there was a tendency to precipitate metallic iridium upon calcination. This was suggested to be due to the partial charge (as calculated using the method of Livage[1]) on the iridium metal centre being too low and that consequently iridium ethoxides are not readily susceptible to hydrolysis. It would appear reasonable to assume the same of ruthenium in this case as the electronegativity is the same as for Ir (2.2 in Pauling's scale). The absence of metallic Ru in the ammonia hydrolysed sample may be due to efficient alcoxolation by hydroxide groups bound to Ti removing coordinated ethoxide groups bound to Ru rather than these groups being hydrolysed as follows :-

$$\equiv\text{Ti-OH} + \text{RO-Ru}\equiv \rightarrow \equiv\text{Ti-O-Ru}\equiv + \text{ROH}$$

Acid catalysis retards this condensation reaction as the hydrolysed species involved are often protonated and thus less likely to interact with one another. This means that titanium species more likely to condense with themselves than with the low partial charge ruthenium centres leaving unreacted R-OR units which can pyrolyse to the metal. It has also been postulated[5] that ruthenium disproportionates to the metal and the oxide under sol-gel conditions. This may happen in this system; however, the lack of metal in the ammonia hydrolysed sample (1, Fig 4.6)) suggests that this is not the case, since if disproportionation were occurring then this sample should also contain some metal.

The third important feature of these patterns concerns the impurities present in

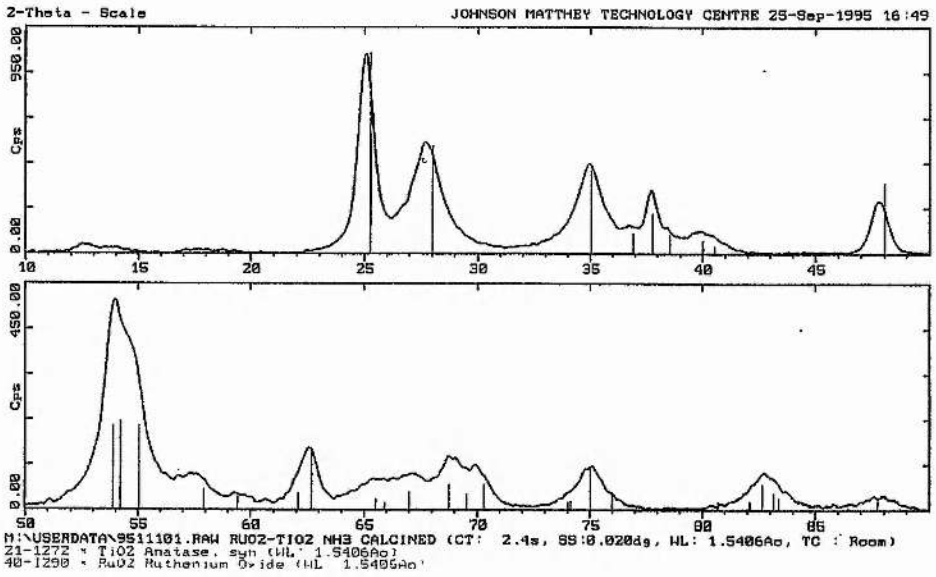

Fig. 4.6: X-ray powder diffraction pattern (Cu Kα) for ammonia hydrolysed RuO_2-TiO_2 sample (1). Vertical peaks represents library values for species present.

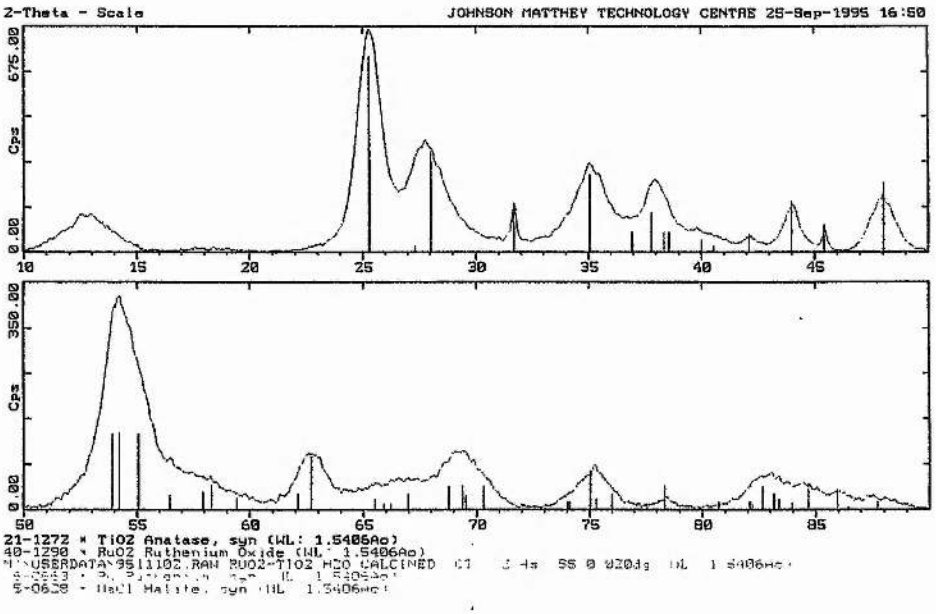

Fig. 4.7: X-ray powder diffraction pattern (Cu Kα) for water hydrolysed RuO_2-TiO_2 sample (2)

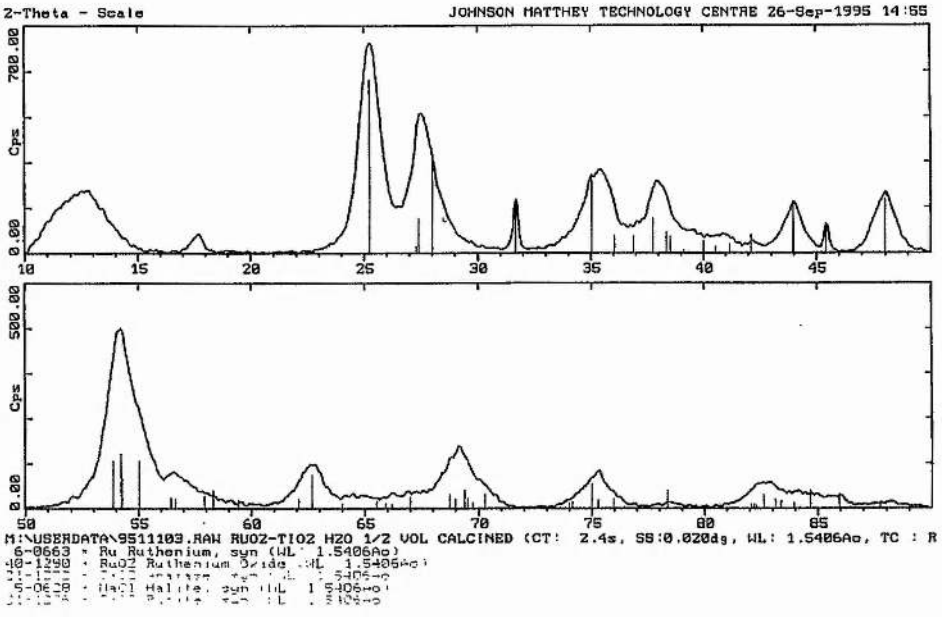

Fig. 4.8: X-ray powder diffraction pattern (Cu Kα) for water hydrolysed, low volume, RuO_2-TiO_2 sample (3).

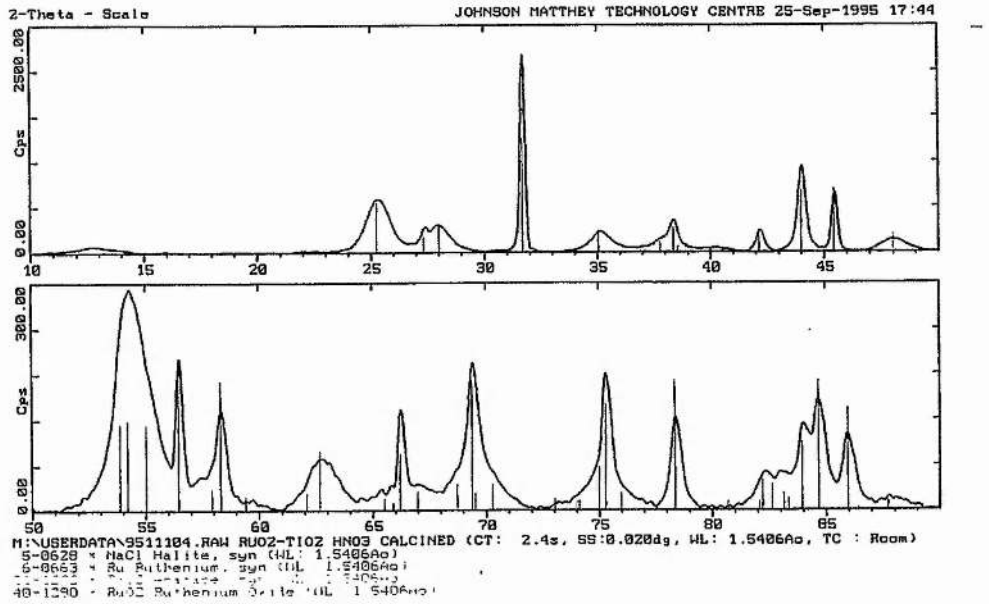

Fig. 4.9: X-ray powder diffraction pattern (Cu Kα) for HNO_3 hydrolysed RuO_2-TiO_2 sample (4).

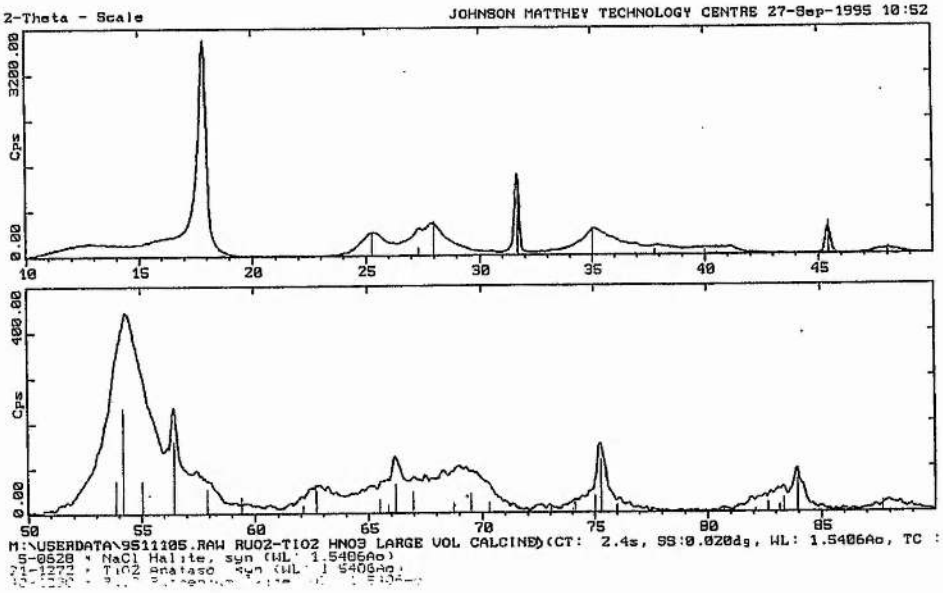

Fig. 4.10: X-ray powder diffraction pattern (Cu Kα) for HNO_3 hydrolysed, large volume, RuO_2-TiO_2 sample (5).

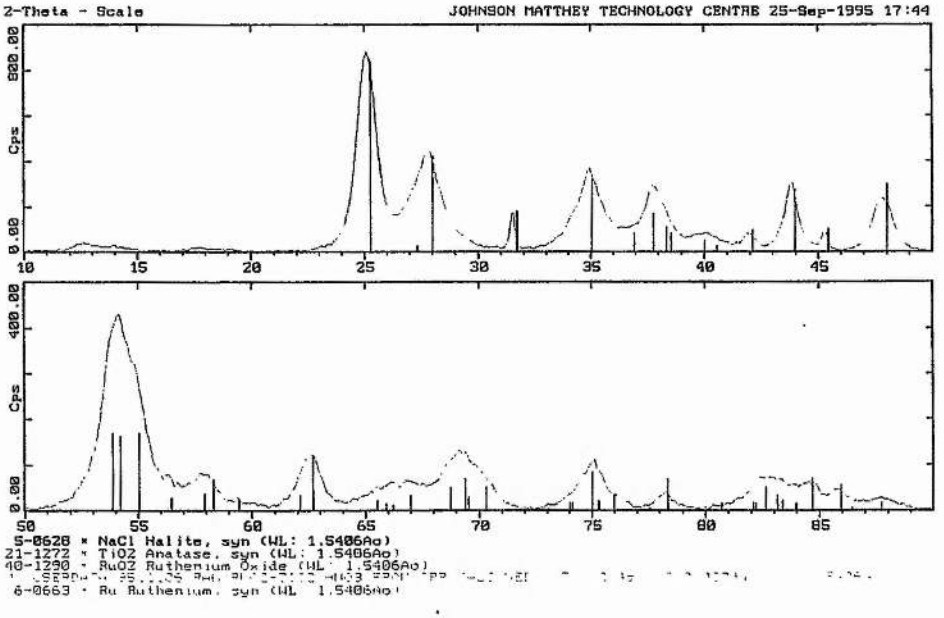

Fig. 4.11: X-ray powder diffraction pattern (Cu Kα) for HNO_3 hydrolysed, O^{i}Pr precursor, RuO_2-TiO_2 sample (6).

the samples. All samples except the ammonia hydrolysed sample contain varying quantities of sodium chloride, NaCl. In the case of the powder samples (4.6-4.8 and 4.10) this might be assigned to poor washing. But in the case of the acid hydrolysed ethoxide sample it is not surprising that NaCl appears as a major peak. Gels encase the whole solvent system and it is clear that in this case the NaCl produced by the generation of the ruthenium alkoxides will get trapped within this gel network and will not be removed by drying. This will not be a problem for powder samples as the NaCl will remain in solution when these precipitate leading to less contamination.

The TGA patterns for samples in which ruthenium metal is found after calcination show greater overall weight loss than the ammonia hydrolysed sample (1) in which no metallic ruthenium is found. Clearly, not only residual carbon and hydrogen are being lost on heating, but also oxygen, probably due to ruthenium mediated oxidation of the ethoxide to H_2O and CO_2. The differential thermal analysis (DTA) pattern is also different for sample 1 compared to other samples. The fact that no metallic ruthenium is found for the ammonia hydrolysed sample suggests that all the weight loss observed in this system is due principally to the loss of coordinated solvent, with very little being due to combustion of unreacted material. It also explains why this sample has a sharp single peak in the DTA curve between 190°C and 275°C whereas other samples have a broad peak due to loss of residual alkoxide groups.

4.3.5 XPS Analysis of the Uncalcined RuO_2-TiO_2 Mixed Oxide System

X-ray photoelectron spectroscopy (XPS) typically gives compositional data for the surface layers ($\approx$ 30 A) corresponding to the penetration depth of the sof X-rays into the sample.

The ratios of Ru:Ti at the surface of the samples and the positions of the Ru $3d_{5/2}$ lines from the XPS spectra are given in Table 4.4, along with the bulk ratios from XRF for comparison purposes. The XPS spectrum of the ammonia hydrolysed sample (1) and the enlarged spectrum around the Ru $3d_{5/2}$ line are given in Figs 4.12 and 4.13 respectively.

Sample	Position of Ru $3d_{5/2}$ Line /eV	Surface Ru:Ti Ratio (XPS)	Bulk Ru:Ti Ratio (XRF)
1	281.3	0.15	0.38
2	280.9	0.16	0.28
3	281.7	0.25	0.38
4	280.7	0.25	0.41
5	281.9	0.33	0.33
6	281.0	0.19	0.41

Table 4.4: XPS Results for the RuO_2-TiO_2 samples obtained using sol-gel techniques

Surface analysis of Ru/Ti samples is complicated by the presence of overlapping peaks. In this case the Ru 3d levels are obscured by the C 1s level (Fig 4.13) and the Ru 3p levels are partially obscured by the overlaying Ti 2p level. The data were therefore quantified for the Ru/Ti system by using the peak-fitting program in the software used for the analysis to fit a Ru $3d_{5/2}$ level alongside the C 1s peak and to ratio this with the Ti 3p level[13].

The position of the Ru $3d_{5/2}$ line is at the same energy value in all cases and is assigned to an oxidised Ru species which could be either Ru(III) or Ru(IV)[9]. In none of

the uncalcined samples examined was any Ru(0) detected. This suggests that the metallic ruthenium found in the XRD analysis of the samples after calcination arises from a thermal process, namely the thermal degradation of unreacted ruthenium alkoxides as postulated in section 4.3.4, rather than from disproportionation of Ru(III) to Ru(IV) and Ru(0), although this disproproportionation may be occurring in the bulk. This is further evidence that simple ruthenium alkoxides may not be reactive enough for this system to work efficiently.

The XPS analysis also detects impurities present at the surface of the samples. In all cases traces of four elements, sodium, chlorine, nitrogen and silicon are detected. The largest amount of sodium and chlorine (the powder XRD evidence suggesting that these elements are in the form of sodium chloride) is found in the dried gel sample (4). The presence of silicon and nitrogen in the samples may be due to contamination from glassware, reaction with the nitric acid used to catalyse hydrolysis or possibly as a contaminant arising present in the ethanol solution. The ethanol used was dried over molecular sieves and it has been suggested[6] recently that these sieves can introduce salts into the solvent through zeolite-induced autopyrolysis of trace water in the system.

Concerning the variation in the values for the Ru:Ti ratios at the surface, the values are consistently lower than those for the bulk in all cases apart from that of the value for the high dilution experiment (sample 5). The trend in the samples prepared from ethoxide precursors is that the surface concentration of titanium increases as follows: base $\rightarrow$ none $\rightarrow$ acid catalyst. Experimental observations suggest that black RuO_2 precipitates are forming before the titanium precursor is added to the system, suggesting that hydrolysis and condensation of the ruthenium alkoxide precursor is occurring as it is generated and before the introduction of catalyst. Obviously this

process should be unaffected by the variation in catalyst, and will lead to the particles

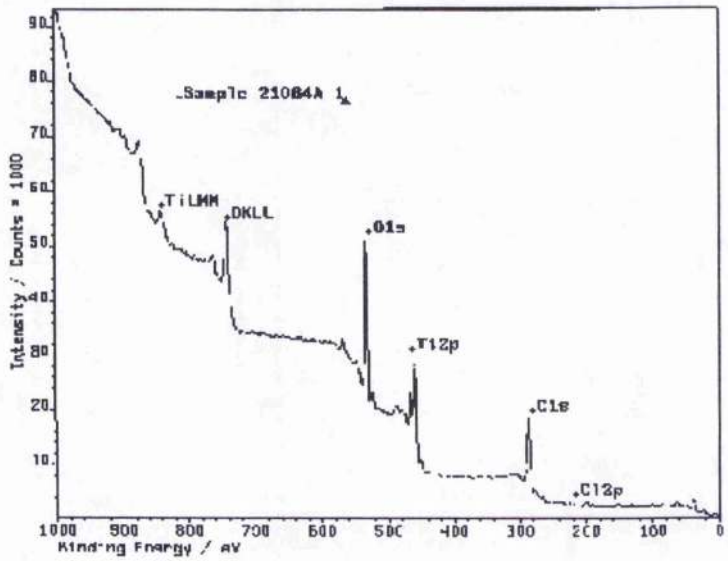

Fig. 4.12: XPS spectrum of ammonia hydrolysed RuO_2-TiO_2 sample (1).

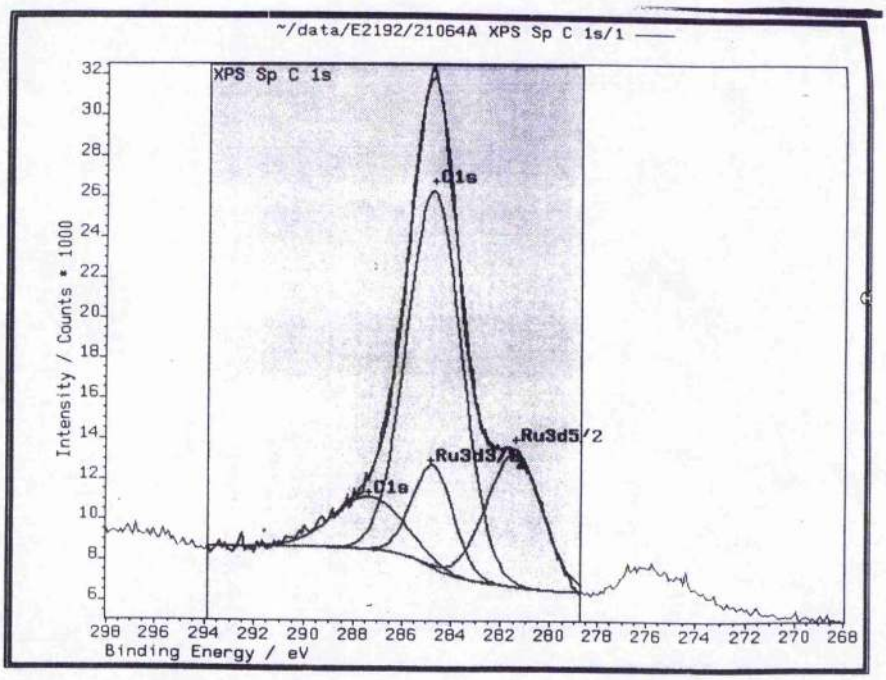

Fig. 4.13: XPS spectrum of NH_3 hydrolysed RuO_2-TiO_2 sample (1), expansion of area around Ru $3d_{5/2}$ line.

of RuO_2 being approximately the same size in each experiment. Thus any comparison with the bulk values is more likely to represent the variation of surface to bulk titanium with catalyst than any variation for a mixed oxide. Base catalysis tends to favour the formation of small TiO_2 particles whereas acid catalysis leads to larger for particles. Hence, for base catalysis, the surface area per unit volume will be higher than catalysed system, leading to a higher overall ratio of Ti surface to Ti bulk for this system if the same initial amount of $Ti(OEt)_4$ is used. Thus, if the RuO_2 particles should be roughly consistent in size in each experiment and are condensing separately from the TiO_2 particles/gels, the base catalysed sample should have the lowest Ru:Ti ratio at the surface. Daolio et al[10] measured the surface and bulk concentrations of ruthenium and titanium in mixed oxide coatings by secondary ion mass spectrometry and found that on heat treatment the ruthenium accumulated in the bulk. However, our XPS analysis was performed on uncalcined samples and it is less likely that the same segregation phenomenon is being observed.

One further point arises. If it is assumed that not all of the ruthenium precursor is precipitating as RuO_2 before the $Ti(OEt)_4$ is added then the surrounding gel network of will be depleted in ruthenium. Evidence for this arises from the three acid hydrolysed samples. The highest Ru:Ti value is observed in the high dilution experiment where the bulk and surface values are the same. The dilution means that condensation is slower for both metals and thus the precursors will be better mixed and clusters of RuO_2 within a TiO_2 network are less likely to be formed, especially given that this system did not gel.

Similarly, as pointed out earlier, $Ru(O^iPr)_3$ is more reactive than $Ru(OEt)_3$ and thus hydrolysis and condensation during the preparation stage of the reaction are likely

to be more extensive for $Ru(O^iPr)_3$. Hence bulk RuO_2 particles are more likely to be trapped within a gel network of TiO_2. This sample would then have a lower value for the surface Ru:Ti ratio than the other acid-catalysed systems.

4.3.6 Electron Microscopy Studies on the Uncalcined RuO_2-TiO_2 Mixed Oxide System

4.3.6.1 SEM Studies

Scanning electron micrographs of the six samples are shown in Figs 4.14-4.19.

Previous work[3] has shown that, by using ammonia as a catalyst, fine (< 1 μm) particles of RuO_2-TiO_2 mixed oxides could be formed using sol-gel techniques. From the XRD data shown earlier and the microscopy it is clear that our attempt to repeat these results (sample 1) has not been successful as a solid solution was not obtained. Figure 4.14 shows that the particle size distribution is large in this sample and is in general of the order of microns rather than nanometers. Higher magnification (1000X, not shown) indicates that large particles are covered by much smaller particles.

The two systems prepared in the absence of a catalyst (samples 2 and 3, Figs 4.15 and 4.16) give similar micrographs to the sample prepared using ammonia as a catalyst. Again, particle size varies dramatically, but is in general larger when no catalyst is present than for the ammonia-catalysed sample. An interesting feature of the micrograph for sample 2 is that there appear to be two species present as indicated by the presence of particles of different shades. It is conceivable that the more conductive darker particles are RuO_2 rich and that the lighter particles (non-conducting and therefore liable to charging) are TiO_2 rich. This is evidence for the ruthenium

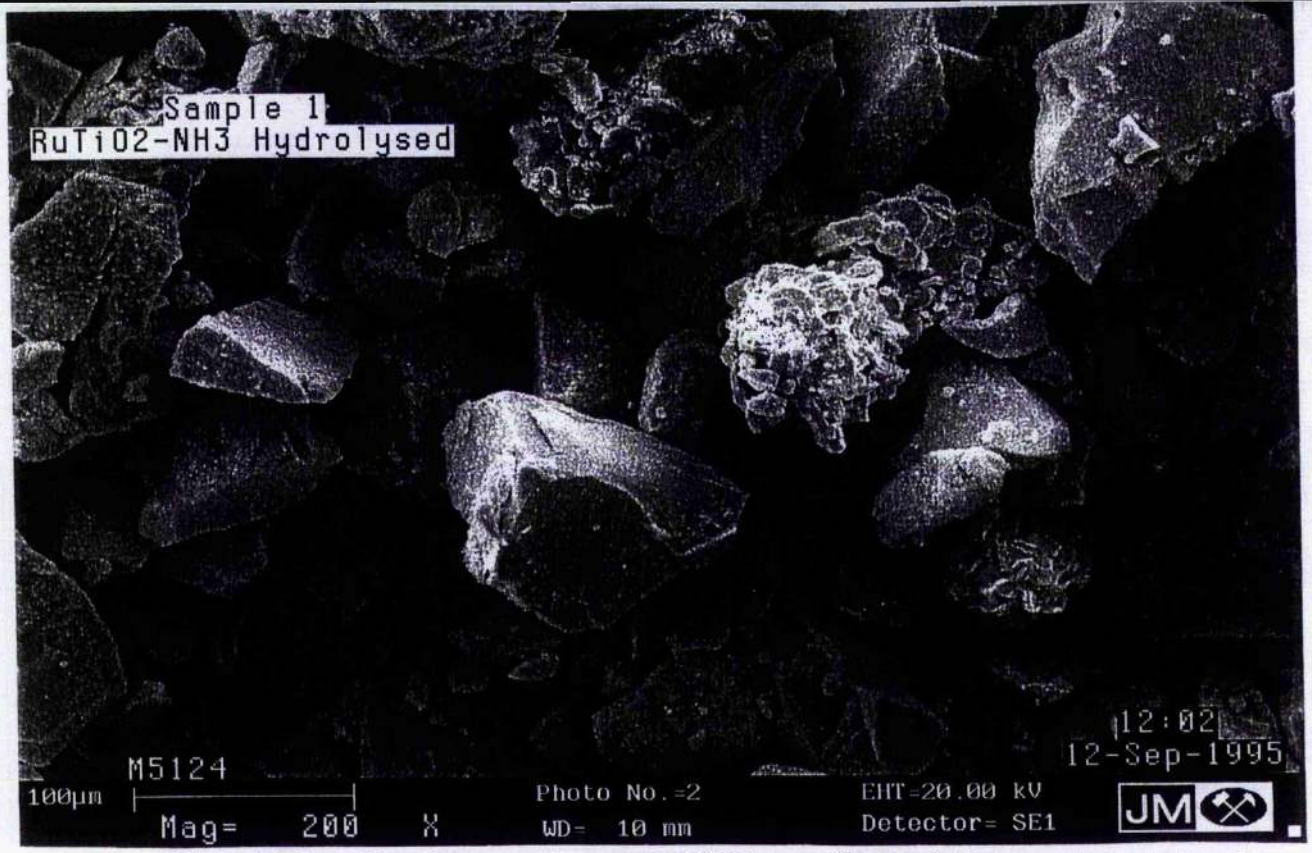

Fig. 4.14: Scanning electron micrograph (200X magnification) of ammonia hydrolysed RuO_2-TiO_2 sample (1).

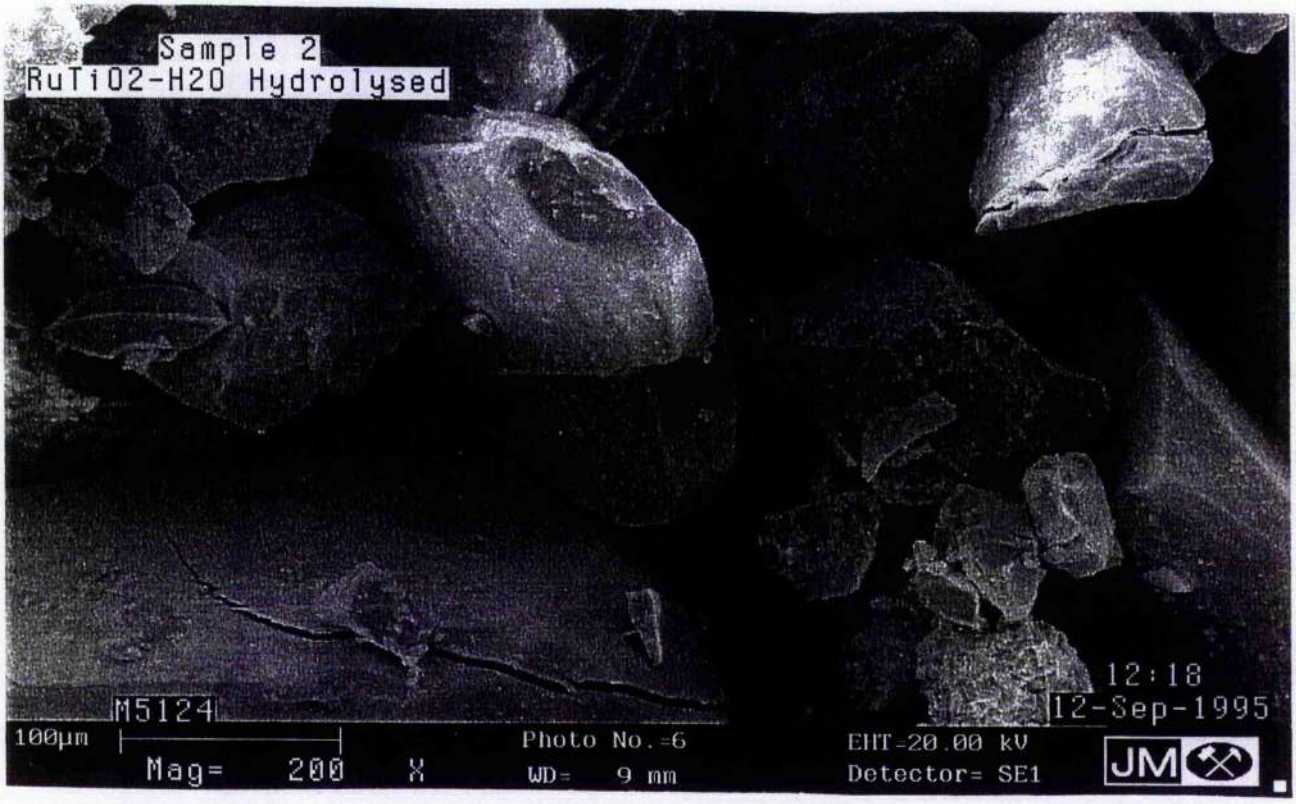

Fig. 4.15: Scanning electron micrograph (50X magnification) of water hydrolysed RuO_2-TiO_2 sample (2).

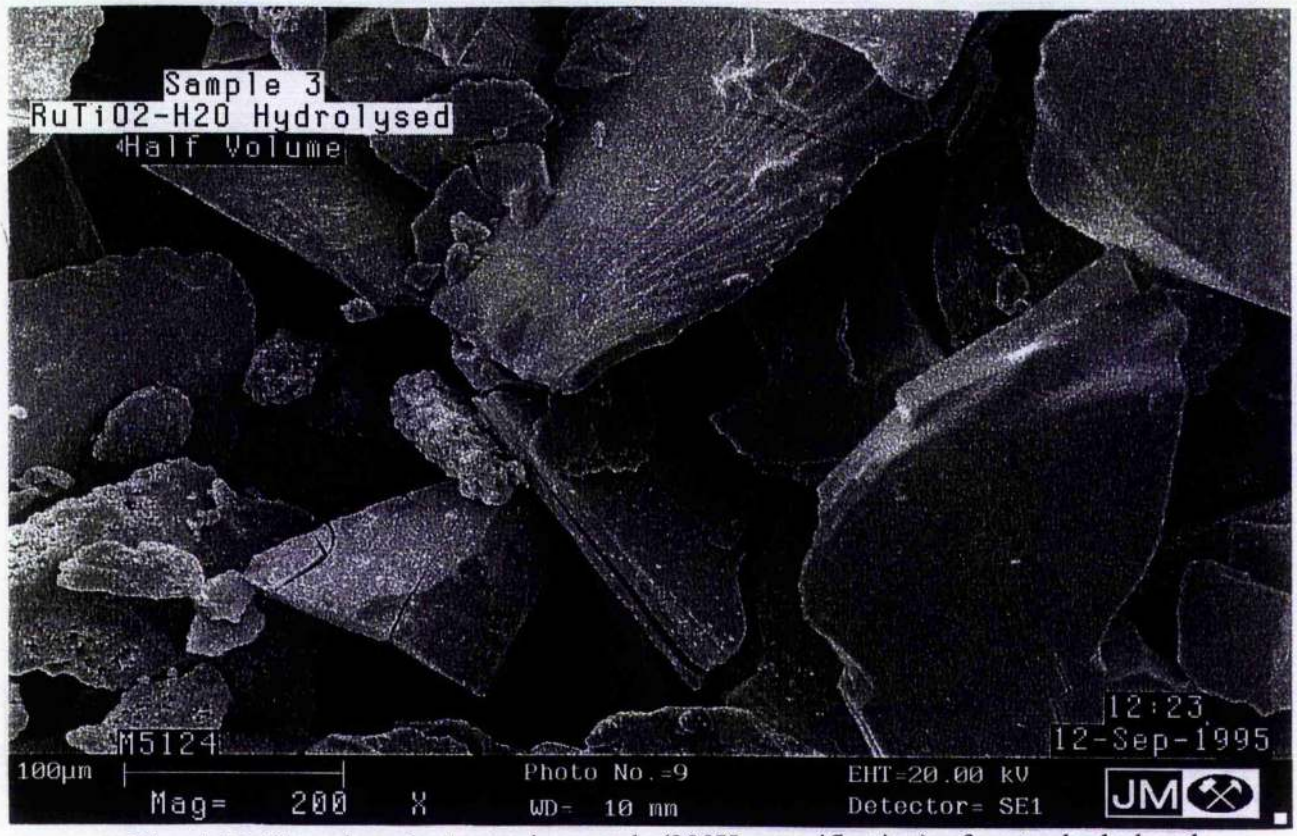

Fig. 4.16: Scanning electron micrograph (200X magnification) of water hydrolysed, low volume, RuO_2-TiO_2 sample (3).

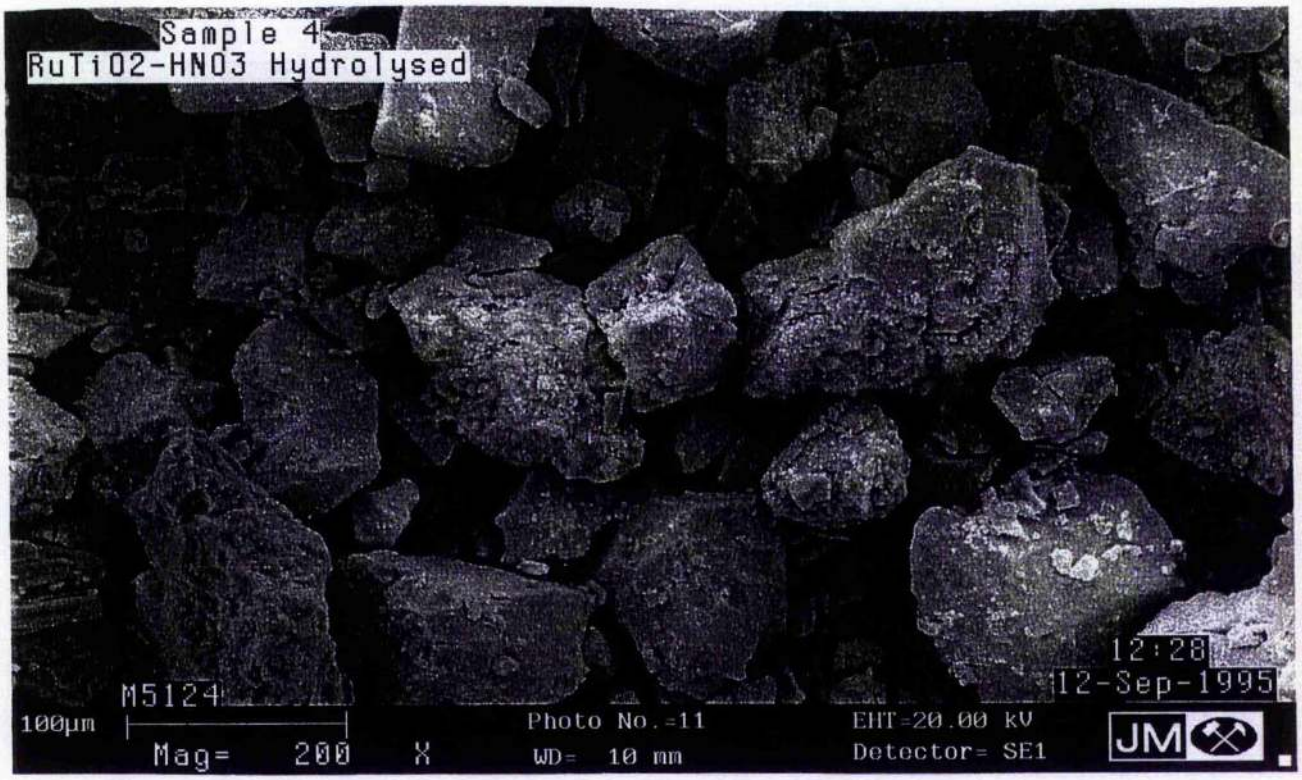

Fig. 4.17: Scanning electron micrograph (200X magnification) of HNO_3 hydrolysed RuO_2-TiO_2 sample (4).

Fig. 4.18: Scanning electron micrograph (200X magnification) of HNO_3 hydrolysed, large volume, RuO_2-TiO_2 sample (5).

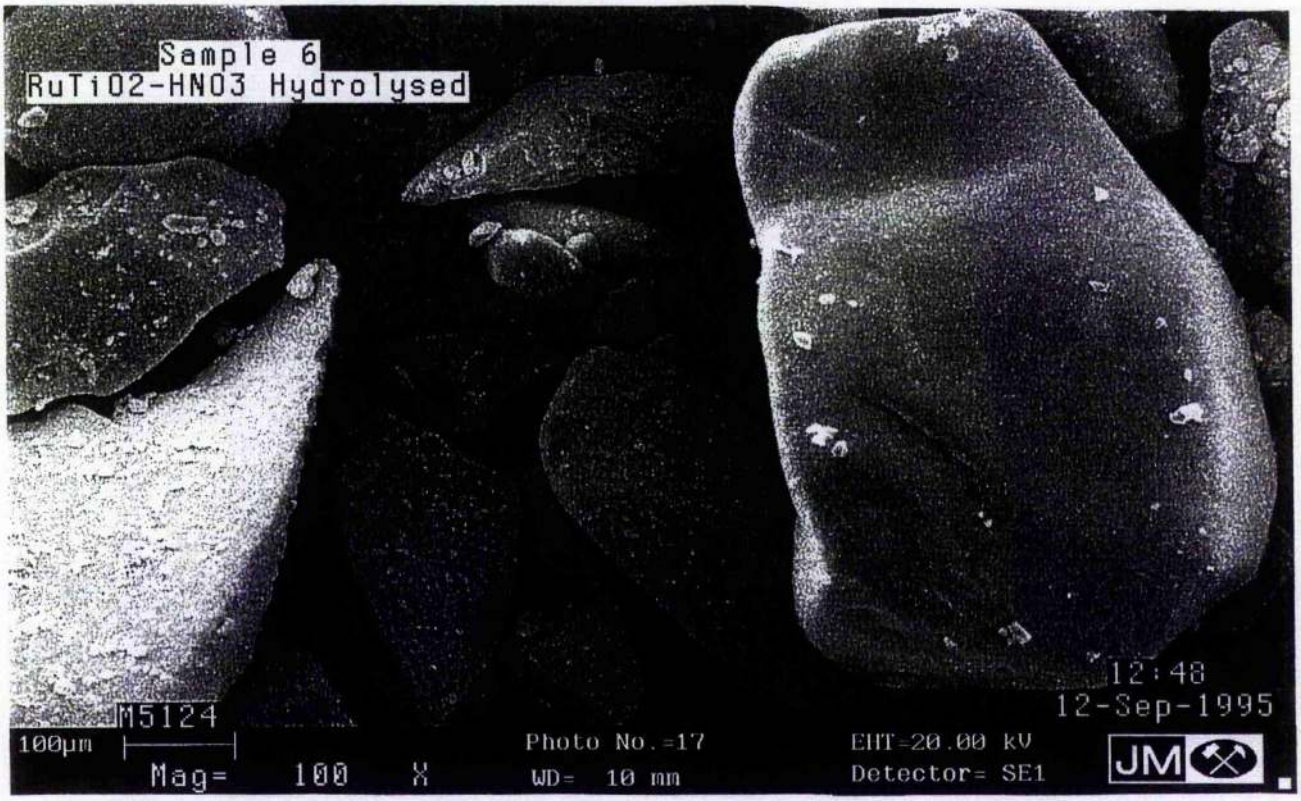

Fig. 4.19: Scanning electron micrograph (100X magnification) of HNO_3 hydrolysed, O^iPr precursor, RuO_2-TiO_2 sample (6).

precursor.undergoing hydrolysis and condensation separately, most likely before $Ti(OEt)_4$ is added to the system

The morphology of the micrograph for the acid hydrolysed ethoxide sample (4, Fig. 4.17) is significantly different to that of the base-catalysed and catalyst-free samples (1-3). Whereas previous samples showed plates or smooth particles in this sample the grains are rough. Examination at a magnification of 1000X (not shown) reveals that the particles are covered with much smaller particles. In contrast (Fig. 4.18 for sample 5), the micrograph of the acid-hydrolysed, high dilution mixture is dominated by these small particles (< 1μm diameter) The size of the particles at low concentration is expected to be small given that the large molecular separation of the reactants will lead to less extensive condensation. The small particles on the surface of the dried gel particles in sample 4 might therefore be identified as uncondensed Ru or Ti ethoxide or hydroxide species.

The micrograph for the acid hydrolysed isopropoxide sample, 6, (Figure 4.19), like sample 2, reveals the presence of two distinct species, as indicated by the presence of particles of different shades. Particle size varies dramatically from fractions of millimetres to a few microns. The particles are less granular than those produced using ethoxide precursors. $Ru(O^iPr)_3$ will hydrolyse quicker than $Ru(OEt)_3$ and thus will also be more condensed prior to the mixing in of the titanium precursor leading to segregated RuO_2 and TiO_2 particles.

4.3.6.2 TEM Studies

The EDX/electron diffraction analysis of the six samples reveals several interesting features. Firstly, the analysis gives an indication of the positions of

ruthenium oxide and ruthenium aggregate clusters within the titanium oxide network. Examination of each of the micrographs (e.g Fig. 4.20 which shows the micrograph at 115000X magnification for sample 1) shows two dark aggregate clusters (0.5 μm in diameter) of RuO_2 nanocrystallites (2-4 nm in size) within the surrounding TiO_2 particulate matrix. Although there appears to be some mixing in all cases, most of the ruthenium present seems to be concentrated in these clusters, as is apparent in Fig 4.20. This is further evidence of the pre-hydrolysis and condensation of the ruthenium precursor before addition of $Ti(OEt)_4$ and hydrolysis catalyst. The presence of nanocrystalline RuO_2 in the samples 1-3 suggests that the condensation is reversible in these systems. Reversible condensation has been observed in systems where base is used as the catalyst[14], as the base can regenerate either alkoxide or hydroxide groups. This may explain why other base-catalysed sol-gel RuO_2-TiO_2 systems have given mixed oxides, as the base catalyst may be redissolving the RuO_2 produced during generation of the ruthenium alkoxide, allowing better mixing with the titanium precursor. It is surprising that the catalyst-free and acid-hydrolysed isopropoxide samples show the presence of crystalline RuO_2. This may arise from crystallization occurring during solvent removal.

The selected area diffraction patterns for the six samples indicate a monoclinic TiO_2 structure for the uncalcined samples with the ammonia hydrolysed sample (1) also containing some of the anatase phase of TiO_2. The base and water hydrolysed ethoxide samples (1-3) along with the acid hydrolysed isopropoxide sample (6) all contain nanometre scale ruthenium oxide crystallites. The precursor that gave the smallest particles (< 1nm) was sample 3, where hydrolysis has been performed in a smaller volume of solvent. The small size of the particles in this sample suggest that condensation of the ruthenium and titanium is occurring together and that a partial

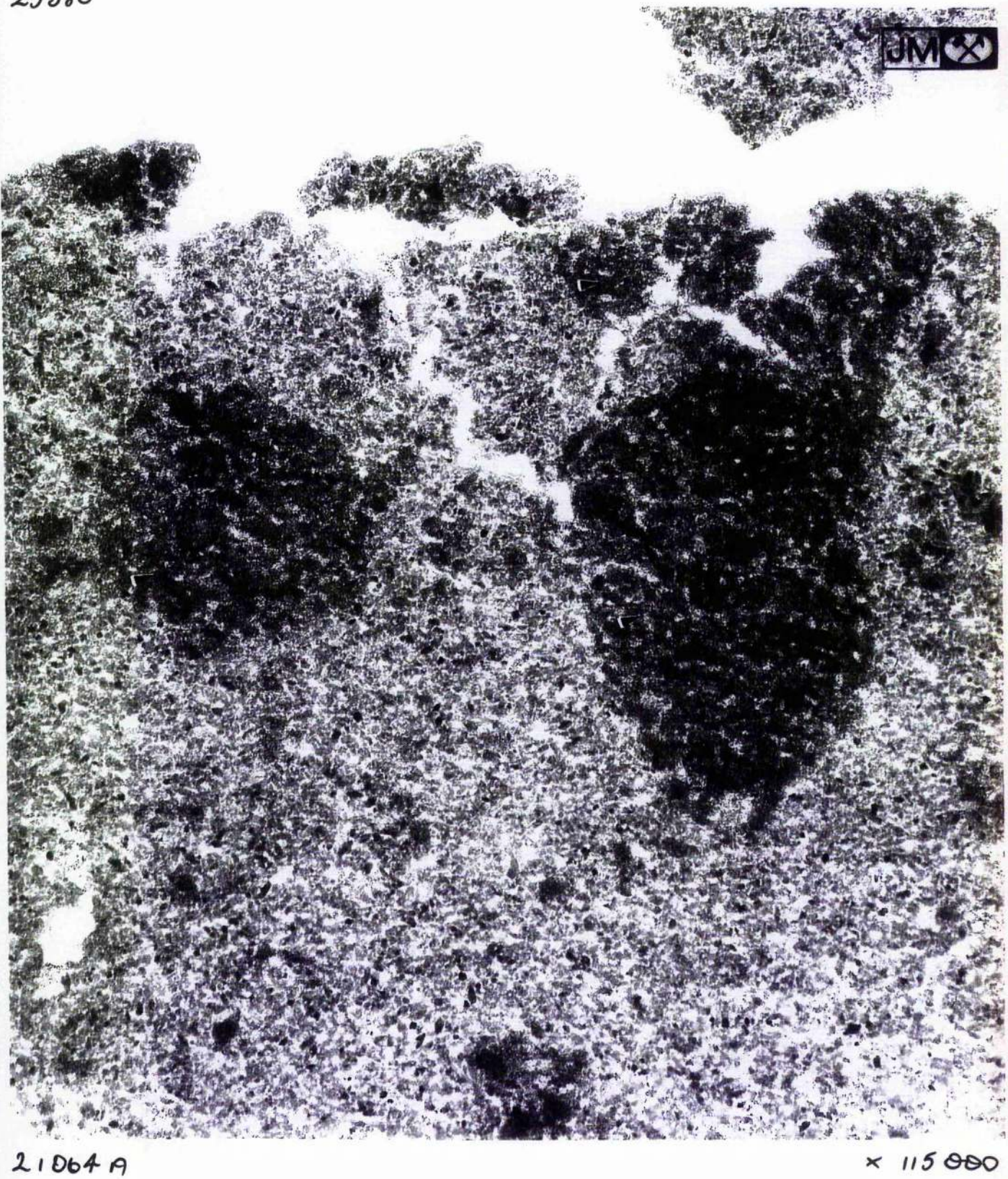

Fig. 4.20: Transmission electron micrograph (115000X magnification) of the ammonia hydrolysed RuO_2-TiO_2 sample (1)

solid solution formation is occurring, confirming the XRD results, although the presence of larger clusters of RuO_2 suggest that some reaction is still occurring prior to addition of $Ti(OEt)_4$. For the ethoxide samples the nanocrystallite size increased by changing from base catalysed to uncatalysed hydrolysis although the cluster size showed no such trend. The acid hydrolysed ethoxide samples (4 and 5) contained only amorphous ruthenium particles of a size comparable to that of the ruthenium oxide crystallites found in the acid hydrolysed isopropoxide sample 6. This is further evidence of the increased reactivity of the isopropoxide precursor as it suggests either: i) complete hydrolysis of the precursor; or ii) the ability of the monomeric precursor to, once hydrolysed, to attack other molecules in an attempt to achieve coordinative saturation. The absence of any crystalline ruthenium oxide in the acid hydrolysed ethoxide based samples is further evidence of the unreactivity of these species. The regions of amorphous ruthenium possibly correspond to partially hydrolysed and condensed ruthenium ethoxide species which pyrolyse or disproportionate upon heating to give the metallic ruthenium found in the XRD patterns.

4.3.7 Attempted Sol-Gel Processing of Pure RuO_2

Solutions of ruthenium ethoxide were prepared from a number of different starting materials by reaction with sodium ethoxide. These solutions were hydrolysed using water or a solution of HNO_3.

The results obtained from these experiments were surprising. The ruthenium ethoxide generated had a blue colour in some cases, which progressed through a series of other colours when hydrolysed: blue, green, and finally brown or red before in some cases, small amounts of black powder were deposited. The most likely explanation for

these colour changes is the sequential formation of Ru-O-Ru bridged species in solution, although attempts to isolate these species were unsuccessful due to their reactivity. The rate of colour change was dependent upon the concentration of acid in the system: With no acid the solution remained green whereas the change to red/brown became quicker as $[H^+]$ was increased, with the $Ru:H^+$ =1:0.75 solution going brown almost instantly. Without addition of peroxide no gelation is observed but some of the solutions gave tiny amounts of particles. If peroxide is added precipitation of particles is observed. It would appear then that the ruthenium ethoxide is undergoing hydrolysis very slowly and that peroxide modification is required to speed up the reaction.

One thing that is noticable about all the syntheses performed is that a varying amount of black powder is obtained during the reflux stage and often the product of the reflux is a black colloid rather than a blue solution. This should not be the case, and even if it were, the amount of powder deposited varies from reaction to reaction even though the conditions are not varied. Commercial $RuCl_3.3H_2O$ is in fact a mixture of chlorides, nitrites and oxides of Ru(III) and Ru(IV) and thus it may be that this inconsistency in the nature of the starting material could explain the inconsistencies in the results. As the amount of ruthenium in the starting material is not known, the amount of base added to produce the ethoxide is a non stoichiometric one. Add to this the fact that the starting material has coordinated water and it becomes possible that the alkoxide precursor might hydrolyse during its synthesis or the reaction not go to completion. It is also possible that reaction of the coordinated water with the sodium ethoxide might lead to substitution by OH^- followed by condensation. However, variations were also seen when using the same batch of $RuCl_3.nH_2O$ The presence of black powders after refluxing also suggests that the concentration of ruthenium present in solution during the hydrolysis step is lower than is desired and this will

affect gel times, possibly even making the concentrations too low for gelation. Certainly this may be one reason why the gel times for the RuO_2-TiO_2 mixed oxide varied from seconds to hours and also why its composition varied. It was for this reason that other precursors, $(NEt_4)[RuCl_5MeCN]$ and anhydrous $RuCl_3$ were used. However, these have not proved to be satisfactory replacements for $RuCl_3.nH_2O$: No gels are obtained from $(NEt_4)[RuCl_5MeCN]$and anhydrous $RuCl_3$ proved insoluble in ethanol. Other solvents may have to be used if this is to be used as a precursor.

Previously, as described in section 4.3.1, when ruthenium alkoxides have been generated from $RuCl_3$ without first refluxing in ethanol for several hours, black precipitates are formed on the side of the flask. This is not apparent when the starting material is refluxed for several hours prior to generation of the ethoxides in the experiments performed. Indeed, with all the precursors tried the ruthenium species generated remained in solution until peroxide was added and in the case of the sample prepared from $(DMSO)_2H[trans\text{-}RuCl_4(DMSO)_2]$ hydrolysed at high temperature remain in solution to a great extent even after the peroxide oxidation step. The samples to which no peroxide is added exhibit a number of different colours after refluxing with NaOEt: The species produced from $RuCl_3$ start black before turning blue through green and turquoise and ultimately to red brown. In no cases was gelation or precipitation observed even after many months.

In the experiments performed with partial substition of chloride with OEt, the experiment in which only one Cl atom was replaced appeared to undergo the colour changes more slowly than the experiment in which two Cl atoms were replaced.

The results suggest one of two things: i) The first possibility is that the ethoxides are not being formed and hence not being hydrolysed and condensing, which is unlikely given the fact that the only difference in the synthesis is the refluxing prior to

addition of NaOEt, and that there are no extra reagents added. This possibility is more likely with ruthenium starting materials other than $RuCl_3$; ii) The second possibility is that the alkoxides generated are too inert to react due to the high electronegativity of ruthenium and this possibility has been analysed in the following section by calculating the partial charges on several of the possible ruthenium species that may arise in these systems.

4.3.8 Partial Charge Calculations for Possible Ruthenium Species in a Sol-Gel System

Partial charge calculations have been performed using the method of Livage. This method uses the electronegativities of the elements or groups constituting the molecule to determine the distribution of charge around the molecule thus giving an indication of the relative likelihood of the extent and rates of hydrolysis and condensation. In this case the group electronegativites have been calculated as these are of greater interest than the individual atoms comprising the groups. Calculations have been performed on hydrated and non hydrated starting materials to investigate whether removal of the initial coordinated water present in $RuCl_3.nH_2O$ would be significant. Calculations have also been performed on compounds with remaining coordinated chloride to determine if leaving a highly electronegative ligand bound to the metal centre could make a significant difference to the hydrolysis rates.

The Pauling scale electronegativities of the relevant species used in these calculations are as follows: Ru, 2.20; Cl, 3.16; OEt, 2.41 (C, 2.55; H, 2.20; O, 3.44); HOEt, 2.39; OH, 2.75; H2O, 2.55. The results of partial charge calculations for a simplified ruthenium ethoxide system (one assuming a monomeric species with no

solvent coordination) are shown in Table 4.5.

The values for the partial charge on the ruthenium metal centre are much lower than those on most first row transition elements. Titanium tetraethoxide, for example, has a partial charge of 0.63, almost a factor of ten higher than for this ruthenium system. Hydrolysis occurs by nucleophilic attack and coordination of water molecules to the metal centre and the low partial charge on ruthenium suggests that this process will be slow, although substitution of bound solvent molecules or other coordinated ruthenium

		Partial Charges δ on component groups of ruthenium ethoxide				
	Molecule formula	δRu	δOEt	δH_2O	δHOEt	δOH
1	$Ru(OEt)_3$	0.077	-0.026			
2	$Ru(OEt)_3.H_2O$	0.096	-0.008	-0.072		
3	$Ru(OEt)_2.OH.HOEt$	0.112	0.007		0.017	-0.143
4	$Ru(OEt)_2.OH$	0.116	0.012			-0.051
5	$Ru(OEt)_2.OH.H_2O$	0.128	0.022	-0.043		-0.130
6	$Ru(OEt).(OH)_2.HOEt$	0.144	0.038		0.048	-0.115
7	$Ru(OEt).(OH)_2$	0.157	0.050			-0.104
8	$Ru(OEt).(OH)_2.H_2O$	0.160	0.054	-0.012		-0.101
9	$Ru(OH)_3.HOEt$	0.177			0.079	-0.086
10	$Ru(OH)_3$	0.199				-0.066

Table 4.5 Partial charges on component species of a simplified ruthenium ethoxide system.

ethoxides may be relatively facile as these will be weakly bound. Hydrolysis of the first ethoxide group should be fast once a water molecule is bound to the centre, as loss of the positively charged ethanol molecule from (3) is thermodynamically favourable. Hydrolysis of the remaining ethoxide groups is less facile (4)-(8) as this now involves proton transfer to a positively charged ethoxide group. Acid catalysis allows protonation of the bound ethoxide without the need for proton transfer and hydrolysis should therefore be more extensive if this is used. Condensation in ruthenium alkoxide systems will also be slower as this involves attack of hydroxide groups on the metal centre. The partial charge on the hydroxide groups bound to ruthenium is again lower than that of first row transition elements suggesting that condensation will be slower e.g. (3) has a partial charge δ of –0.14 whereas in the OH groups in hydrolysed titanium alkoxides typically have a charge δ of 0.3-0.4.

4.5 Conclusions

It is clear from the X-ray diffraction analysis of the sol-gel processed RuO_2-TiO_2 samples that instead of the desired homogenous $Ru_{(1-x)}Ti_xO_2$ a heterogeneous mixture of RuO_2 and TiO_2 and in most cases ruthenium metal is produced. If, as the partial charge calculations suggest, the ruthenium precursor is too inert to react, new or modified precursors perhaps based on the ruthenium acetates developed by Wilkinson[15] must be used to allow single phase mixed oxides or gels of RuO_2 to be produced. In the less likely event that ruthenium metal arises from disproportionation, precursors in the correct Ru(IV) oxidation state must be developed. The XRD data correlates well with the TEM data, with both indicating the presence of clusters of crystalline or amorphous RuO_2 within a TiO_2 matrix and confirming the presence of

two phases. Given the variation in the XRD and TEM patterns obtained for different systems, the nature of the final calcined product can be rationalized by precursor catalyst chemistry with base catalyst or no catalyst systems giving powders and acid catalyst systems giving gels as expected. Other work has shown that RuO_2 can diffuse within a TiO_2-RuO_2 system during heating. Therefore, to some extent the heterogeneous nature of the final product may be due to the less forcing calcination conditions that we have used. In future work this could be simply checked by a study of the powder XRD patterns as a function of calcination temperature

The observation that the final ratio of Ru:Ti is different to the initial ratio may be due to removal of Ru during the preparation of the alkoxide through precipitation of RuO_2. Further to this, the ratio of Ru:Ti at the surface is different to that at the bulk. To support the former, experimental observations suggest that the ruthenium precursor is hydrolysing and condensing as it is generated and before $Ti(OEt)_4$ is added. This is surprising, as Ru has a low electronegativity and any alkoxide complex generated should therefore be relatively unreactive. But the reflux conditions used to generate them may be sufficient to allow hydrolysis and condensation. Indeed, the presence of water coordinated to ruthenium in the $RuCl_3.nH_2O$ starting material and the presence of a base, (NaOEt) during generation of the alkoxide, could promote these reactions before mixing with the titanium precursor. We have found that refluxing of the RuCl3.nH2O/EtOH mixture prior to the addition of NaOEt is an effective dehydrating procedure. In general, efforts must be made to use an anhydrous Ru starting material to prevent uncontrolled hydrolysis and condensation and also to isolate, if possible, the alkoxide precursor. Isolation of the alkoxide may also allow removal of the NaCl by-product and lead to a pure final gel. The difference in bulk and surface Ru:Ti ratios arises either from diffusion of RuO_2 into the bulk or from TiO_2 particles condensing

around condensed RuO_2 particles.

The large difference in electronegativity between Ru and Ti means that the rates of hydrolysis and condensation under the same conditions will be vastly different and modification of the precursors, either by making the ruthenium precursor more reactive or making the titanium precursor less reactive, will be necessary if gels are to be obtained with Ru and Ti mixed on a molecular scale. On the other hand, as will be shown in the next chapter it is relatively easy for a titanium alkoxide to gel around a solution of an unreactive platinum group metal oxide molecular precursor, which then gives a solid solution.

4.5 Experimental Section

4.5.1 Attempted Application of Sol-gel Processing Techniques to the Production of RuO_2-TiO_2 Mixed Metal Oxides

4.5.1.1 Hydrolysis Using NH_3

Commercial $RuCl_3$ (Johnson Matthey) and $Ti(OC_2H_5)_4$ (Aldrich) were used as starting materials. Due to the moisture sensitivity of the species involved in the reactions all glassware was dried in an oven at at least 140 °C for at least 6 hrs prior to performing any experiment. Flame drying under nitrogen or argon was also used to dry much of the equipment in later experiments.

Fresh sodium ethoxide in ethanol was prepared for each experiment using clean sodium[16a] via the method described in Vogel[16b].

$RuCl_3$ (1.05g, 4 mmol) was dissolved in 25 cm^3 of anhydrous ethanol and freshly prepared sodium ethoxide in ethanol (12 mmol) was added. Ruthenium alkoxide was prepared by refluxing the solution for 3 hours at 78 °C under a dry nitrogen or argon atmosphere. After cooling to room temperature $Ti(OC_2H_5)_4$ (2.2 cm^3, 1 mmol) was added and the mixture stirred. Hydrolysis was performed by adding 50 cm^3 of an ammonia ethanol solution (20 mmol $NH_{3(g)}$ in 1 dm^3 ethanol) whilst the mixture continued to be stirred. After 5 minutes 11 cm^3 of 30% H_2O_2 were added slowly to the reaction vessel. The product was separated by centrifugation, washed with 3% H_2O_2 and dried in an oven at 90 °C overnight.

4.5.1.2 Hydrolysis Using H_2O

The mixture of ruthenium and titanium alkoxides was prepared as before but in this case hydrolysis was performed using water (0.36 cm^3, 20 mmol). All other steps were as for 4.5.1.1 above.

4.6.1.3 Hydrolysis Using H_2O in Half Solvent Volume

As 4.5.1.2 above except the total volume of the reaction was halved.

4.6.1.4 Hydrolysis Using HNO_3

Preparation of the alkoxide mixture was the same as i) above. In this experiment HNO_3 (2.25 cm^3 of 0.21 M acid to give a H_2O:Ru+Ti ratio of 5:1 and a H^+:Ru+Ti ratio of 0.075) was added and stirring was continued for several hours before addition of H_2O_2. The product could not be centrifuged as it was gelatinous in nature and this step was ignored. The gel was dried in an oven overnight as before.

4.6.1.5 Hydrolysis Using HNO_3 in a Large Volume of Solvent

Synthesis and hydrolysis as for 4.5.1.4 above except the $RuCl_3$ starting material was dissolved in 100 cm^3 of anhydrous ethanol. The finely divided nature of the precipitate demanded that it be separated by centrifugation.

4.5.1.6 Hydrolysis of an Isopropoxide Precursor Using HNO_3

Ruthenium isopropoxide was prepared from $NaOC_3H_8$ in dry isopropanol. $Ti(OC_2H_5)_4$ was again used as the titanium precursor. Hydrolysis was performed using 0.21 M HNO_3 and the mixture stirred until gelation occured prior to adding 11 cm^3 of H_2O_2. Separation and drying steps were as for 4.5.1.1.

4.5.2 Preparation of potential sol-gel precursors

4.5.2.1 Preparation of $(Et_4N)[RuCl_5MeCN]$

The procedure followed was a slight modification of that followed by Dehand and Rose[8]. Commercial $RuCl_3.3H_2O$ (Johnson Matthey, 2g) was dissolved in 100 cm^3 acetonitrile (Aldrich) with 1.2g of Et_4NCl. and heated under reflux for 4 hours. After cooling to room temperature the red solution was filtered and precipitation was induced by addition of a large excess of diethyl ether. The oily product was extensively triturated using diethyl ether in a bath of acetone and solid CO_2. The red brown precipitate obtained was filtered, washed with diethyl ether and dried in vacuo.

The final product was characterized by IR spectroscopy and found to contain the correct bands at 2250, 2303 and 2316 cm^{-1} corresponding to the coordinated acetonitrile and 412 cm^{-1} corresponding to bonds to the metal centre.

4.5.2.2 Preparation of $(DMSO)_2H[$*trans*-$RuCl_4(DMSO)_2]$

The procedure followed was that of Alessio et al[7].

$RuCl_3.nH_2O$ (5.39 g) was refluxed in 175 cm^3 of ethanol for 3 hours to give a deep green solution. The solution was filtered and vacuum evaporated to about 15 cm^3. To the solution 5.5 cm^3 of concentrated HCl (37%, 12M) were added followed by 11 cm^3 of DMSO with rapid stirring.After slow heating to 80 °C the colour changed from green to red orange and the solution was allowed to cool to room temperature. The solution was reheated to 50 °C, 50 cm^3 of acetone were added and the the solution left to crystallize. The product, red orange crystals, was filtered, washed with ice cold acetone and diethyl ether before being dried under vacuum.

4.5.2.3 Preparation of Na[*trans*-$RuCl_4(DMSO)_2$]

Again the procedure was that of Alessio et al[7].

Finely ground $(DMSO)_2H$[*trans*-$RuCl_4(DMSO)_2$] (6.5g) was dissolved in 275 cm^3 of ethanol and 3 cm^3 of water. To this solution saturated NaCl solution was added to precipitate a bright orange compound. The product was filtered washed with ice cold acetone and diethyl ether and dried under vacuum.

4.5.3 Application of sol-gel Processing Techniques to the Production of RuO_2

4.5.3.1 Attempted Preparation of RuO_2 using $RuCl_3.3H_2O$

Due to the moisture sensitivity of the species involved all glassware was dried in an oven at at least 140 °C for at least 6 hours prior to performing any experiment and cooled under nitrogen or argon. Ethanol was dried by dissolving magnesium turnings (5g/litre), with an iodine catalyst, in the wet solvent followed by refluxing for three

hours minimum and distillation onto 3A molecular sieves. The ethanol was stored under argon and left for 24 hours prior to use.

Fresh sodium ethoxide in ethanol was prepared for each experiment using clean sodium[16a] via the method described in Vogel[16b].

$RuCl_3.3H_2O$ (2.63g 10 mmol) were dissolved in 25 cm^3 of anhydrous ethanol to give a 0.4M solution. A 3M solution of sodium ethoxide (10 cm^3) was added and the mixture refluxed for 3 hrs to produce ruthenium alkoxide. After cooling to room temperature 5 cm^3 portions were removed and an ethanolic solution of HNO_3 was added to hydrolyse the precursor. The concentration of these solutions was such as to give a specific ratio of $Ru:H_2O:H^+$ (Table 4.6).

To some of these solutions 1 cm^3 of 30% H_2O_2 was slowly added either instantly after adding the acid or a certain set period after hydrolysis had been begun.

Solution G was as solution F but the solution was stirred vigourously during addition of the hydrolysis solution. Solution H was as F but the solution was allowed to hydrolyse for 1 hour prior to the slow addition of H_2O_2. Solution I was hydrolysed by direct slow addition of H_2O_2 to the ruthenium ethoxide solution.

4.5.3.2 Attempted Preparation of RuO_2 from $(Et_4N)[RuCl_5MeCN]$

$(Et_4N)[RuCl_5MeCN]$ (2.25g, 5 mmol), prepared as above was added to 25 cm^3 of anhydrous ethanol and the solution heated to dissolve the solid. To this solution 13.3 cm^3 of a 1.5M NaOEt (20 mmol) was added and the mixture refluxed for three hours before 11 cm^3 of 30% H_2O_2 was slowly added.

Solution	Ru	H_20	H^+	Peroxide added
A	1	5	0	NO
B	1	5	0.075	NO
C	1	5	0.30	NO
D	1	50	0.075	NO
E	1	5	0.75	NO
F	1	5	0.75	YES
G	1	5	0.75	YES
H	1	5	0.75	YES
I	1	HIGH	0	YES

Table 4.6: Ratios of $Ru:H_2O:H^+$ used to hydrolyse ruthenium alkoxide precursors

4.5.3.3 Attempted Preparation of RuO_2 from Anhydrous $RuCl_3$

Anhydrous $RuCl_3$ (Johnson Matthey, 1.77g) was added to 25 cm^3 of anhydrous ethanol and heated in an unsuccessful attempt to dissolve to $RuCl_3$. To this mixture 20 cm^3 of 1.5M NaOEt were added and refluxed with the solid $RuCl_3$ in an attempt to produce ruthenium alkoxide. A 10 cm^3 portion was removed and hydrolysis was attempted with 0.11M HNO_3.

4.5.3.4 Attempted Preparation of RuO_2 from $Ru(OEt)_3$ with prior refluxing

$RuCl_3$ (Johnson Matthey, 2.63g, 10 mmol) was dissolved in 25 cm^3 of anhydrous ethanol and refluxed at 78 °C under a dry argon atmosphere for 2 hours until a green solution was obtained. To this solution 1.5M sodium ethoxide (either freshly prepared via the method of Vogel[16] or from Aldrich, 20 cm^3, 30 mmol) was added and refluxing continued for a further 3 hrs after which a brown species, postulated to be ruthenium ethoxide had formed. After cooling to room temperature HNO_3 (9 cm^3 of 1.1M acid diluted to 0.11M with anhydrous ethanol to give a Ru:H_2O ratio of 1:5 and a Ru:H+ ratio of 10:1) was added to this solution with stirring and the solution left to hydrolyse and condense for 30 minutes after which 30% H_2O_2 (Aldrich, 10 cm^3 was added). The final product was collected by centrifugation and dried at 90 °C under vacuum for 10 hours.

4.5.3.5 Attempted Preparation of RuO_2 from Partially Substituted $RuCl_3$

Method was as for 4.5.3.4 with the following modifications: Two experiments were performed, in the first 13.33 cm^3 rather than 20 cm^3 of 1.5M NaOEt were added to the green $RuCl_3$ solution and in the second 6.66 cm^3 of 1.5M NaOEt were added. These amounts would allow only two and one of the Cl atoms bound to the ruthenium centre to be substituted. The ethoxides were again hydrolysed with HNO_3 but no peroxide has been added to date to determine whether any gelation will occur over a prolonged period.

4.5.3.6 Attempted Preparation of RuO_2 from Chloride-Dimethyl Sulphoxide-Ruthenium (III) Compounds

Method was as for 4.5.3.4 above only in these cases $(DMSO)_2H[trans\text{-}RuCl_4(DMSO)_2]$ (5.56g, 10mmol) or $Na[trans\text{-}RuCl_4(DMSO)_2]$ (4.2g,10mmol) were used as the starting materials . Again no peroxide has to date been added to investigate whether gelation is possible before the oxidation step.

4.5.3.7 Attempted Preparation of RuO_2 from $(Et_4N)[RuCl_5MeCN]$ with prior refluxing

1.27g (2.8 mmol) of $(Et_4N)[RuCl_5MeCN]$ were dissolved in 8 cm^3 of anhydrous ethanol and heated to reflux. After 30 minutes 7.5 cm^3 (11 mmol) of 1.5M NaOEt were added and refluxing continued for three hours. After cooling to room temperature 0.25 cm^3 of 1.1M HNO_3 were added. Product was left overnight to observe whether any gelation had occured. A further 0.25 cm^3 of 1.1M HNO_3 was added.

4.5.3.8 High Temperature Hydrolysis Experiments

These experiments have to date been performed using $RuCl_3$ and $(DMSO)_2H[trans\text{-}RuCl_4(DMSO)_2]$. The ethoxides were generated as above. Cooling to room temperature was not allowed, HNO_3 was added to the reaction while the ethoxide species were still at 78 °C. Refluxing was continued for 15 hrs to allow hydrolysis and condensation at this higher temperature. After this time H_2O_2 was added with stirring to oxidize the system which was then left to gel. In the experiment using $RuCl_3$ the product was separated by centrifugation and dried at 90 °C under vacuum overnight.

4.6 References

1) J. Livage, M. Henry and C. Sanchez, *Prog. Sol. St. Chem.*, 1988, **18**, 1.

2) M. Gugliemi, P. Columbo, V. Rigato, G. Battaglin, A. Boscolo-Boscoletto and A. Debattisti, *J. Electrochem. Soc.*, 1992, **139**, 1655.

3) K. Kameyama, S. Shohji, S. Onoue, K. Nishimura, K. Yahikozawa and Y Takasu, *J. Electrochem. Soc.*,1993, **140**, 1034.

4) Y. Takusu, S. Onoue, K. Kameyama, Y. Murakami and K. Yahikozawa. *Electrochim. Acta.*,1993, **39**, 1994.

5) Y. Murakami, K. Miwa, M. Ueno, M. Ito, K. Yahikozawa and Y. Takasu, *J. Electrochem. Soc.*, 1994, **141**, L118.

6) K. E. Swider, C. I. Merzbacher, P. L. Hagans and D. R. Rolison, *Chem Mater.*, 1997, **9**, 1248.

7) E. Alessio, G. Balducci, A. Lutman, G. Mestroni, M. Calligaris and W. M. Attia, *Inorg. Chim. Acta*, 1993, **203**, 205.

8) J. Dehand and J. Rose, *Inorg. Chim. Acta*, 1979, **37**, 249.

9) J. Moreno, J. M. Dominguez, A. Montoya, L. Vicente and T. Viveros, *J. Mater. Chem.*, 1995, **5**, 509.

10) A. Mills, *Chem. Soc. Rev.*, 1989, **18**, 285.

11) B. D.Yoldas, *J. Mater. Sci.*, 1986, **12**, 1087.

12) A. Osaka, T. Takatsuna and Y. Miura, *J. Non-Cryst. Solids*, 1994, **178**, 313.

13) J. A. Busby, Electron Optics Unit Report, Johnson Matthey plc, September 1995.

14) C. J. Brinker, G. W. Scherer, *Sol-Gel Science, The Physics and Chemistry of Sol-Gel Processing*, Academic Press, San Diego, 1990.

15) A. Spencer and G. Wilkinson, *J. Chem. Soc. Dalton Trans.*, 1972, 1570.

16) A. I. Vogel, *Textbook of Practical Organic Chemistry 4th Ed.*, Longman, London, 1978.

CHAPTER 5

Attempted Aqueous and Non-Aqueous Sol-gel Processing of IrO_2 and IrO_2-TiO_2 Mixed Metal Oxides

5.1 Introduction

Iridium dioxide, IrO_2, has a number of uses, principally as an electrode material, but also as a catalyst for oxygen evolution and as an electrochromic material as was reported in Chapter 1. It is traditionally prepared from solutions of the chloride or by the Adams method of heating iridium trichloride with sodium nitrate.

Sol-gel processing as a technique for producing iridium dioxide and indeed other platinum group metals, has not been extensively studied. For example as far as I am aware no aqueous sol-gel routes to IrO_2 have been reported. The $[Ir(OH_2)_6]^{3+}$ ion has been partially characterized and its behaviour on oxidation studied[1]. This ion is thought to have potential as an aqueous sol-gel precursor. Furthermore routes analogous to those to RuO_2 from RuO_4 via reduction of higher valent precursors are less viable; Ir(V) is the highest oxidation state available for Ir and compounds with the metal in this state are reduced extremely quickly. Iridium alkoxides, unlike those of ruthenium, are known, These iridium alkoxides are in the +3 oxidation state rather than the +4 state of the desired IrO_2 product. Studies on alkoxide based sol-gel routes to IrO_2 films and powders have been reported[2,3] along with sol-gel routes to mixed oxides of IrO_2 with tin[4], tantalum[5], ruthenium[6] and a ternary mixed oxide of iridium, ruthenium and titanium[7]. The powders of the mixed oxides formed

are found to be rutile phase solid solutions.

This work on alkoxide routes to iridium dioxide via sol-gel processing has concentrated on powders and films, but no intermediate gels have been reported for IrO_2 or of mixed oxides in which Ir is a component. The low partial charge on iridium in its alkoxides is due to its low electronegativity (iridium has the same electronegativity as ruthenium). This suggests that the reactivity of these species will be low and that single metal IrO_2 gels will be difficult to obtain, with gels of IrO_2 combined with a more reactive metal such as titanium being a more realistic target. The trinuclear iridium acetate molecule $[Ir(III)_3O(OAc)_6(HOAc)_3](OAc)$ is well characterized and soluble in both water and ethanol providing another potential precursor.

In this chapter our attempts at producing the first single metal gels of IrO_2 and mixed metal oxide gels and powders of IrO_2-TiO_2 mixed oxides are reported along with analysis of the gel and powder products for the latter. Both aqueous and non-aqueous routes have been studied with a variety of precursors to determine the optimum conditions for developing this system. For mixed oxides studies have been performed to determine the minimum amount of a more reactive metal is required to obtain gels.

5.2 Results and discussion

5.2.1 Studies on the $[Ir(H_2O)_6^{3+}]$ aqua ion

The ion was prepared via the method of Castillo-Blum[1] et al. It was purified and concentrated using ion-exchange chromatography and characterized by UV-vis

spectrophotometry. Spectra of solutions of the ion in 2M perchloric acid contained the expected bands at 315 and 264 nm (Fig. 5.1). The concentration of the final solutions was in general around 0.02 M.

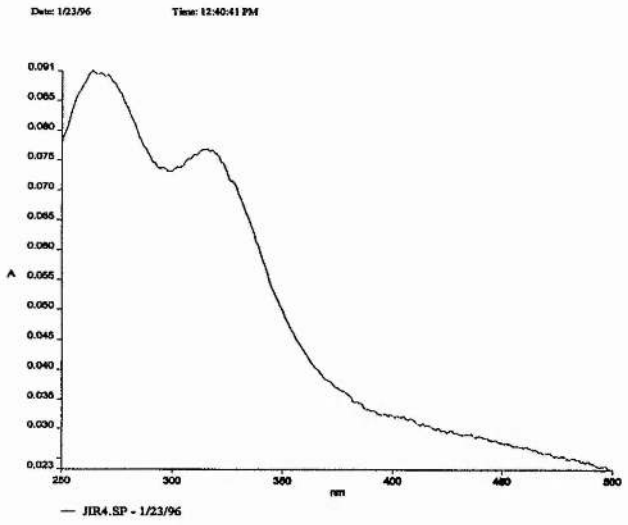

Fig. 5.1 UV-Vis spectrum of the $[Ir(H_2O)_6^{3+}]$ aqua ion.

On slowly raising the pH of the solution from pH 0 to pH 2 a colour change from pale yellow/green to purple is observed. On further addition of base a dramatic rise to pH 4.5 is noted. This rise in pH is accompanied by the transition from a clear purple to a cloudy white solution with a fine white precipitate that required isolation by centrifugation being obtained on further raising the pH to 8. This cream solid obtained at higher pHs is almost certainly $Ir(OH)_3(OH_2)_3$. Consistent with this is the observation that the precipitate can be converted back to the aqua ion by isolation, dissolution in 1 M $HClO_4$ and purification by chromatography.

If the precipitate is left at room temperature for a matter of weeks it darkens

and ultimately forms a black solid. In contrast to the case of the ruthenium aqua ion, at no point during the experiment was any precipitate corresponding to the metal dioxide observed. However, the black powder obtained by allowing the cream $Ir(OH_2)_3(OH)_3$ precipitate obtained to undergo solid state reaction may well be IrO_2 produced by olation as postulated for chromium by Ardon et al[8] via formation of hydroxo bridges with elimination of water.

The absence of any IrO_2 precipitates from solution can be ascribed principally to the concentration of the sample: the solution starts at <0.02 M two orders of magnitude less than is typical for aqueous sol-gel experiments and there is too little iridium oxide precursor present to from a gel network. It might also be suggested that condensation is not occuring due to the inertness of the iridium metal centre with loss of water being an extremely slow process. The purple solution obtained on raising the pH to 2 can be assigned to small amounts of the Ir(IV) species observed by Castillo-Blum et al[1] on electrochemical reduction of solutions of Ir(V) (derived initially from the iridium aqua ion $Ir(H_2O)_6^{3+}$) as it has the same band at 550 nm in the UV-Visible spectrum as was reported for this species (Fig. 5.2).

Electrochemical oxidation of the $[Ir(H_2O)_6]^{3+}$ ion using a platinum gauze electrode sample prepared was also performed as it was thought that this might provide a means of obtaining IrO_2 gels. The initial pale yellow-green Ir(III) solution turning to brown-green Ir(V) shortly after current was applied. The solution turned blue-purple (corresponding to Ir(IV)) on reduction (performed by reversing the polarity of the Pt gauze electrode) and on further reduction converted to yellow Ir(III) although in this case the product is mostly a dimeric hydroxo bridged species rather than the $[Ir(H_2O)_6]^{3+}$ aqua ion with some oligomeric Ir(III) also being present. However, without being able to concentrate the sample readily to facilitate gel

formation, no further work has been performed on the $[Ir(H_2O)_6^{3+}]$ aqua ion.

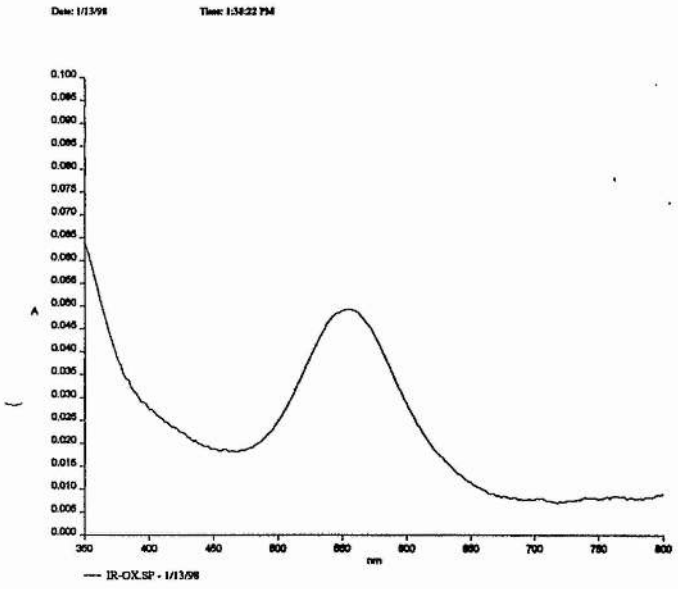

Fig. 5.2 UV-Vis spectrum of the purple solution observed on raising the pH of a solution of $[Ir(H_2O)_6]^{3+}$ in perchloric acid.

5.2.2 Attempted Non-aqueous Sol-gel Processing of IrO_2 based on Alkoxide Precursors

Attempts were made to prepare IrO_2 from "iridium alkoxide" precursors derived from two different starting materials, H_2IrCl_6 and Na_2IrCl_6. On addition of NaOEt to an ethanolic solution of H_2IrCl_6 a cloudy grey solution is obtained which precipitates a black powder shortly after heating is commenced. In all likelihood the base is hydrolysing the Ir-Cl bonds after which condensation of the Ir-OH groups to give IrO_2 is happening in an uncontrolled manner. If the sodium salt of the hexachloroiridate, Na_2IrCl_6, is used the ethanol solution turns orange on initial

addition of NaOEt and turns black shortly after refluxing is commenced. The orange colour may arise from the oxidation of the ethanol and partial conversion of red Ir(IV) to yellow green Ir(III). After cooling and addition of the hydrolysis catalyst (HNO_3 solution) the solution remains stable indefinitely if solvent is not allowed to evaporate, although precipitate is evident on some occasions before the hydrolysis is begun. If base is added to catalyse condensation, then gelation or precipitation still does not occur. Precipitation of powder does occur if an "iridium alkoxide" solution is left to evaporate overnight at room temperature. This phenomenon is independent of the hydrolysis catalyst used. The Na_2IrCl_6 precursor showed the most promise and was subsequently used in the mixed-metal oxide gelation experiments described in section 5.2.3.

Sol-gel processing of IrO_2 from the "iridium alkoxide (IV)" system was expected to be simpler than the analogous ruthenium alkoxide system as no oxidation with peroxide is required. The iridium precursor should also be more reactive as the iridium metal centre is in a higher oxidation state. If solutions of the alkoxide are obtained these would appear to be stable until a certain concentration is reached after which precipitation occurs. As mentioned in section 5.1 iridium has the same electronegativity as ruthenium and, although the partial charges on the metal centre and substituent groups (0.082 and -0.0206 respectively for a simple $Ir(OEt)_4$ model) are slightly higher, calculations suggest that hydrolysis will not be favourable. The reason for the precipitation observed before hydrolysis in some experiments may arise from either a rearrangement of the alkoxide to form a more stable but less soluble intermediate or, more likely, from wet base or solvent leading to substitution of bound chloride on Na_2IrCl_6 with OH^- rather than OEt^- allowing condensation, a process made more facile due to the refluxing conditions employed.

Thus it is likely that the black solution observed after attempted preparation of the alkoxide is in fact colloidal IrO_2. If colloidal IrO_2 is obtained this could explain why the expected condensation of the hydrolysed Ir precursor is not observed if extra base is added to the system. Given that condensation does occur if OH groups are present this would appear to be further evidence that the metal alkoxide itself is too unreactive to undergo hydrolysis. A final point concerns the nature of the precursor itself: the initial starting material has six coordinated chlorine atoms of which only 4 are substituted (any more and the system would contain too much base for gels to be obtained). It may be that a mixed sodium/iridium chloroalkoxide is being formed as no sodium chloride (which is not soluble in ethanol) precipitate is observed during the experiments.

5.2.3 Attempted Non-aqueous sol-gel processing of IrO_2-TiO_2 mixed oxides

5.2.3.1 Preparation of samples

In this series of experiments four IrO_2-TiO_2 mixed oxide samples were prepared from "iridium alkoxides" generated from Na_2IrCl_6 in ethanol, mixed with $Ti(OEt)_4$ (to give a total metal concentration of $\approx$ 0.25 mol dm^{-3}). These were hydrolysed by a water ethanol solution with an acid catalyst (HNO_3) with a ratio H_2O:M:H^+ = 5:1:0.1. The aim of this experiment was firstly to see if mixed solid IrO_2-TiO_2 solid solutions could be obtained and secondly to determine how much $Ti(OEt)_4$ was necessary to obtain gels. The gel times for the each sample are given in Table 5.1.

SAMPLE[a]	RATIO Ir:Ti	PRODUCT	GEL TIME
1	1:4	GEL	15 min
2	2:3	GEL	19 h
3	3:2	GEL	24 h[b]
4	4:1	POWDER	3 days[b]

a) Typically water and HNO_3 are added to x mmol Ir and (5-x) mmol Ti (after 4x mmol NaOEt added to generate iridium ethoxide) to give final ratio $H_2O:M:H^+ = 5:1:0.1$. b) These solutions were allowed to evaporate to obtain a product.

Table 5.1 Product natures and gel times for IrO_2-TiO_2 samples produced by hydrolysis and condensation of alkoxide precursors in ethanol.

The sample containing the most titanium gelled the fastest, and, as expected the gel times, decreased as the amount of iridium in the sample was increased. In the case of sample 3 a certain amount of evaporation and concentration of the sample at room temperature after hydrolysis proved necessary before gelation could occur. In the case of the last sample the product nature upon extensive room temperature evaporation of the precursor solution was necessary before a precipitate was observed. The table only lists the average gel times since these varied slightly when each experiment was repeated under identical conditions. The gel times and product nature for all samples varied somewhat with each experiment; on some occasions powders were obtained instead of gels for samples 2 and 3. Different morphologies were obtained using the same batch of starting material and the results can most likely be explained in terms of either trace water in the ethanol solvent or the NaOEt solution or from impurities arising from drying of the solvent.

This would lead to hydrolysis and condensation of the iridium precursor before the hydrolysis solution and catalyst were added giving colloidal IrO_2 which can be incorporated into the gel nework by the hydrolysed $Ti(OEt)_4$ condensing around it.

5.2.3.2 Thermal analysis of the IrO_2-TiO_2 samples.

The DTA/TGA traces of the Ir:Ti 3:2 oxide sample dried under vacuum at 90-100 °C and heated under oxygen (Fig. 5.3) display the main features of all the samples with, in particular, two main areas of weight loss and thermal events at around 100 °C and 200-300 °C. These results are typical of the TGA and DTA patterns of sol-gel processed materials, with the weight loss at 100 °C corresponding to loss of water and coordinated water and possibly some further condensation within the sample, while the exothermic weight loss between 200 and 300 °C corresponds to cracking of organic material.

The overall weight losses are reported in Table 5.2. The derivatives of the TGA patterns show that the highest rate of combustion of organic material occurs at lower temperatures as the amount of iridium in the sample increases. This suggests that iridium alkoxides are less thermally stable than those of titanium and will decompose at lower temperatures.

The patterns in the overall weight lost are not what was expected: the overall weight loss would be expected to decrease as the amount of iridium is increased given iridium's much greater atomic mass. In fact rather similar weight losses are observed for samples 1-3. This may be due to the presence of the sodium chloride by-product of iridium alkoxide generation, which is trapped within the gel network thus reducing the fraction of a sample analysed that is IrO_2 and hence producing a lower than expected

value. This trend and the anomalously high weight loss for sample 4 may indicate again the presence of substantial amounts of incompletely hydrolysed iridium alkoxides and that the gel is formed by condensation of the hydrolysed titanium species around the unhydrolysed iridium alkoxide.

SAMPLE	RATIO Ir:Ti	OVERALL % WT LOSS
1	1:4	9
2	2:3	12
3	3:2	9
4	4:1	60

Table 5.2 Overall weight loss in IrO_2-TiO_2 mixed oxide samples heated under oxygen at 10 °C/min to 450 °C. For experimental details see 5.3.2.1 and table 5.1.

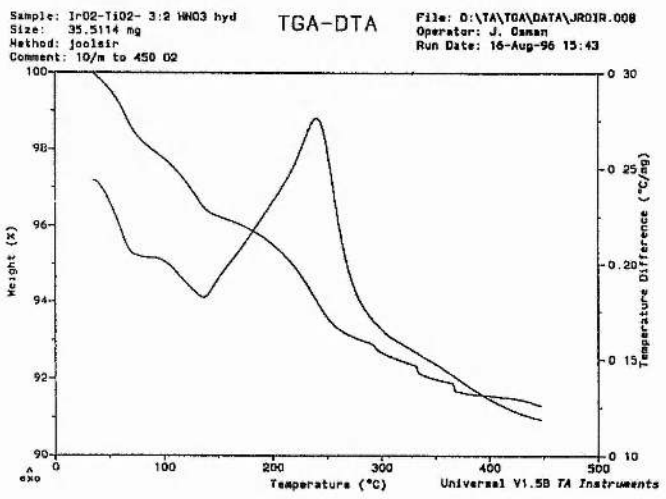

Fig. 5.3 TGA/DTA pattern for IrO_2-TiO_2 mixed oxide, ratio Ir:Ti 3:2 heated under oxygen at 10 °C/min to 450 °C.

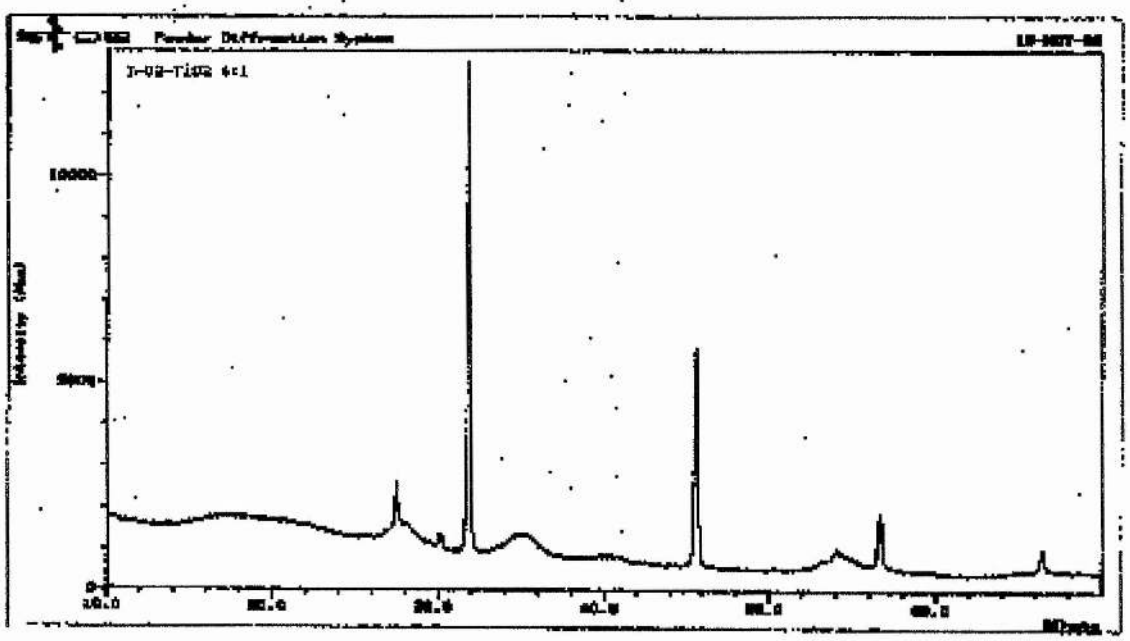

Fig.5.4: Powder X-ray diffraction pattern of IrO_2-TiO_2 mixed oxide, ratio Ir:Ti 4:1 calcined at 250°C for 3 hrs then 450°C for 3 hrs.

5.2.3.3 X-ray diffraction studies

After calcination at 250°C for 3 hours followed by further calcination at 450°C for 3 hours the samples were studied by powder X-ray diffraction. The X-ray diffraction pattern for the sample 1 is shown in Fig. 5.4. From this pattern it is clear that there is a major problem when it comes to trying to produce gels containing IrO_2 from ethoxides derived using Na_2IrCl_6 as the starting material. The major phase present in all the sample is found to be a cubic phase and is assigned to NaCl produced during reaction of the hexachloroiridate with sodium ethoxide or perhaps during hydrolysis and condensation of the Ir:Ti precursor mixture. The presence of NaCl is unsurprising

as the gel network encases the whole solvent system and thus any impurity will remain trapped within the gel when the solvent is driven off. In the hope of obtaining better diffraction patterns the samples were washed with distilled water. The subsequent patterns obtained contained very broad peaks which did not allow us to ascertain whether a solid solution had been formed.

Some analysis was possible by examination of the data file associated with the Ir:Ti 3:2 system : It is found that anatase TiO_2 is present in the sample and it is also clear that some rutile phase IrO_2 is present and in this way the samples are similar to the RuO_2-TiO_2 mixed oxide samples reported in chapter 4. It is found though that a second rutile phase is present with 2θ values of 27.84 and 35.24. These values are between the values expected for either the TiO_2 or IrO_2 rutile structures and are evidence for the partial formation of a solid solution. Unlike the analogous ruthenium system there is no XRD evidence of any metal in the samples. The iridium starting material has the same oxidation state as the final product so there is less likelihood of disproportionation although were the starting material to be reduced by the solvent this possibility could arise. It was postulated by Osaka[2] that thermolysis of iridium alkoxides leads to the metal due to the high covalency of the Ir-OR bond and the unlikelihood of its undergoing hydrolysis. This phenomenon is not observed in our experiments perhaps as a consequence of the postulated hydrolysis and condensation of the Na_2IrCl_6 starting material.

5.2.3.3 Analysis of surface samples by XPS

The XPS spectrum of the Ir:Ti 4:1 sample is shown in Fig. 5.5 and the expanded region around the Ir 4f peaks is shown in Fig. 5.6.

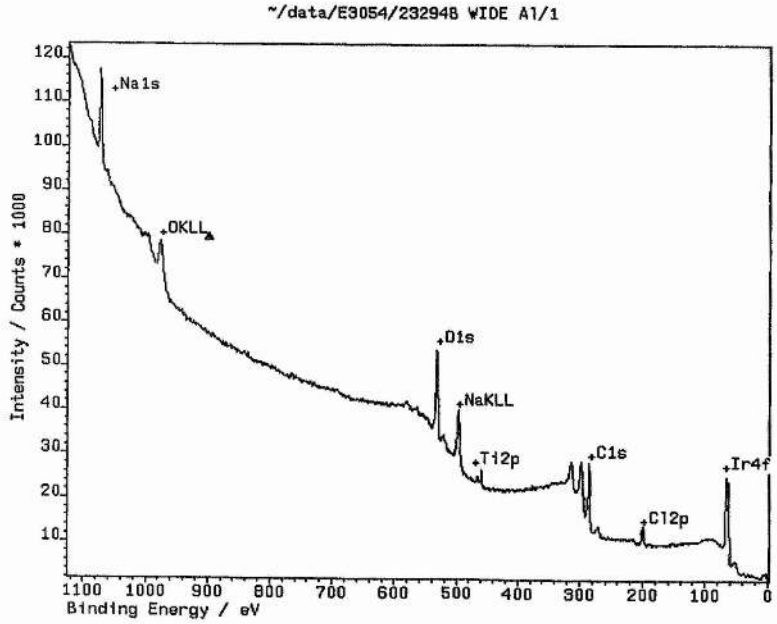

Fig. 5.5 XPS spectrum of IrO_2-TiO_2 sample ratio Ir:Ti 4:1

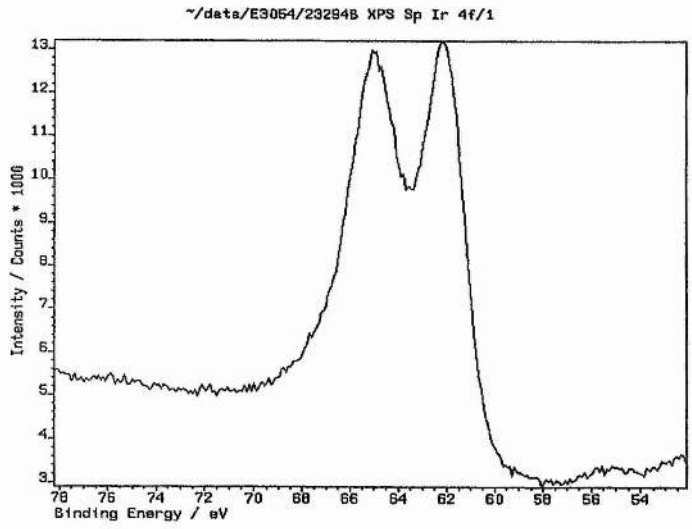

Fig. 5.6 XPS spectrum of IrO_2-TiO_2 sample ratio Ir:Ti 4:1. Expanded area around Ir 4f peak

SAMPLE	INITIAL RATIO Ir:Ti	Ir:Ti SURFACE	RATIO Ir(IV)/(III)
1	4	2.8	NO Ir(IV)
2	1.5	0.7	0.12
3	0.66	1.2	0.4
4	0.2	0.66	0.7

Table 5.3 Ratios of Ir:Ti and Ir(IV):Ir(III) in mixed IrO_2-TiO_2 samples determined from the 60-65 eV Ir 4f peak area and the 458 eV Ti 2p peak area of the XPS spectra.

The results are similar to those for the RuO_2-TiO_2 samples reported in Chapter 4. It is found that the ratio of iridium to titanium at the surface of the samples as measured by XPS does not match the figure for the bulk. It was found for ruthenium systems that surface depletion in RuO_2 had occurred and this phenomenon is also observed for two of the IrO_2-TiO_2 mixed oxides, those with higher ratios of iridium to titanium. For samples that contain lower concentrations of iridium, however, the converse is true with the concentration of iridium at the surface being higher than expected. XPS studies on IrO_2-Ta_2O_5 films produced from chloride solution[9] explained an enrichment of tantalum at the surface in terms of phase segregation at the surface due to the lower density of the amorphous tantalum phase. This might explain why there is surface enrichment of TiO_2 but does not explain enrichment of IrO_2. In titanium-rich samples homocondensation between Ti-OH and Ti-OR groups is more likely than reaction between Ti and Ir species which might lead to highly condensed large particles of TiO_2 and much smaller IrO_2 rich particles. The greater exposed

surface area of these small particles leads to apparent iridium enrichment at a surface.

An unexpected result was the discovery of the presence of iridium(III) in the samples. This species must arise either during the generation of the alkoxide or by corrosion of the IrO_2 product. It is most likely that the tetravalent alkoxide is not stable and that the hexachloroiridate is reduced when treated with sodium ethoxide or by the ethanol solvent. Osaka[2] noted that nitric acid could be used to oxidize the Ir(III) to Ir(IV) as well as catalysing the hydrolysis of the ethoxide groups and there is some evidence that this may happen in the IrO_2-TiO_2 system. Thus the ratio of iridium to titanium is lowered and thus the ratio of nitrate to iridium increases as the ratio of Ir(IV):Ir(III) increases. Mehrotra and Singh have reported many examples in which metal alkoxides[10] have proved to be far more complicated molecules than had been thought and it may be that the species generated from Na_2IrCl_6 and NaOEt is not the simple $Ir(OEt)_4$ species assumed.

The XPS results also confirm the presence of large quantities of sodium and chlorine in the samples from the NaCl impurity which was detected in the X-ray diffraction patterns. Some spectra also detect the presence of nitrogen species in the samples, a feature that could arise from the reduction of nitrate by Ir(III).

5.2.3.4 Analysis of the samples using electron microscopy

The samples were analysed by both scanning and transmission electron microscopy. In the case of the former the presence of large quantities of sodium chloride (as determined by EDX spectroscopy) again made analysis difficult as it proved impossible to ascertain whether the particles of varying size found were composed of smaller particles or whether they formed a continuous network. The TEM

study included examination by EDX to analyse typical features of the samples. Fig. 5.7 show the micrograph at 530 000 times magnification for the sample with ratio Ir:Ti 4:1 and Fig. 5.8 the EDX spectrum of the same sample.

The results of the TEM study provide strong evidence for the partial formation of solid solutions or a dispersion of oxide phases on the nanometer scale in some of the samples although, in the samples with Ir:Ti ratios of 3:2 and 2:3, there is evidence of some cluster formation in addition to the solid solution with the size of these clusters for the former being up to 0.9 μm across. Close examination of these clusters shows them to be composed of IrO_2 particles with diameters in the range 0.5-20 nm. In all cases the iridium particles were surrounded by a titanium dioxide coating, a crystalline TiO_2 coating in the case of sample 1. The analysis confirms the X-ray diffraction evidence that there are many phases present in the samples. Clearly heating the gels to 450 °C does not give a homogenous solid solution, rather a mixture of rutile IrO_2, anatase TiO_2 and some mixed IrO_2-TiO_2 oxide. The presence of clusters of IrO_2 particles rather than their even distribution throughout suggests that the formation of any solid solution is a consequence of titanium dioxide condensing and gelling around the iridium precursor particles rather than reacting with them. Certainly for the higher iridium concentration samples it would be expected that the iridium dioxide particles would coat the titanium dioxide particles if the iridium precursor were hydrolysing and condensing to any great extent. This is further evidence, along with the slow gel times, of the poor reactivity of the iridium ethoxide in a sol-gel system although it would appear that this is not detrimental to the formation of solid solutions of the mixed oxide.

Fig. 5.7 Transmission electron micrograph of IrO_2-TiO_2 sample ratio Ir:Ti 4:1

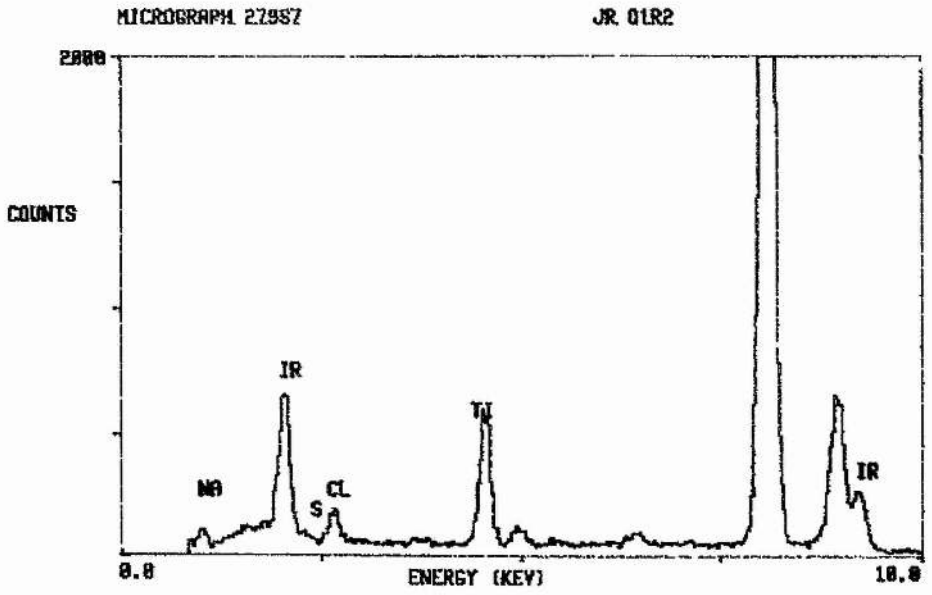

Fig. 5.8 EDX spectrum of IrO_2-TiO_2 sample ratio Ir:Ti 4:1

5.2.4 Attempted Aqueous and non-aqueous routes to IrO_2-TiO_2 mixed oxides based on an iridium acetate precursor

5.2.4.1 Preparation of samples and gel times

The iridium acetate precursor $[Ir(III)_3(\mu_3\text{-}O)(\mu\text{-}O_2CCH_3)_6(HOAc)_3](OAc)$ is, unlike the "iridum ethoxide" species used in previous attempts to produce mixed oxides, a well defined species. It has been shown to be highly soluble in acetic acid and water and it was also found to be reasonably soluble in ethanol. The use of acetates in sol-gel processing is well known and they can be used in both hydrolytic and non hydrolytic procedures for producing oxide gels. Bearing in mind theresults discussed in the previous section in which separate regions of TiO_2 and IrO_2 are observed in the

electron micrographs, it was decided to try and equalize the rates of hydrolysis and condensation for Ir and Ti . A well known way of doing this is the addition of a chemical modifier, usually a chelating ligand, to slow down the rates of hydrolysis and condensation of the more reactive precursor in this case the $Ti(OEt)_4$. A further advantage of using the acetate over a chloride based starting material is that it, like other easily decomposed oxyanions such as nitrate and carbonate, contains only metal and elements that can be easily removed during heat treatment.

For colloidal processing of an IrO_2-TiO_2 mixed oxide the titanium precursor, again $Ti(OEt)_4$, was stabilized against fast hydrolysis and precipitation using 2,4 pentanedione (acac). It was found that during the addition of aqueous solutions of the iridium acetate to stabilized $Ti(OEt)_4$ a white precipitate, postulated to be TiO_2 was formed initially but that this redissolved after stirring. These solutions were then used to prepare gels (Table 5.4, samples 5-7). It was found that if glacial acetic acid, also known to stabilize $Ti(OEt)_4$ against fast hydrolysis, is used instead of acac the white TiO_2 precipitate does not redissolve.

In addition to the attempts to produce IrO_2-TiO_2 mixed oxides from aqueous solution, attempts were made to produce gels of an IrO_2-TiO_2 by non-hydrolytic sol-gel processing. Ethanol had to be used as a solvent as it was found that iridium acetate was not soluble in any of the typical aprotic solvents used for non-hydrolytic sol-gel processing and this may have affected the results to some extent. It was found that shortly after heating the colour of the solution changes from green to red brown suggesting that either the iridium species is rearranging or that some mixed iridium and titanium precursor is being produced. If the iridium acetate is dissolved in ethanol and refluxed on its own the colour change is not observed suggesting that the second of these possibilities is more likely. However, all attempts to isolate this precursor

were unsuccessful. The red-brown colour persists for several weeks suggesting that condensation is not occurring, possibly due to the choice of solvent. If water is added to the solution, gelation occurs (Table 5.4, sample 8).

Sample	Ratio Ir:Ti	Gel Time /Days	Volume of Final Gel/cm^3
5[a]	3:1	29	12
6[a]	1:1	18	17
7[a]	1:3	14	15
8[b]	1:1	5	20

a) Solutions of iridium acetate in water (x mmol in 20 cm^3) were added to (4-x) mmol of $Ti(OEt)_4$ stabilised with (4-x) mmol Hacac with stirring and left to gel. b) $Ti(OEt)_4$ stabilised with (4-x) mmol Hacac was added to a solution of iridium acetate dissolved in 20 cm^3 of anhydrous ethanol and refluxed. 5x mmol of water mixed with ethanol was added to hydrolyse the precursors and the solution left to gel.

Table 5.4: Gel times and final volumes for iridium acetate based gels. Samples 1-3 are obtained from aqueous solutions of iridium acetate and $Ti(OEt)_4$ stabilised with acac. Sample 4 represents the gel produced from ethanolic solution by refluxing the same precursors followed by hydrolysis.

The times taken to produce dark green monolithic gels from aqueous solution after leaving the solutions on the open bench to evaporate and the time taken for the red-brown ethanolic solution to gel are given in Table 5.4. No gelation is seen if the samples are not allowed to evaporate, suggesting that the concentrations are too low to

allow condensation at the concentrations necessary to completely dissolve the iridium acetate precursor. No precipitation occurred at any time during this evaporation suggesting that the iridium species did react to form the gel to some extent although in all cases addition of water to the dried gel gave a weakly green solution of the soluble iridium acetate precursor. The gel samples were also investigated under conditions for supercritical drying as after several washes with dry methanol to remove water the green colour of the samples had virtually disappeared. The persistent green colour of the gels suggests at least that the core of the iridium species remains intact. The gel time of the gel produced from ethanolic solution is measured from the addition of water to the alkoxide/acetate solution.

The gel times for the aqueous samples increase with iridium content as expected as once again the iridium precursor is less reactive than the titanium precursor. The gel times are slower than for ethoxide based systems principally due to the modification of the titanium precursor to prevent fast hydrolysis and precipitation at the high hydrolysis ratios used. It is interesting to note that the alcoholic solution of the precursors (sample 4) gave relatively fast gelation, even though the volume of solvent used was larger. It is possible that partial condensation is occurring during the reflux stage of experiment to give either polymers, which is unlikely given that there is no water in the system before hydrolysis and that gelation did not occur after many days of heating, or a distinct mixed metal precursor species. The ruthenium analogue of the iridium acetate has shown to undergo substitution of coordinated ligands faster than expected due to a trans effect produced by the μ-3 oxygen atom[11]. The oxygen atoms of the alkoxide groups in $Ti(OEt)_3(acac)$ have a partial negative charge and are thus nucleophilic. Hence it is possible that substitution of the acetic acid molecules coordinated to the iridium atoms might occur, hence the colour change. This would

produce a reactive precursor as the coordinated titanium groups could hydrolyse and condense amongst themselves. It is, however, clear that gels can be obtained even for samples containing low concentrations of the more reactive metal a phenomenon that was not observed for the alkoxide system studied in which samples containing lower concentrations of titanium gave powders rather than gels (Table 5.1).

All attempts at supercritical drying lead to a collapse of the gel network. The dry methanol solvent used to extract the water from the gel may have reacted with residual OH and OR groups on the gel leading to this collapse and in addition to this there were also problems with the iridium acetate precursor being extracted into methanol solution.

5.2.4.2 Thermal analysis of the samples

The samples 5-8 were analysed by simultaneous TGA/DTA by heating at 10 °C/min to 550 °C under oxygen. The traces obtained were almost identical for all samples with a typical pattern, that of the sample (6) containing iridium and titanium in a ratio of 1:1 derived from aqueous solution being shown in Fig 5.9. The overall weight losses are listed in Table 5.5.

In all the samples analysed there is weight loss of about 10% between 100 and 150 °C corresponding to the loss of solvent and water. The principal weight loss occurs at around 200 °C accompanied by a large peak in the DTA trace. This loss is assigned to combustion of organic material, with the weight loss increasing with the amount of iridium in the samples. No peak is seen that might correspond to crystallization in the samples.

Sample	wt loss /%
5	77
6	65
7	35
8	70

Table 5.5: Overall weight loss observed during thermal analysis under oxygen of IrO_2-TiO_2 mixed oxides. Samples 5-7 are obtained from aqueous solution, sample 8 from ethanolic solution.

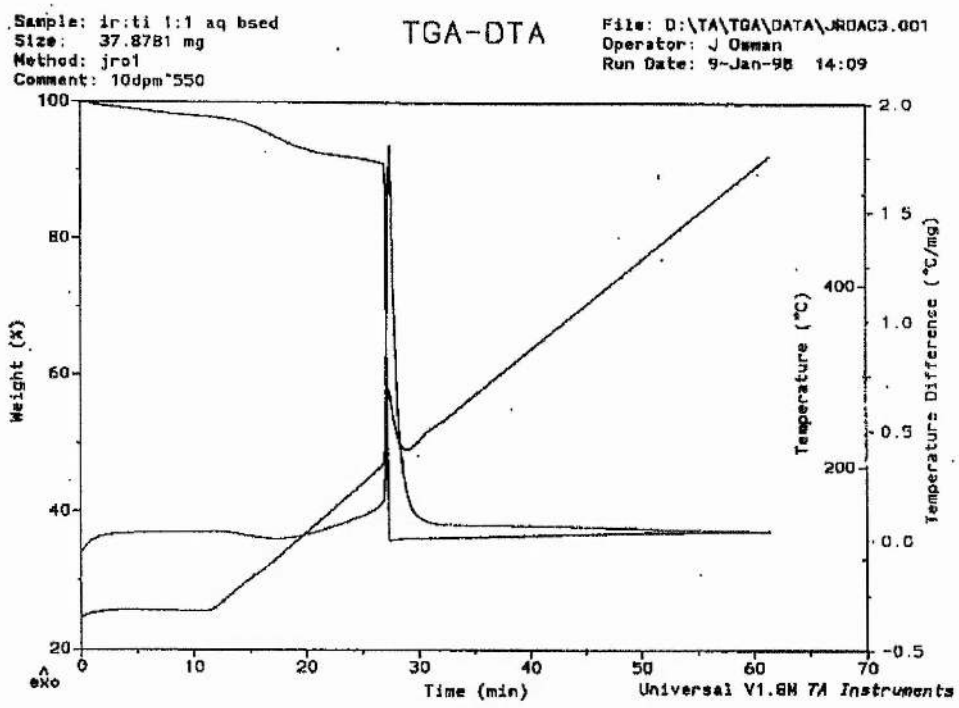

Fig 5.9 TGA/DTA traces under oxygen for IrO_2-TiO_2 (ratio Ir:Ti 1:1) mixed oxide derived from aqueous solution heated at 10°C/min to 550°C

The overall weight losses observed in this system are much higher than expected and are certainly higher in most cases than for the corresponding oxides produced from alkoxide precursors. The results suggest that hydrolysis and condensation are not extensive with many of the organic groups on both the precursors being unhydrolysed, this being a further indication that the iridium acetate might not be undergoing reaction at all as was suggested by the green colour of the methanol solutions used to extract water from the gels for supercritical drying. The oxide content of acac stabilised $Ti(OEt)_4$ is 28.3% and that of iridium acetate is 56%. It is thus significant that the overall weight loss increases when the amount of titanium in a sample decreases when the reverse is expected. It is likely that as the amount of titanium is increased in each sample the extent of hydrolysis and condensation is greater hence the smaller weight loss.

5.2.5.1 Analysis of the samples by X-ray diffraction

The samples 5-8 produced from aqueous and ethanolic solution were calcined in the same way as the IrO_2-TiO_2 gels and powders produced from iridium ethoxide precursors. It was found that final calcination at 450 °C was sufficient to satisfactorily crystallize two of the aqueous samples (6 and 7). The other aqueous sample (5) and the sample obtained using ethanol as a solvent (8) needed calcination at 550 °C to obtain a crystalline sample as, although there was some evidence of a crystallinity at 450 °C, the peaks were too broad to allow analysis.

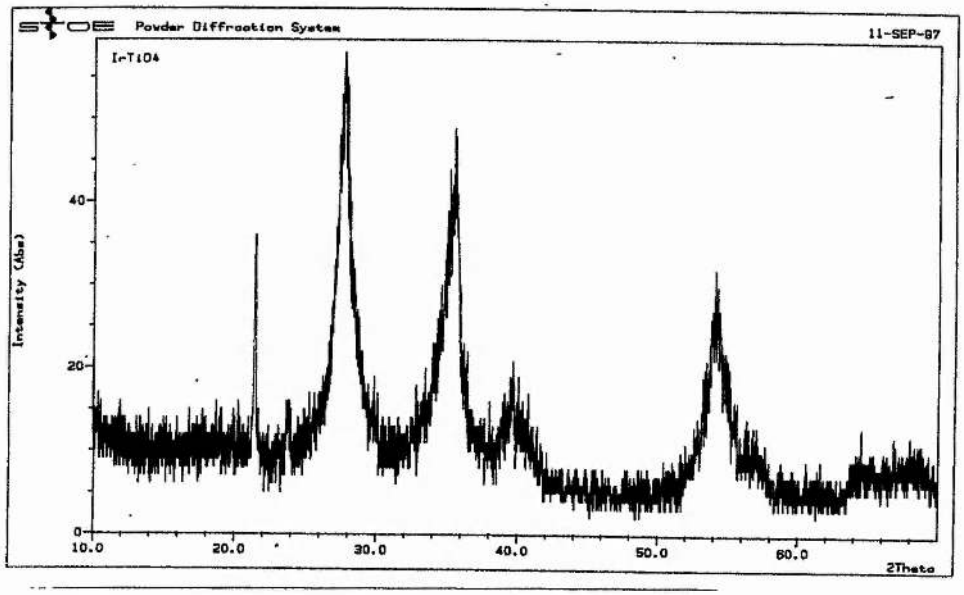

Fig. 5.10: X-ray powder diffraction pattern (Cu kα) for IrO_2-TiO_2 (ratio Ir:Ti 1:3) mixed oxide calcined at 250°C and 450°C.

The results are a clear indication that the procedures have indeed provided a novel route to an IrO_2-TiO_2 solid solution. Fig. 5.10 show the X-ray diffraction pattern for the Ir:Ti 1:3 sample. The patterns clearly show firstly that there are no peaks corresponding to anatase phase TiO_2, this being the case for all the samples studied. There only appears to be one rutile phase and the positions of selected peaks for each sample along with the positions of the peaks for the pure materials are given in Table 5.6. The positions of the peaks are between the values for the rutile phases of pure IrO_2 and TiO_2 although the extent of these peaks shifts does not correspond exactly to the ratio of the metals in the sample as would be expected if intimate mixing were occurring as is shown in Fig. 5.11. For the samples 5 and 7, obtained from aqueous solution, the peak positions tend to be closer to the values for a sample with a Ir:Ti 1:1 ratio suggesting the presence of some single phase IrO_2 or TiO_2 (whichever is of the

highest percentage in the sample), the peaks of which are hidden by the broad mixed oxide peaks. Analysis of sample 4, obtained from ethanolic solution, shows the position of the peaks to be much closer to those expected of rutile phase TiO_2 suggesting that the sample might not be a solid solution and that in this sample only TiO_2 is crystallizing even at the higher calcination temperature of 550°C. The peaks are relatively broad in all cases suggesting that the size of the particles is relatively small with the samples at ratios of Ir:Ti 1:1 seeming to have the broadest peaks.

Reflection		Sample				
hkl	IrO_2	1	2	3	4	TiO_2
110	28.026	27.9341	27.789	27.345	27.5701	27.445
101	34.699	35.2819	35.445	35.667	35.8254	36.084
211	54.018	54.1744	54.071	54.071	54.3232	54.319

Table 5.6: Positions of selected peaks 2θ in X-ray powder diffraction patterns (Cu $k\alpha$) for IrO_2-TiO_2 mixed oxides obtained from aqueous (samples 1-3) and ethanolic solution (sample 4).

One of the principal advantages of using an acetate-based route over the ethoxide route initially tried is in the composition of the final gel product. As no sodium ethoxide was used to prepare the gel none of the sodium salt impurity that was such a problem in the ethoxide based gels is present in the final product. It is also found that this route to the oxide does not produce any iridium metal after calcination as no peak is seen at $2\theta = 47.311°$ which would be present along with a major peak at 40.660° (indistinguishable from the (1 1 1) reflection of the rutile phase in these patterns).

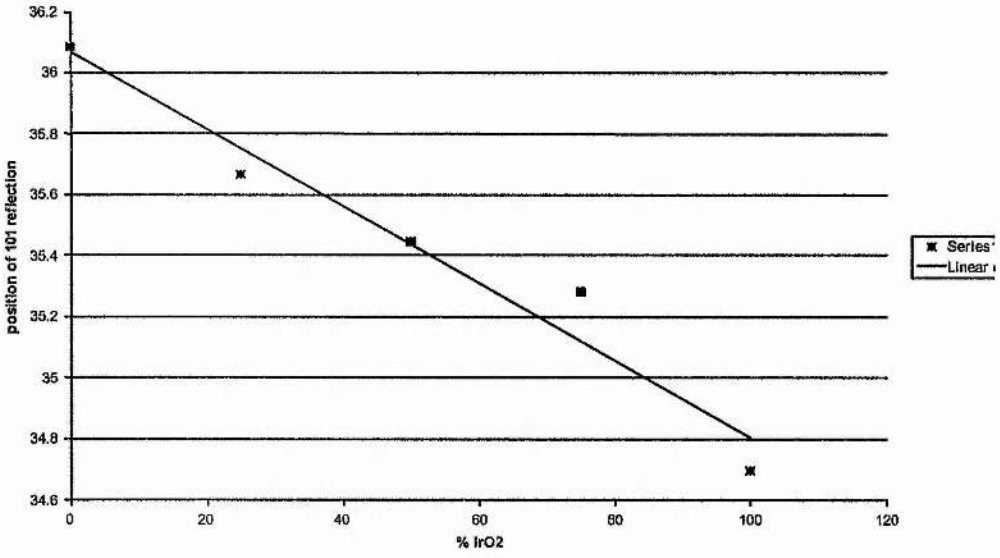

Fig. 5.11: Positions of 101 plane reflections 2θ in X-ray powder diffraction patterns (Cu kα) for IrO_2-TiO_2 mixed oxides obtained from aqueous (samples 1-3) and ethanolic solution (sample 4)

5.2.5.4 Analysis by electron microscopy

The samples were all studied by both scanning and transmission electron microscopy. The SEM pictures (Fig. 5.12 shows the micrograph for sample 6) and is typical of all the samples analysed) show broken particles of the gels of varying size and higher magnifications suggest that, unlike in previous gel samples, the particles would appear to be parts of a continuous network which has cracked under capillary pressure and not an aggregation of smaller particles. Examination by TEM (Fig. 5.13 shows sample 6) confirms the high degree of dispersion in the uncalcined samples as unlike previous samples no distinct regions of TiO_2 and IrO_2 can be found and the

Fig. 5.12 Scanning electron micrograph of IrO_2-TiO_2 mixed oxide (ratio Ir:Ti 1:1) derived from aqueous solution

Fig. 5.13 Transmission electron micrograph (115 000 times magnification) of IrO_2-TiO_2 mixed oxide (ratio Ir:Ti 1:1) derived from aqueous solution

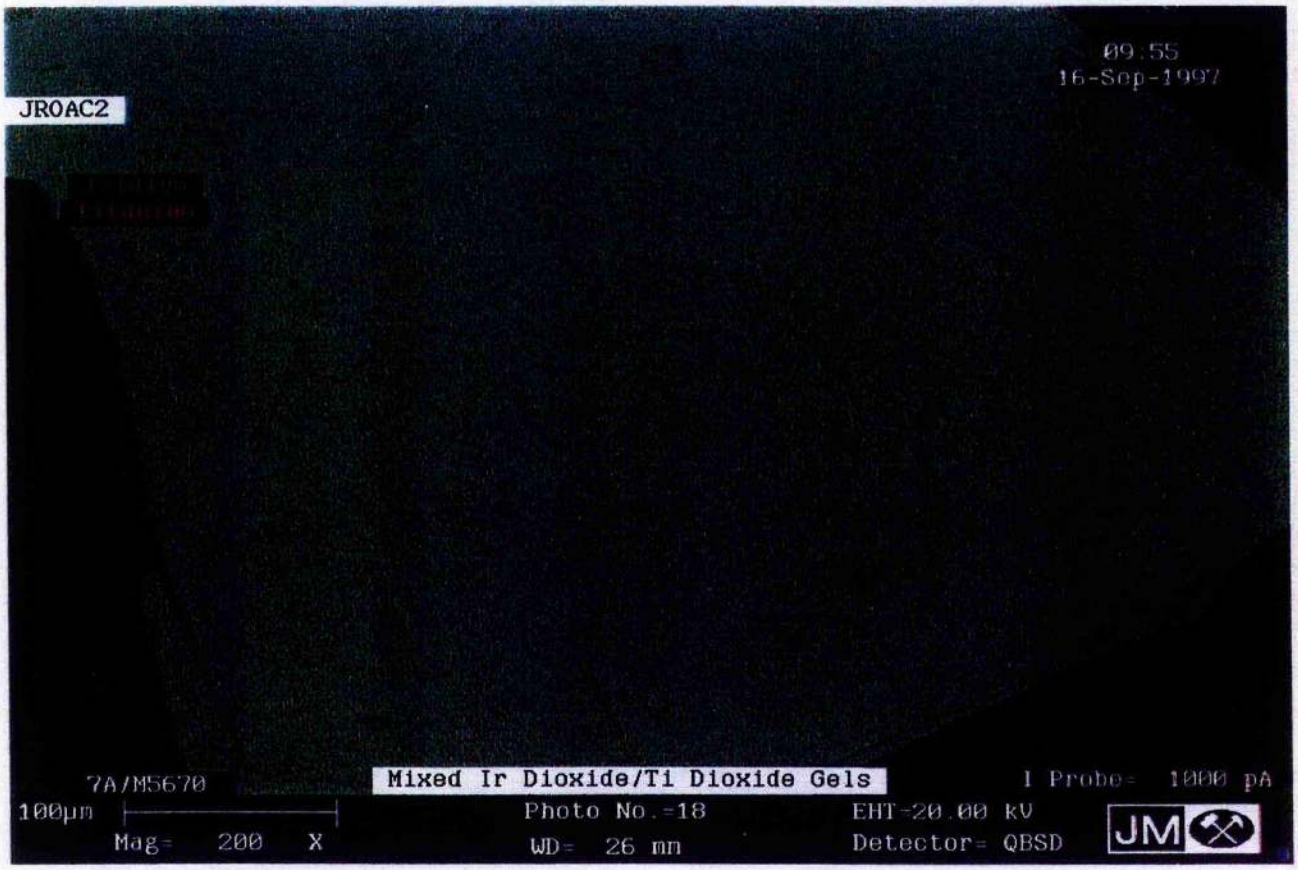

Fig. 5.14 Scanning electron micrograph of IrO_2-TiO_2 mixed oxide (ratio Ir:Ti 1:1) derived from aqueous solution showing the distribution of Ir and Ti .

samples are found to be an amorphous mixture of tiny particles of titanium and iridium oxides, with the EDX results for the analysis indicating that titanium is the predominant region in all the samples tested. EDX analysis of the SEM results allow determination of the distribution of the different species within each gel fragment. Fig. 5.14 shows an even distribution of titanium and iridium within the Ir:Ti 50:50 gel as determined by EDX and again shows that there are no independent regions of IrO_2 and TiO_2, rather an intimate mixture of the two with TiO_2 clearly being the predominant species at the surface.

5.3 Conclusions

The principal conclusion to be drawn from these experiments is that it is possible to produce highly dispersed mixed metal oxide gels containing iridium and titanium dioxides, but only if an iridium acetate precursor and acac modified titanium precursor are used. The final product is intimately mixed as shown by the electron microscopy studies, crystallizes at 450-550 °C to a single rutile phase solid solution, with oxidation of Ir(III) to Ir(IV) occuring during calcination, and contains no impurities or iridium metal. The gel times are relatively slow reflecting the nature of the precursors, modified $Ti(OEt)_4$ and iridium acetate. If controlled hydrolysis of an ethanolic solution is used gelation is quicker although this sample requires a higher calcination temperature to obtain a cystalline sample and there is some doubt, arising from the powder X-ray diffraction data, as to whether a genuine solid solution is being produced after calcination. However, the choice of sol-gel route, be it from aqueous or ethanolic solution, had little effect on the nature of the gels obtained with both aqueous and non-aqueous routes giving an intimately mixed final product with differences only

noticable after heat treatment.

Attempted Non-hydrolytic routes to the mixed oxide and supercritical drying of the gel product have been unsuccessful although a non-hydrolytic route should work if a non polar solvent in which the iridium acetate is soluble can be found. It is clear, from the green colour of the solutions obtained during the methanol soaking stage of supercritical drying and the large weight loss observed in the thermal analysis of the samples, that the gelation reaction is at least partially reversible in all the samples prepared and that reaction of the iridium acetate molecule is not extensive.

Attempts to produce mixed gels from "iridium alkoxides" and titanium ethoxide precursors have been relatively successful with partial solid solution formation being achieved albeit with some regions of single metal oxide within the samples. The principal problem arising form the route starting from sodium hexachloroiridate is that the final product is contaminated extensively with sodium chloride, with the XPS analysis of the system suggesting some reduction from Ir(IV) to Ir(III) taking place. The NaCl contamination should not prove a problem if powder samples are required. Attempts to produce single metal IrO_2 gels from "alkoxide" precursors have been unsuccessful and this is thought to be due to the reactivity of the "iridium alkoxide" itself and whether this species is actually being generated.

The aqueous route via hydrolytic polymerization of the iridium aqua ion, $[Ir(H_2O)_6]^{3+}$ has been investigated and a number of colour changes are observed. It is found that gels cannot be obtained at the concentrations used, instead a cream precipitate of $Ir(OH)_3(OH_2)_3$ that can reconverted to the aqua ion or allowed to olate to form IrO_2 is produced by controlled raising of the pH of a solution of the aqua ion in perchloric acid.

5.4) Experimental Section

5.4.1 Preparation of the $[Ir(H_2O)_6]^{3+}$ aqua ion

The procedure used was that of Beutler and Gamsjager[12]. 2.2g of H_2IrCl_6 (Johnson Matthey) were dissolved in 600 cm^3 of 0.2M NaOH (Aldrich) and maintained at 35-40°C for 3-4 hours. 400 mg of ascorbic acid (Aldrich) were added after approximately 2 hours to prevent air oxidation of the Ir(III) produced. Oxygen evolution was observed and the colour of the solution changed from red to green/yellow. The solution was slowly neutralised to pH 8 by slow addition of 4M $HClO_4$ and the cream precipitate of $Ir(OH)_3(H_2O)_3$ formed was cooled and centrifuged. The cream precipitate was dissolved in 2M $HClO_4$ and loaded onto a column of Dowex 50W-X2 50-100 mesh (H^+ form). The column was washed with 0.2M $HClO_4$ before elution of the product with 2M $HClO_4$.

5.4.2 Attempted preparation of IrO_2 gels

In this experiment and in all experiments using ethoxide precursors the glassware used was dried in an oven for at least 6 hours prior to use to remove trace water.

Na_2IrCl_6 (4.51g, 10 mmol, Johnson Matthey) was added to a dry 3 necked flask under argon. 25 cm^3 of anhydrous ethanol were added and the solution heated under reflux to dissolve the solid. 27 cm^3 (40 mmol) of 1.5M sodium ethoxide (NaOEt) (Aldrich) were added to the solution which turned orange and then black. The solution was heated under reflux for 3 hours after which 9 cm^3 of a 10% by mole solution of

HNO_3 in anhydrous ethanol (to give a ratio of H_2O:Ir:H^+ of 5:1:0.1) were added to hydrolyse the IrO_2 precursor. Neither gelation or precipitation occured.

The experiment was repeated using a more concentrated solution of the Na_2IrCl_6 but again no precipitation or gelation occured. The experiment was also repeated using H_2IrCl_6 (Johnson Matthey)

5.4.3 Attempted preparation of IrO_2-TiO_2 gels from alkoxide precursors

5.4.3.1 Preparation of IrO_2-TiO_2 1:4 gel

0.451g (1 mmol) of Na_2IrCl_6 (Johnson Matthey) was placed in a dry 3 necked flask under argon and dissolved in 20 cm^3 of anhydrous ethanol. To this solution was added 0.9 cm^3 (4 mmol) of 3M NaOEt (Aldrich). The mixture was refluxed for three hours to generate iridium (IV) alkoxide after which 0.84 cm^3 (4 mmol) of $Ti(OEt)_4$ was added. The solution was left to cool after which 4.5cm^3 of HNO_3 (10% by mole in absolute ethanol) was added with stirring to hydrolyse the ethoxide mixture (ratio of H_2O:M:H^+ of 5:1:0.1). A black gel was obtained after 15 minutes. The gel was air dried to remove most of the solvent and then dried under vacuum overnight.

5.4.3.2 Preparation of IrO_2-TiO_2 2:3 gel

Experimental procedure was as for section 7.4.3.1. 0.90g (2 mmol) of Na_2IrCl_6 was dissolved in 20cm^3 of absolute ethanol under argon and heated after which 0.63 cm^3 (3 mmol) of $Ti(OEt)_4$ was added. Hydrolysis was performed using 4.5cm^3 of HNO_3 in ethanol. The solution gelled in 19 hours although on some occasions when

the experiment was repeated a powder product was obtained.

5.4.3.3 Preparation of IrO_2-TiO_2 3:2 gel

Experimental procedure was as for section 7.4.3.1. 1.35g (3 mmol) of Na_2IrCl_6 was dissolved in 20cm^3 under argon and heated. After cooling the solution 0.42 cm^3 (2 mmol) of $Ti(OEt)_4$ was added. Hydrolysis was performed using 4.5cm^3 of HNO_3 in ethanol. Initially gelation did not occur and the solution appeared stable. It was found that if the solution were allowed to evaporate partially gelation occured within 24 hours. Again it was found that precipitation rather than gelation occured in some repeats of the experiment.

5.4.3.4 Preparation of IrO_2-TiO_2 2:3 gel

Experimental procedure was as for section 7.4.3.1. 1.80g (4 mmol) of Na_2IrCl_6 was dissolved in 20cm^3 under argon and heated. After cooling 0.21 cm^3 (1 mmol) of $Ti(OEt)_4$ was added. Hydrolysis was performed using 4.5cm^3 of HNO_3 in ethanol. The solution did not gel even after partial evaporation rather a powder product was obtained, centrifuged and dried as for the gel samples

5.4.4 Attempted preparation of IrO_2-TiO_2 gels from Iridium acetate and $Ti(OEt)_4$

5.4.4.1 Preparation of IrO_2:TiO_2 1:1 gel from aqueous solution

1.976g (5 mmol) of $[Ir_3(OAc)_6O(HOAc)_3]OAc$ (iridium acetate) (Johnson

Matthey) were dissolved in 20cm^3 of distilled water to give a 0.25M solution. $Ti(OEt)_4$ (1.05cm^3, 5 mmol, Aldrich) were placed in a dried beaker and 2,4,Pentanedione (acac, 0.51cm^3, 5 mmol, Aldrich) were added with stirring to stabilise the titanium precursor against fast hydrolysis and condensation. The aqueous solution of iridium acetate was added dropwise with stirring to the modified $Ti(OEt)_4$. The mixture was covered with Nescofilm® in which a number of holes had been pierced and allowed to gel. A dark green gel was obtained after 18 days and dried under vacuum at 90°C overnight to remove solvent.

The experiment was repeated using with the iridium acetate precursor dissolved in 0.5M acetic acid rather than water and using no acac to stabilise the $Ti(OEt)_4$. This gave a white precipitate on mixing which would not redissolve and gelation did not occur.

For supercritical drying purposes a portion of the gel obtained from iridium acetate and acac stabilised $Ti(OEt)_4$ was soaked in 5 baths of dry methanol to remove water. It was observed that the methanol solution developed a green colour suggesting that the iridium acetate was being leached from the gel. Supercritical drying was unsuccessful with all attempts leading to a collapse of the gel network.

5.4.4.2 Preparation of IrO_2:TiO_2 1:3 gel from aqueous solution

Experimental procedure was the same as 7.4.4.1. 0.79g (2 mmol) of iridium acetate in 20cm^3 of distilled water were added to $Ti(OEt)_4$ (1.26 cm^3, 6 mmol) stabilised with 0.61 cm^3 (6 mmol) of acac with stirring. The solution gelled after 14 days again giving a green gel which was dried under vacuum as before.

5.4.4.3 Preparation of IrO_2:TiO_2 3:1 gel from aqueous solution

Experimental procedure was for 7.4.4.1. 2.964g (7.5 mmol) of iridium acetate in 20 cm^3 of distilled water was added to a mixture of 0.53cm^3 (2.5 mmol) of $Ti(OEt)_4$ and 0.25 (2.5 mmol) of acac with stirring. The solution gave a green gel after 29 days which was dried under vacuum.

5.4.4.4 Preparation of IrO_2:TiO_2 1:1 gel from ethanolic solution.

1.97g (5 mmol) of iridium acetate were placed in a dry 3 necked flask under argon. 20 cm^3 of anhydrous ethanol were added and the mixture heated to 70°C with stirring to dissolve the acetate. To the resulting solution was added 0.51 cm^3 (5 mmol) of acac and 1.05 cm^3 (5 mmol) of $Ti(OEt)_4$. The mixture was initially heated for one week in an attempt to obtain a non-hydrolytic gel which was not formed nor could the solution species be isolated after removal of the solvent under vacuum. During heating the colour of the solution changed from green to red/brown and a white precipitate was observed which later redissolved. In experiments after the attempt to produce the non-hydrolytic gel 3.6 cm^3 of a mixture of 10% water in absolute ethanol (20 mmol water) were added 3 hours after addition of the acac and $Ti(OEt)_4$. Gelation occured within 5 days of the addition of the hydrolysis water and the resultant red/brown gel was dried under vacuum overnight.

5.5) References

1) S. E. Castillo-Blum, D.T. Richens and A.G. Sykes, *Inorg. Chem.*, 1989, **28**, 954

2) A. Osaka, T. Takatsuna and Y. Miura, *J. Non-Cryst. Solids*, 1994, **178**, 313.

3) Y. Murakami, S. Tsuchiya, K. Yahikozawa and Y. Takasu, *J. Mater. Sci.Lett.*,1994, **13**, 1773.

4) Y. Murakami, H. Ohkawauchi, M. Ito, K. Yahikozawa and Y. Takasu, *Electrochim. Acta*, 1994, **39**, 2551.

5) Y. Murakami, S.Tsuchiya, K. Yahikozawa and Y. Takasu, *Electrochim. Acta*, 1994, **39**, 651.

6) Y. Murakami, K. Miira, M. Ueno, M. Ito, K. Yahikozawa and Y. Takasu, *J. Electrochem. Soc.*, 1994, **141**, L118.

7) Y. Takasu, S. Onoue, K. Kameyama, Y. Murakami and K. Yahikozawa, *Electrocchim. Acta*, 1994, **39**, 1993

8) M. Ardon, A. Bino and K. Michelson, *J. Am. Chem. Soc.*, 1987, **109**, 1986.

9) Y. E. Roginskaya, O. V. Morozova, E. N. Loubnin, A. V. Popov, Y. I. Ulitina,V. V. Zhurov, S. A. Ivanov and S. Trasatti, *J. Chem. Soc., Faraday Trans.*,1993, **89**, 1707.

10) R. C. Mehrotra and A. Singh, *Chem. Soc. Rev.*, 1996, **25**, 1.

11) D. T. Richens, *The Chemistry of Aqua ions*, Wiley, Chicester, 1997.

12) P. Beutler and H. Gamsjager, *J. Chem. Soc. Chem. Commun.*, 1976, 554.

CHAPTER 6

Oxygen Evolution and Electrochemical Studies on Sol-Gel Derived Iridium Dioxide.

6.1 Introduction

One of the most important uses of RuO_2 and IrO_2 is in the catalysis of oxygen evolution (equation 6.1).

$$4Ce^{IV} + 2H_2O \rightarrow 4Ce^{III} + 4H^+ + O_2 \qquad (6.1)$$

A solution of cerium (IV) is an example of a species which is thermodynamically unstable as it has a redox potential greater than that of the O_2/H_2O and Cl_2/Cl^- couples[1]. This species is, however, stable kinetically due to a large activation barrier arising from the multi-electron transfer processes involved. Hence the need for a redox catalyst to allow production of oxygen hydrogen and chlorine at reasonable rates.

The group of Mills[2] has studied the kinetics of water oxidation of a number of different catalysts including RuO_2 and IrO_2 in the oxidation of water by $Ce^{4+}_{(aq)}$ using an oxygen evolution cell and in situ UV-Vis spectrophotometry. It was found that RuO_2 and IrO_2 catalysts showed high activity after heat treatment, and that this activity remained high when the catalysts were mixed with an inert metal support. The same techniques have been used to study chlorine evolution by $Ce^{4+}_{(aq)}$ catalysed by RuO_2 and IrO_2 prepared by different methods[3].

It has been shown that for most examples of redox catalysis the catalyst acts as a microelectrode[4] (Fig. 6.1), that is to say that the that the particles have two redox reactions occurring at their surfaces and that the particles provide a medium for electrons to flow between these couples. At a given time, t, during the reaction the current, $i_{mix,t}$, due to the electrons flowing through the particles is related to the rate of reaction at that instant by equation 6.2

$$R(t) = i_{mix,t} / F \qquad (6.2)$$

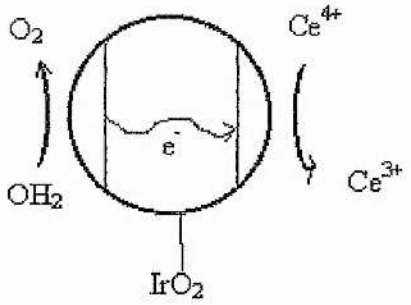

Fig. 6.1: Schematic representation of an IrO_2 microelectrode.

If the redox catalyst is not affected by the reaction conditions and if the redox couples act independently of each other it is possible to predict, using this model, the kinetics of catalysis from a knowledge of the current vs voltage behaviour of the two redox couples on the redox catalyst[5,6].

The acid medium in which oxidation is performed can affect the kinetics. These are diffusion controlled if the difference between the two equilibrium potentials involved in the reaction is large. If $Ce^{4+}_{(aq)}$ is used as the oxidant in 1M $HClO_4$ the $Ce^{IV/III}$ couple is sufficiently separated from the O_2/H_2O couple and the electrochemical

model of redox catalysis[1] predicts that the current will tend to its diffusion controlled limit, given in equation 6.3 (where n is the number of electrons transferred in the reduction of Ce(IV) to Ce(III), D is the diffusion coefficient of the Ce(IV) ions ($=k_d\delta$), δ is the thickness of the diffusion layer and A_{cat} is the effective catalyst surface area) i.e the kinetics of the reaction are first order with respect to [Ce(IV)].

$$I_{mix} = nFD[Ce^{IV}]A_{cat}/\delta \qquad (6.3)$$

A detailed study of the the kinetics of water oxidation by Ce(IV)[7] using thermally activated $RuO_2.nH_2O$ as the redox catalyst, has shown that the kinetics of Ce(IV) reduction are indeed first order with respect to [Ce(IV)] and that thus, subject to there being no corrosion of the catalyst, the kinetics of reduction of the Ce(IV) ions should be a direct measure of the catalytic activity of a redox catalyst.

It has been observed that first order behaviour is observed for particles with a mean diameter of > 100 nm. If the particle size is smaller than this there have been reports of the reaction showing a dependence on catalyst concentration approaching second order[8]. The explanations that have been put forward to explain this phenomenon include rate enhancement by particle collision, diffusion layer restriction of particle proximity, catalyst poisoning or corrosion and finally coagulation of the particles. Prevention of coagulation has been performed using antiflocculants such as polystyrene sulphonate[8] and the inert oxide AEROSIL COK 84[9] (an 84% SiO2, 16% aluminium oxide C mixture). By adding the antiflocculant it has been found that the overall rate increases which has led to the conclusion[8] that it is the chemical characteristics of the surface, rather than the state of catalyst dispersion or gas evolution, that gives rise to second order dependence on catalyst concentration.

The aim of our work was to apply the techniques used above to study the catalytic activity of the sol-gel derived IrO_2-TiO_2 mixed oxide catalysts produced by sol-gel processing and to compare them to the published data for oxides prepared by other methods. Attempts were also made to prepare electrodes coated with the sol-gel derived mixed oxides but the adhesion of the oxide layer to the titanium substrate used proved poor. In the limited time available no electrochemical experiment could be performed on these electrodes.

6.2 Instrumentation

Oxygen evolution studies were performed using a Rank Brothers oxygen electrode system (Fig. 6.1). This consists of a quartz cell with a platinum working electrode covered by a teflon membrane. This was surrounded by a silver reference electrode. The working electrode was poised at –0.4 V relative to the reference electrode and the current due to oxygen evolution (equation 6.1) was converted to a voltage by a Pine Instrument company RDE 4 potentiostat. This voltage was recorded on a Graphtec WX 3000 chart recorder.

The rate of oxygen evolution, was also studied by monitoring of the rate of disappearance of the UV band of $Ce^{4+}_{(aq)}$ at 400 nm using a Perkin Elmer Lambda 14 spectrophotometer. Plots of absorbance against time were recorded and smoothed using the UV Winlab software package for the IBM PC.

Full details of the method are provided in section 6.5

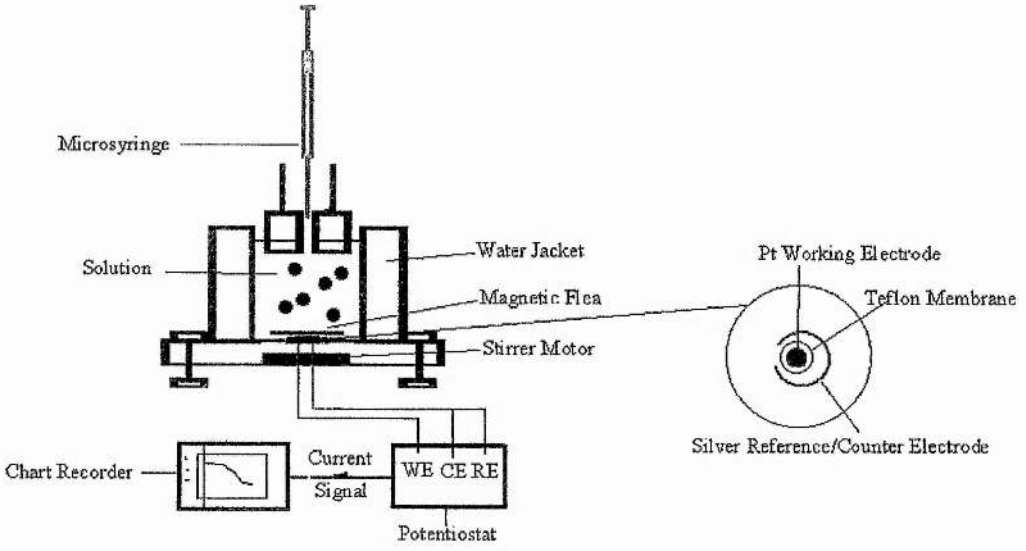

Fig. 6.1 Schematic representation of the experimental system used to monitor the IrO_2 catalysed oxidation of water to oxygen by Ce (IV) ions.

6.3 Results and Discussion

6.3.1 UV-Vis Spectrophotometric studies on iridium oxide electrocatalysts

The oxygen evolving properties IrO_2-TiO_2 samples produced from ethoxide and acetate precursors was initially studied by examining the rate of absorbance change, and hence the rate of consumption of the UV-Vis band at 400 nm of a solution of Ce (IV) added to suspensions of the catalyst samples in 1M $HClO_4$.

The results obtained for the ethoxide based samples are plotted in Fig. 6.2 and the rate constants obtained in Table 6.1, where k_1 is the first order rate constant, k_1' is the k_1/(amount of catalyst used) and k_1'' is rate constant per mole of active metal.

Sample	Gradient k_1	Intercept	r^2	k_1' /g^{-1} s^{-1}	k_1'' /mol^{-1} s^{-1}
IrO_2	-0.010	-0.143	0.940	32.46	7303.5
Ir:Ti 4:1	-0.009	-0.006	0.987	29.22	8218.3
Ir:Ti 3:2	-0.010	0.004	0.997	32.46	12175.3
Ir:Ti 2:3	-0.02	-0.196	0.981	64.94	36525.9

Table 6.1: Rate Constant data for IrO_2 and IrO_2-TiO_2 mixed oxides derived from UV-Vis spectrophotometry. k_1 is the first order rate constant, k_1' is the k_1/(amount of catalyst used) and k_1'' is rate constant per mole of active metal.

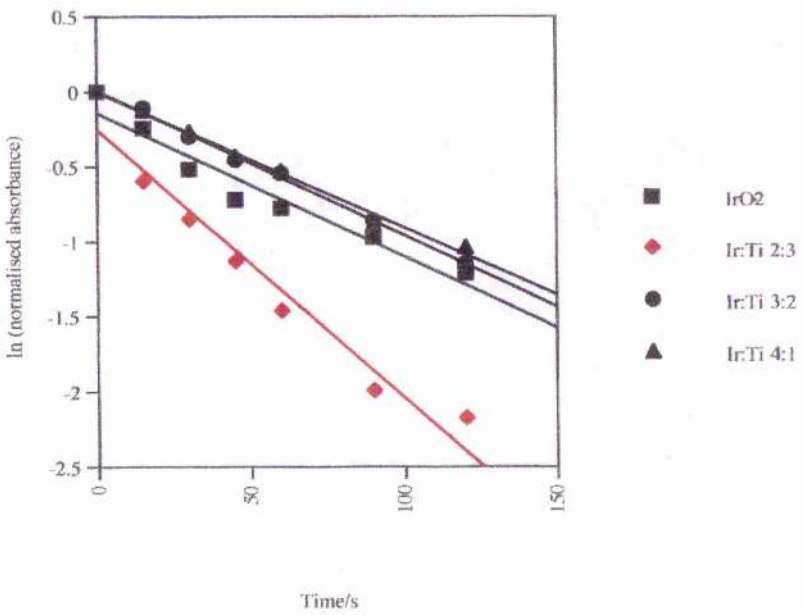

Fig. 6.2: Kinetics of $Ce^{4+}_{(aq)}$ disappearance during the oxygen evolution reaction catalysed by of sol-gel derived IrO_2 powders.

Surprisingly, the results for the IrO_2-TiO_2 samples generated from ethoxides have very similar rate constants, k_1, and, as was found for the samples of Mills[2], the addition of a base metal is found to increase the rates. It is found that as the amount of TiO_2 in a sample is increased then so does the activity per mole of IrO_2. This improved activity as more TiO_2 is mixed in has the added advantage of lowering the potential cost of any catalyst based on this system.

The overall rates are higher for sol-gel derived IrO_2 than for IrO_2 produced by base hydrolysis of the trichloride followed by thermal activation but lower than those obtained from an Adams catalyst[2]. When other factors are taken into account however, these iridium catalysts are found to be extremely effective. The measure of activity per gram of catalyst, k_1', used is significantly higher for thermally activated mixed oxide compounds and even than for IrO_2 produced by any other means. Further to this, the results are comparable, and in some cases higher than for mixed IrO_2-SnO_2 catalysts, the most active catalysts reported[2]. The values of k_1" are also high. This is a measure of the activity per mole of the active species and it is found here that the activity values obtained for the sol-gel derived species are of the same order of magnitude as the best known oxygen evolution catalysts reported.

The high activity of the samples can be explained by considering their nature. Mills and Russell[2] found that addition of SnO_2 to an IrO_2 sample increases the rate constants for oxygen evolution when compared to pure IrO_2 and the same is found here. It was shown in the electron micrographs of the mixed oxide samples (section 5.2.3) that the IrO_2 in the samples is in the form of small (0.5-20 nm) highly dispersed particles within a TiO_2 matrix. This provides a larger surface area and a larger number of microelectrodes (Fig. 6.4), for water oxidation to occur at than for a pure IrO_2

sample in which much of the active species will be in the bulk, hence the higher activity. It may be necessary however, to get an accurate measure the size of the dispersed mixed oxide particles in the reaction mixture to provide a full explanation of the high activity of these catalysts.

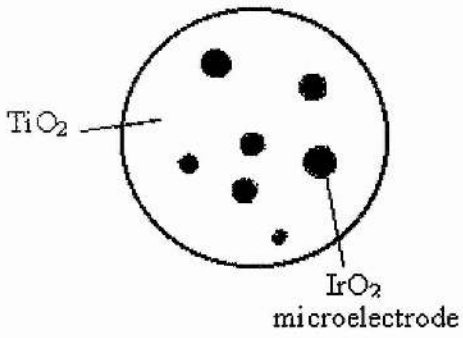

Fig. 6.4: A particle of dispersed IrO_2-TiO_2 mixed oxide showing the IrO_2 microelectrodes at the surface of the particles at which water oxidation can occur.

6.3.2 Oxygen evolution measurements on iridium oxide electrocatalysts

The kinetics of catalysis of the IrO_2 based O_2 catalysts can also be determined using the oxygen cell shown in Fig. 6.2. A dispersion of the catalyst in 1M $HClO_4$ is purged of oxygen using argon. Cerium ions are injected and the oxygen generated by the reduction of these ions, catalysed by the platinum group metal oxide, is itself reduced at a platinum electrode. The current is converted to a measurable voltage by the potentiostat and recorded on a chart recorder.

The activity of a number of the iridium acetate based IrO_2-TiO_2 mixed oxide catalysts was studied although the ethoxide based samples could not be examined due to problems with leaks from the cell. The results for samples tested are given in Table 6.2.

Sample	Gradient k_1 /s^{-1}	Intercept	r^2	k_1' /g^{-1} s^{-1}	k_1" /mol^{-1} s^{-1}
Ir:Ti 3:1	-0.018	-6.1132	0.9598	65.40	12569
Ir:Ti 1:1	-0.0476	-5.9538	0.9677	205.2	39402
Ir:Ti 1:3	-0.0285	-6.6358	0.8398	191.7	36801

Table 6.2: Rate constant data for iridium acetate based IrO_2-TiO_2 mixed oxide samples derived from evolved oxygen measurements. k_1, k_1' and k_1" are defined as before.

The cell used in the measurement of the activity of the catalysts was not thermostatted although the temperature was measured as 18 °C ± 1 °C before and after each experiment. It is again found that the electrocatalytic activities of the sol-gel derived IrO_2-TiO_2 mixed oxides are comparable to the most active samples tested previously[2]. The IrO_2-TiO_2 sample with a metal ratio of 1:1 is found to give the best activity of the samples tested: indeed, the activity of this sample, as determined by the rate per mole of catalyst, is found to be higher than any reported electrocatalyst.

The high activity observed can again be put down to the nature of the sol-gel derived products. The IrO_2 is highly dispersed (with the size of the cystallites having been determined as < 5 nm by TEM) within the matrix of the inert support providing a large surface area for reaction to occur at.

Unlike the ethoxide based systems, however, the electrocatalytic activity does not seem to increase as the amount of the inert support is increased. Instead, a maximum value is obtained at a ratio of IrO_2:TiO_2 of 1:1. This may be a consequence of the fact that the TiO_2 and IrO_2 form a solid solution (see X-Ray diffraction results (section 5.2.5.1)) and thus the surface area of IrO_2 available for reaction is lower as the amount of TiO_2 is increased above a ratio of 1:1.

6.4 Conclusions

The IrO_2-TiO_2 mixed oxides, produced by sol-gel processing using iridium ethoxide and iridium acetate as starting materials, have been shown to have amongst the highest electrocatalytic activities, per mole of active species, of any catalyst reported. The high activity can be assigned to the small size of the iridium oxide particles present in the dispersed mixed oxide powders.

It has been shown that the presence of increasing amounts of an inert support (TiO_2) increases the activity of ethoxide based samples whereas the activity increases with increasing inert support only until the amounts of TiO_2 and IrO_2 were equal after which the activity drops.

6.5 Experimental section.

6.5.1 UV-Vis Spectrophotometric studies on iridium oxide electrocatalysts

The calcined IrO_2-TiO_2 electrocatalyst samples, prepared as in sections 5.4.3 and 5.4.4 and were added to 1M $HClO_4$ to give a concentration of 77 mg/dm^{-3}. Each mixture was sonicated for 5 mins to disperse the solid. 4 cm^3 of each dispersion was placed in a quartz cuvette in a UV-Vis spectrophotometer. A 30 μl aliquot of a 0.12 M solution of cerium nitrate (Aldrich) was added to the dispersion in the cuvette and the absorbance at 400 nm monitored for 10 minutes.

6.5.2) Oxygen evolution measurements on iridium oxide electrocatalysts

4 cm^3 of a dispersion (77 mg/dm^{-3}, prepared as for section 6.5.1) of an IrO_2-TiO_2 sample were placed in an oxygen cell. The solution was degassed with argon until no dissolved oxygen remained. A 30 μl aliquot of 0.12M cerium nitrate (Aldrich) was injected into the cell with stirring and the resultant current converted to a voltage and measured on a potentiostat.

6.6 References

1) A. Mills, *Chem. Soc. Rev.*,1989, **18**, 285

2) A. Mills and T. Russell, *J. Chem. Soc., Faraday Trans.*, 1991, **87**, 1245.

3) A. Mills and D Worsley, *J. Chem. Soc., Faraday Trans.*, 1991, **87**, 3275.

4) M. Spiro, *Chem. Soc. Rev.*, 1986, **15**, 141.

5) A. Mills and N. McMurray, *J. Chem. Soc., Faraday Trans. 1*, 1989, **85**, 2047.

6) A. Mills and N. McMurray, *J. Chem. Soc., Faraday Trans. 1*, 1989, **85**, 2055.

7) A. Mills and S. Giddings, *Inorg. Chim. Acta*, 1989, **158**, 49.

8) N. H. McMurray, *J. Phys. Chem.*, 1994, **98**, 9861.

9) A. Mills and G. Meadows, *J. Chem. Soc., Faraday Trans.*, 1993, **89**, 3849.